Journal of Pyrotechnics

Table of Contents - Issue 22, Winter 2005

Interior Pressure in the Mortar and Motion of a No. 3 Shell in a Fireworks Shot

Yuzo Ooki, Dayu Ding, Masamori Higaki and Tadao Yoshida*

Department of Mechanical Engineering, Ashikaga Institute of Technology
268-1 Omae-cho, Ashikaga-shi, Tochigi 326-8558, Japan
*To whom all correspondence should be addressed
email: yoshida@ashitech.ac.jp

Abstract: *Interior pressure in a fireworks mortar and initial velocity for the shot of a no. 3 shell were measured and results were analyzed. The observed initial velocity was mainly explained by the action of the interior pressure during the shot. On the other hand, a delay in pressure propagation in the mortar, the effect of gas flow through the gap between the mortar and shell, and acceleration of the shell just after leaving the muzzle were suggested.*

Keywords: *fireworks, shot, interior ballistics, initial velocity*

Introduction

Spherical shells are typical Japanese fireworks, shot from a mortar, developing in the sky releasing burning stars, in the form of various artificial flowers. These phenomena can be divided into the behavior of the shell in the mortar and in the air, the bursting of the shell, and the motion of the burning stars. In this article, we describe the results of a study on only the interior ballistics, and the relationship between pressure profile in the mortar and initial shell velocity using a no. 3 shell.

There is a pioneering work on the interior ballistics of the shot of a spherical firework shell by Shimizu.[1] His work was based on the interior ballistics of guns and considered the special situation of a firework shell and mortar. His work used a sophisticated theory to understand the situation and modern workers find it hard to use.

The initial velocity of model shells has been measured using a high-speed video camera by Matsunaga, Yoshida *et al*,[2] and the pressure profile in the mortar has been recorded by Matsunaga *et al*.[3] However the relationship between the pressure profile and the initial velocity has not so far been analyzed and reported.

We carried out the shot experiments using a pressure sensor, amplifier, digital oscilloscope and high-speed video camera, and results were analyzed using a personal computer. In our present work, the interior pressure of the mortar for a no. 3 shell and the trajectory of the shell in the air were recorded, and the results are analyzed and discussed.

Experimental

Materials

No. 3 firework shells, lifting charges and electric matches were provided by Sunaga Fireworks Co. Ltd. The lifting charge was grain black powder made by Nippon Kayaku Co. Ltd.

Apparatus

The fireworks mortar is shown in Fig. 1. The inner diameter, wall thickness, depth and total height of the mortar were 0.09 m, 0.006 m, 0.75 m and 0.78 m, respectively. Two pressure sensors were fitted, to the bottom and to a position 0.26 m below the muzzle of the mortar.

The pressure in the mortar during the shot was measured using two pressure sensors (Kistler 60410A), charge amplifiers (Kistler 5011) and a digital oscilloscope (Sony Tektronix TDS3012). Two pressure sensors were fitted at the bottom and middle of the mortar. The front surface of the sensors was covered with grease to protect the surface from the heat of combustion of the gas produced by the lifting charge.The initial velocity

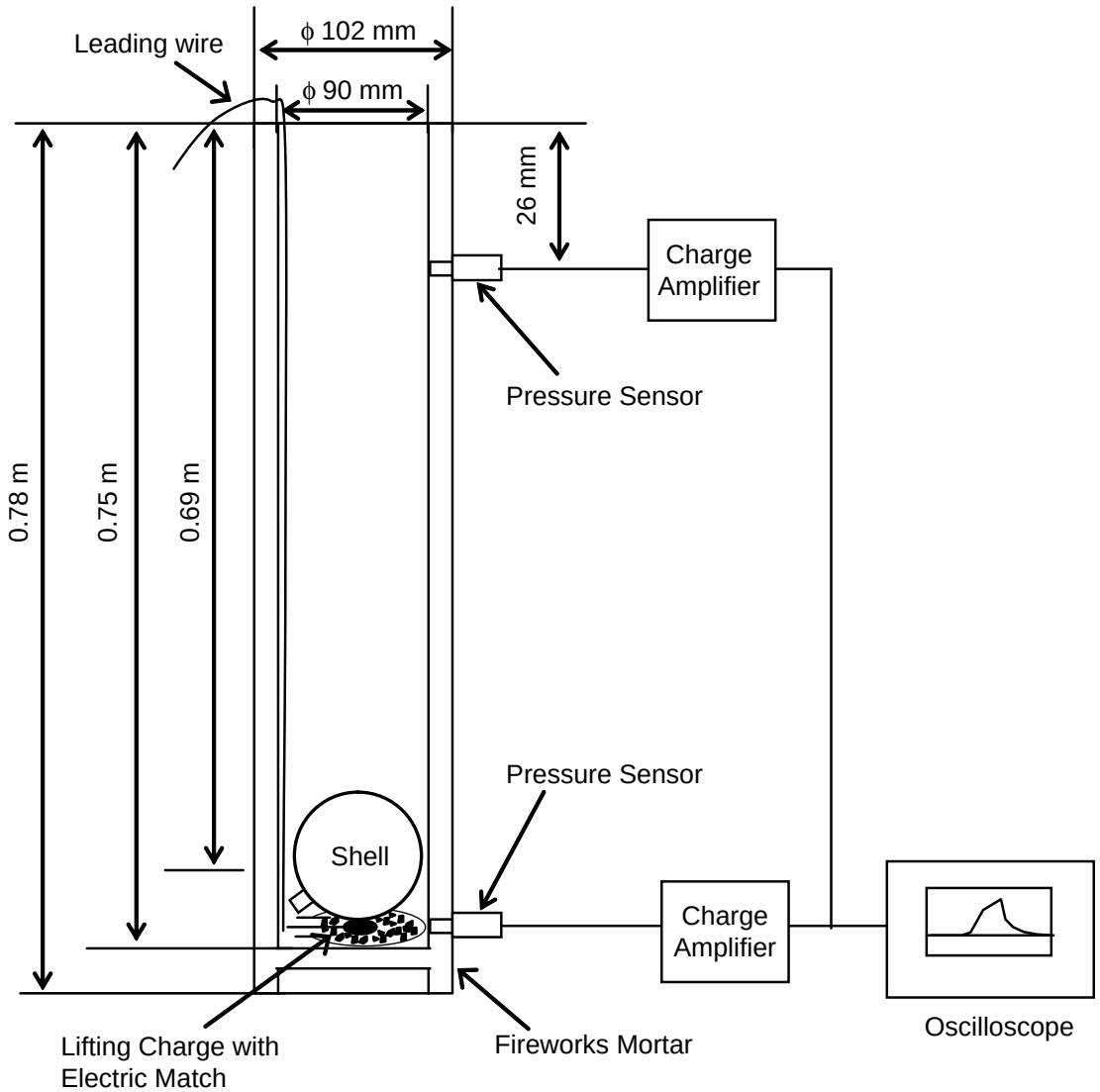

Figure 1. *Fireworks mortar and pressure measuring system.*

of the shell was measured using a high-speed video camera (FOR.A VFC-100SB).

Procedure

The mortar was set on the ground vertically. The lifting charge and electric match in a polyethylene bag were put in the bottom of the mortar. Then a no. 3 shell was placed on the lifting charge. The electric match was ignited by turning on an electric current. The lifting charge burned, pressure developed and the shell moved upwards. The pressure profile was recorded on an oscilloscope and the initial trajectory of the shell in the air was recorded on a high-speed camera. Each frame of the video was reproduced on a video screen and the initial velocity of the shell was determined.

Results and Discussion

Pressure Profile

Pressure profiles in the mortar during shot of the shell are shown in Fig. 2. The pressure profile shown by the thick line was recorded by the bottom sensor, and the profile shown by the fine line by the middle sensor. Both profiles in a figure were recorded simultaneously in a shot.

The profile from the bottom sensor showed an S-shaped curve in the first stage (from the middle pressure sensor to the bottom pressure sensor) and a sharply decreasing curve in the last stage (from the bottom pressure sensor). The first stage corresponds to the period of time during which the

(a)

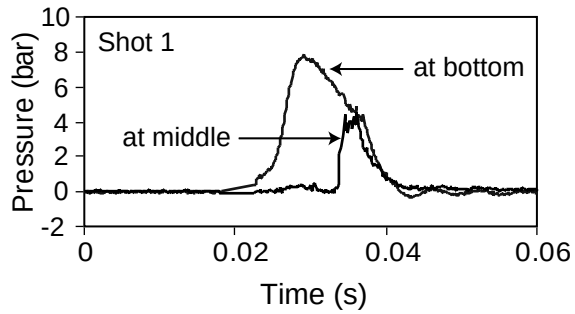

(b)

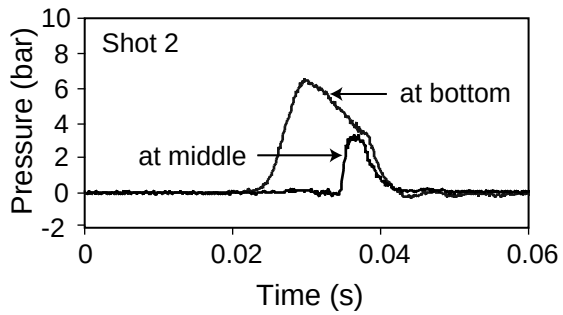

(c)

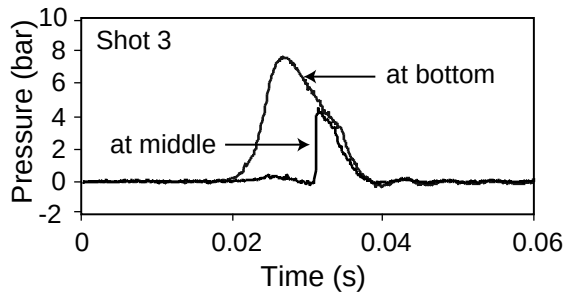

(d)

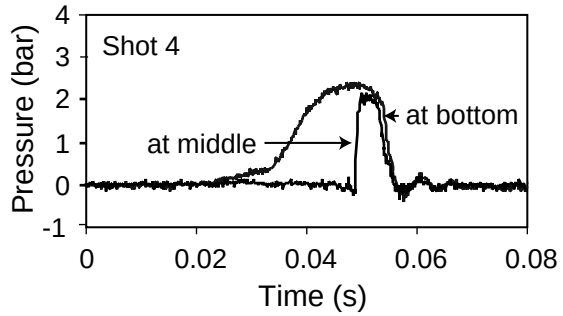

(e)

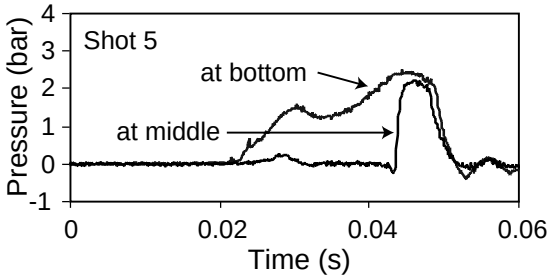

(f)

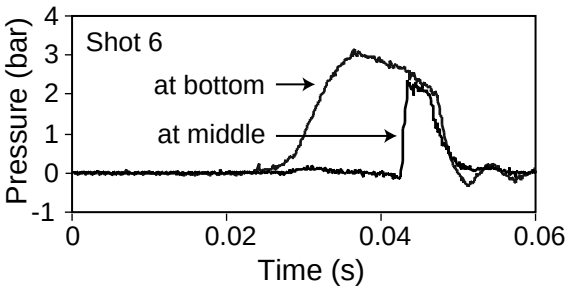

(g)

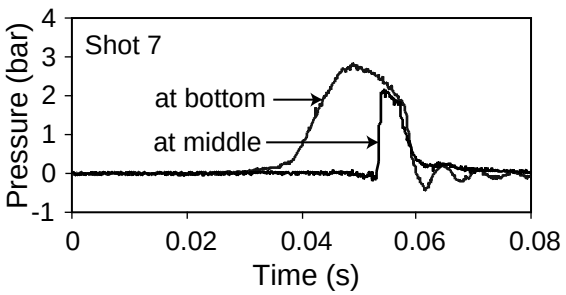

(h)

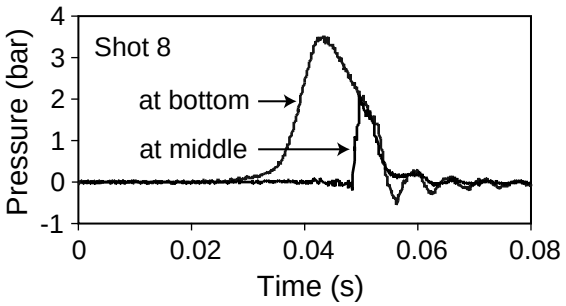

Figure 2(a)–(h). *Pressure profiles in the mortar.*

(i)

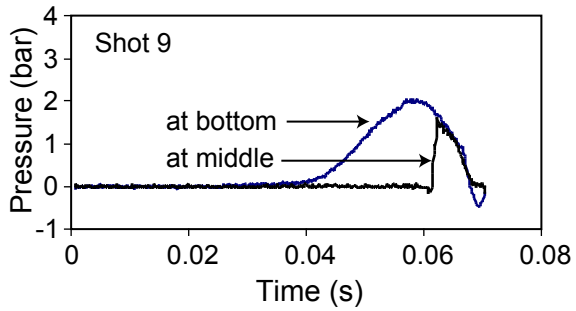

Figure 2 cont. (i). *Pressure profiles in the mortar.*

shell is traveling in the mortar. The later stage corresponds to the period after the shell has left from the muzzle.

The profile from the middle sensor shows a pressure drop just before the sharp pressure increase, and after the sharp pressure increase the pressure profile is similar to that of the bottom sensor. The pressure drop before the sharp increase may be caused by the rapid flow of the combustion gas through the gap between the shell and the mortar wall. This phenomenon may cause the shell to accelerate.

The pressure recorded by the middle sensor is lower than that recorded by the bottom sensor suggesting a delay in pressure propagation in the mortar. At the moment, this is merely our speculation.

Motion of a Shell in the Mortar

The motion of a shell in the mortar was analyzed using a personal computer. The equations of motion of a shell are expressed as follows:

$$M\frac{\mathrm{d}u}{\mathrm{d}t} = p(t)\times A - Mg \qquad (1)$$

$$\frac{\mathrm{d}Z}{\mathrm{d}t} = u \qquad (2)$$

Here, M, u, A, and Z are mass, motion velocity, maximum cross sectional area, and traveling distance of the shell, respectively.

$$A = \frac{\pi D^2}{4} \qquad (3)$$

Here, D is the diameter of the shell, and

$$\frac{\mathrm{d}u}{\mathrm{d}t} = \frac{\pi D^2}{4M}\cdot p(t) - g \qquad (4)$$

$$\frac{\mathrm{d}Z}{\mathrm{d}t} = u \qquad (5)$$

Here, $p(t)$ is observed value and substituted into Equation (4).

Equations (4) and (5) are simultaneously solved by numerical calculation, and acceleration du/dt, velocity u and traveling distance Z are obtained.

In practice, g is much less than

$$\frac{\pi D^2}{4M}\cdot p(t)$$

and can be neglected.

Equations (4) and (5) were solved by the Runge–Kutta method. The time integration process for ordinary differential equations (4) and (5) was performed using a fourth order accuracy Runge–Kutta method.

The digital pressure data were recorded on an oscilloscope and the data were reduced using Excel. These reduced data were used for calculating acceleration, velocity and traveling distance of the shell.

An example of the calculated profiles of the acceleration is shown in Fig. 3(a). A velocity profile is shown in Fig. 3(b), and a distance profile in Fig. 3(c).

The weight of the lifting charge, calculated maximum acceleration, velocity and distance of the shell in the mortar, and observed initial velocity are listed in Table 1.

Observed initial velocity of the shell in the air and calculated muzzle velocity

When a shell is shot, smoke and flame appear from the muzzle and then the shell appears above the smoke. We cannot observe real muzzle velocity. We can only determine initial velocity after the shell appears from the smoke. In the same experiment with the pressure measurement, the initial velocity

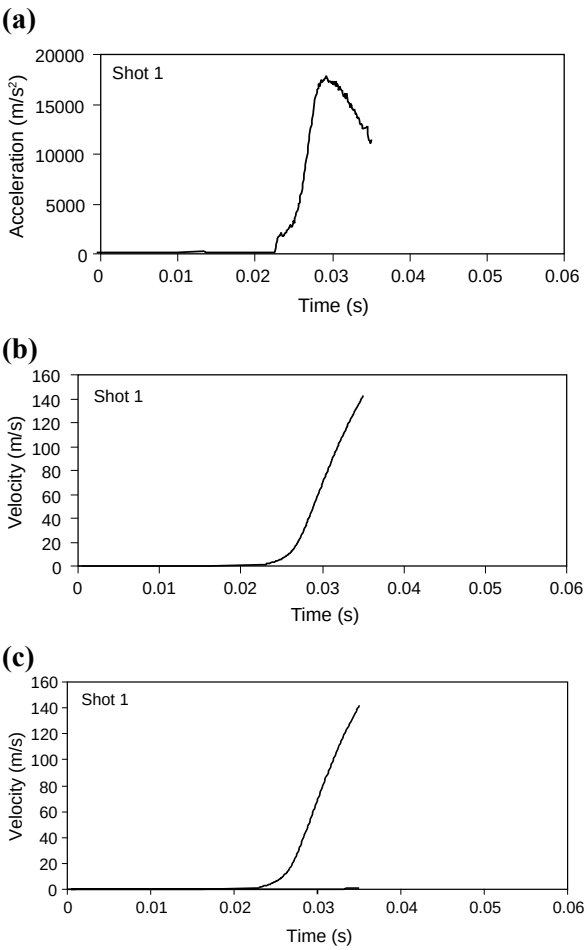

Figure 3(a)–(c). *Profiles of calculated acceleration (a), velocity (b), and traveling distance (c) of a shell for shot 1.*

of the shell was determined. The shell appeared above the smoke at about 2 m above the muzzle and the time difference to about 5 m high was determined. Then the initial velocity was derived. The observed initial velocities were similar to the calculated muzzle velocities from the pressure profiles in the mortar as listed in Table 1.

Effect of residual pressure after a shell has left the muzzle

Pressures at the bottom and middle of the mortar drop sharply after a shell has left the muzzle, but positive pressures remain for a short time. This short-lived pressure accelerates the shell after leaving the muzzle and the velocity of the shell increases in calculation. But this is not realistic and should be made clear in the future.

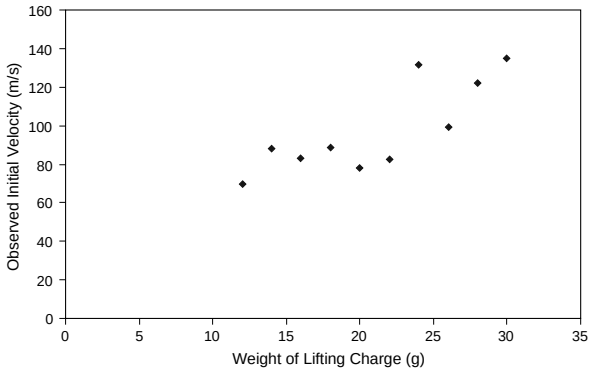

Figure 4. *Plot of observed initial velocity of shell vs. weight of lifting charge.*

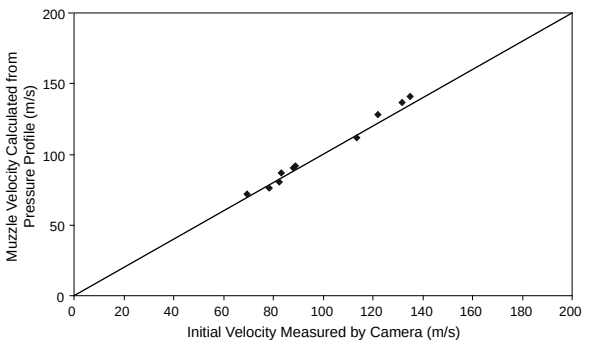

Figure 5. *Correlation of observed initial velocity and muzzle velocity from pressure profile.*

Effect of weight of lifting charge on initial velocity of shell

Initial velocity of the shell is plotted against weight of lifting charge in Figure 4. Correlation between initial velocity and weight of lifting charge is not good, suggesting that the burning of lifting charge is irregular. This must be also proved by suitable experiment.

Correlation of observed initial velocity of shell with calculated muzzle velocity from pressure profile

Calculated muzzle velocity from pressure profile is plotted against observed initial velocity by a high-speed video camera in Figure 5. The correlation is much better than that between observed initial velocity and weight of lifting charge.

Table 1. *Weight of lifting charge, calculated and observed initial velocity, and calculated distance (A to B)*

Test no.	Mass of lifting charge/g	Calculated muzzle velocity/m s^{-1}	Observed initial velocity/m s^{-1}	Calculated distance/m
Shot 1	30	141	135	0.69
Shot 2	28	128	122	0.69
Shot 3	24	137	132	0.69
Shot 4	22	81	82	0.69
Shot 5	20	76	78	0.69
Shot 6	18	92	89	0.70
Shot 7	16	87	83	0.70
Shot 8	14	90	88	0.69
Shot 9	12	72	70	0.70

Practically, the initial velocity of a firework shell can be estimated from the pressure profile, but not by the weight of the lifting charge at the moment.

Calculated maximum distance of shell in the mortar

The real distance of a no. 3 shell from the bottom to the muzzle of the mortar is 0.69 m. Calculated maximum distances of the shell are listed in Table 1. Agreement of both distances is good.

However we should examine whether the observed pressure profile is correct or not. We should examine the effects of delay of pressure propagation and of gas flow through the gap between the shell and the mortar wall in the future.

Acknowledgements

We thank S. Shudo, M. Aoyagi, A. Yatagai, and S. Hukazawa for their assistance.

References

1 (a) T. Shimizu, "On Ballistics of Fireworks Shells", *Journal of the Industrial Explosive Society*, Vol. 212, 1957, p. 18(3); (b) T. Shimizu, "Ballistics of Fireworks Shells", *Proceedings of the 11th International Pyrotechnics Seminar*, July 1988.

2 T. Matsunaga, Y. Wda, E. Ishida, M. Ito, S. Hatanaka, M. Tamura, N. Kobayashi and T. Yoshida, "Study on Safety of Aerial Shell (2). Validation of Exterior Ballistics", *Kogyo Kayaku*, Vol. 478, 1989, p. 50(6).

3 T Matsunaga *et al.,* "Experiment on Interior Pressure in Shot of Fireworks Shells", *National Institute of Chemical Technology Report*, 1993.

Prediction of Aerial Shell and Comet Trajectories Using SHELLCALC©

John Harradine[a] and Tom Smith[b]
[a]Manly, Queensland, Australia
[b] Davas Ltd, 8 Aragon Place, Kimbolton, Cambs PE28 0JD, UK

Abstract: *This paper describes a model for predicting the path of aerial shells and Roman candle comets. This model, incorporated in a Microsoft® Excel-based freeware program, SHELLCALC©, predicts the trajectory of these fireworks using point mass equations for range and height. These equations are modified to take into consideration mortar/candle angle, launch altitude above sea level, wind speed and direction, comet consumption, air density and terrain, and incorporate an approximation of shell drift through tumbling motion and mortar balloting. The graphical output from the model also incorporates typical shell burst diameters.*

Keywords: *Shells, comets, ballistics, trajectory, fall-out*

Introduction

On many occasions it is useful to predict the path of an aerial shell or Roman candle effects (comets) given certain initial conditions. In response to this need, the authors have developed a Microsoft® Excel-based predictor, SHELLCALC©, which is easy to use, and provides graphical outputs which may be readily understood by the lay person and be included in reports and presentations.

SHELLCALC© may be used to assist:

- fireworks operators to plan a display, especially where a risk or hazard assessment is required;
- fireworks regulators to develop safe distances and establish risk regimes for fireworks displays;
- enforcement and investigative agencies to predict possible outcomes of "near misses", or to confirm actual incident data, particularly for presentation in court or in investigation reports;
- fireworks testers to establish a safe template for test firings; and
- fireworks manufacturers to establish safe distances for their products and predict the effect of variable fuse delay times on burst height.

General Layout

The SHELLCALC© data input and output screen is shown in Figure 1. All information is entered and displayed on the same page. In this way it is possible to readily examine the effect of changing a single parameter on the results calculated.

For instance it may be particularly useful to set the fuse delay time to the total flight time of the shell – to examine the possible spread of stars in this, one of the highest consequence failure modes of aerial shells.

Program Input

SHELLCALC© requires that several parameters be input before a meaningful output can be achieved. These inputs, for the aerial shell and roman candle predictors, are shown in Figures 2 and 3, respectively. The user can choose between imperial or metric input, and between calculations on shells or comets. The difference choosing shells or comets is twofold – the graphical output only displays approximate shell burst sizes for shells, and the calculations for shells assume that the shell's mass remains constant throughout its flight. Conversely for comets, no burst diameter information is displayed, and the calculations assume the comet's mass decreases to zero during its flight time.

In addition to choosing the calibre of the shell or comet star, the user can also enter other optional parameters including the fuse delay time for shells

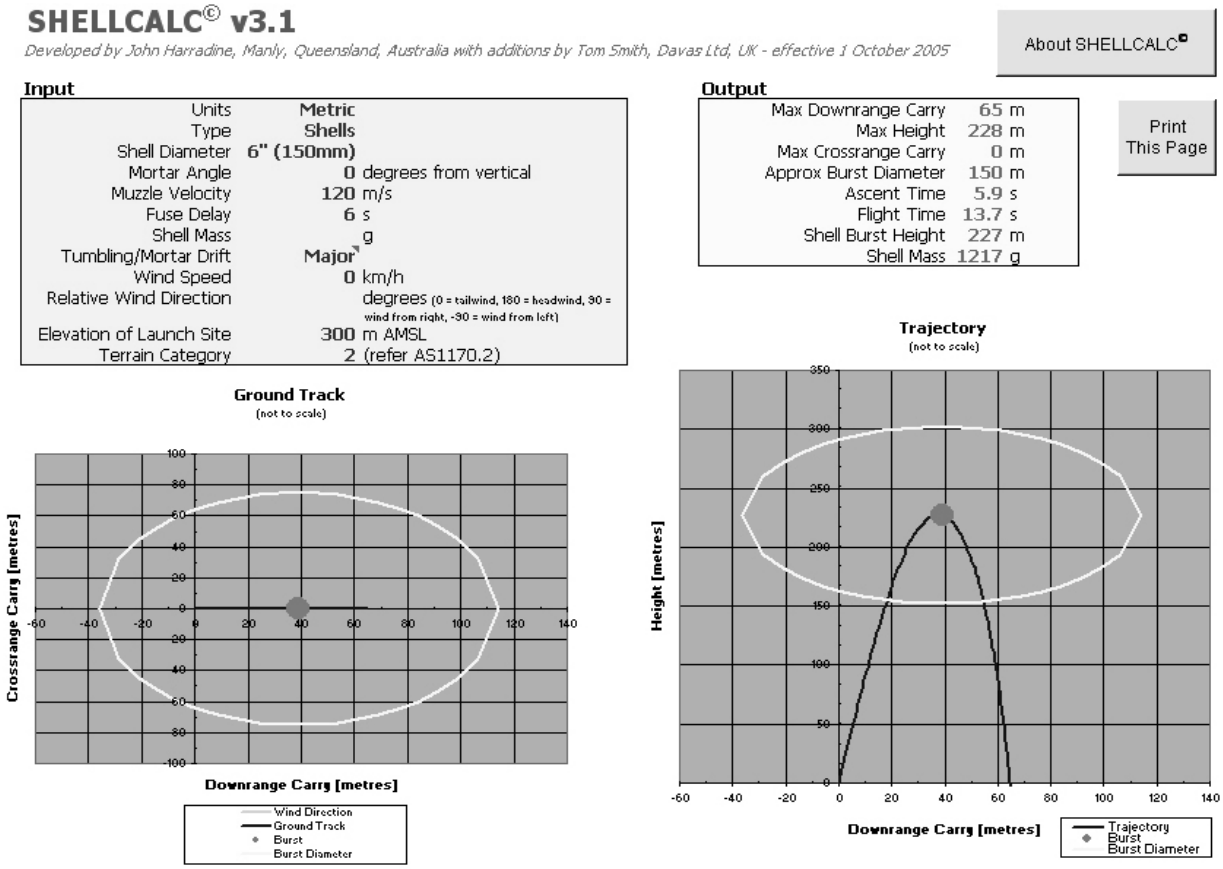

Figure 1. *General layout of SHELLCALC© data input, data output and graphical output screen.*

(if no value is entered the shell is assumed to burst at the apex of its flight), the mass of the shell (if no value is entered the mass is calculated), the muzzle velocity (default values are provided), the wind speed and direction, the elevation of the launch site and a parameter to reflect the terrain category.

Trajectory Prediction

The basis of SHELLCALC©'s trajectory prediction is a point mass trajectory model which, in the case of the Roman candle predictor, has been modified to take into account the burning of the comet during flight (described later). The point mass model is accepted as the simplest useful trajectory prediction technique which takes air resistance into consideration.[1] The point mass model predicts both range (x, y) and height (z) components of acceleration for a projectile of given mass m. The Cartesian points of reference for the point mass model are shown in Figure 4.

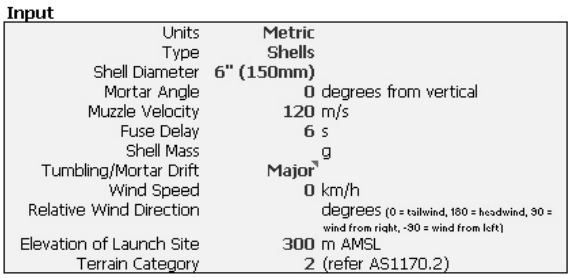

Figure 2. *Aerial Shell input parameters.*

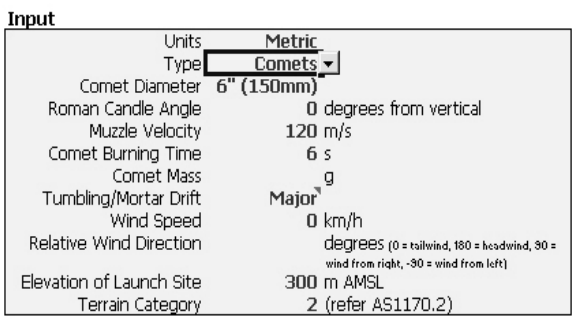

Figure 3. *Comet Shell input parameters.*

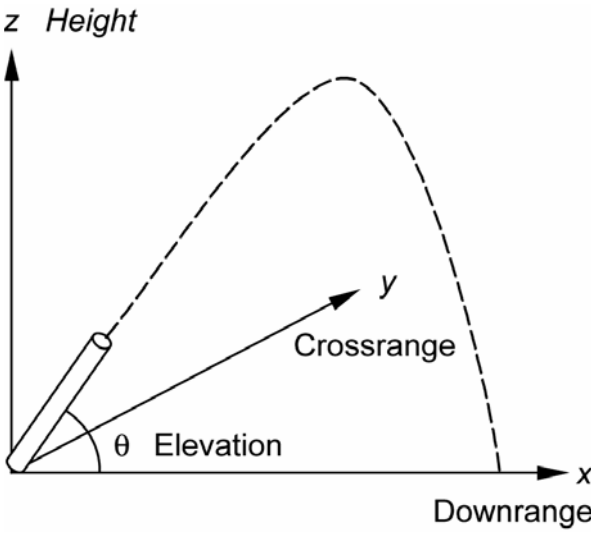

Figure 4. *Cartesian space used in* SHELLCALC©.

The equations for range and height are:

$$m\ddot{x} = \rho V^2 \pi d^2 C_D \left(\frac{\dot{x}}{8V} \right)$$

$$m\ddot{y} = \rho V^2 \pi d^2 C_D \left(\frac{\dot{y}}{8V} \right)$$

$$m\ddot{z} = -\rho V^2 \pi d^2 C_D \left(\frac{\dot{z}}{8V} \right) - mg$$

where: m = mass of projectile [kg]
x = downrange distance [m]
ρ = density of air [kg m^{-3}]
V = velocity of projectile [m s^{-1}]
d = effective diameter of projectile [m]
C_D = drag coefficient of projectile [–]
g = acceleration due to gravity [m s^{-2}]
y = crossrange distance [m]
z = height [m]

These equations are numerically integrated to solve for x, y and z based on a time interval of 0.1 s (this was found to give an acceptable level of accuracy without increasing the file size to an unacceptable level).

Correction for Drag Coefficient

The drag coefficient (C_D) of aerial shells is, at best, difficult to quantify. Such factors as roundness, surface roughness, effective Reynolds number and rotation will vary markedly from shell to shell and affect C_D, in some cases markedly. Given that these vagaries exist, an approximate value of C_D for shell diameters of 2 in (50 mm) to 12 in (300 mm) was determined by applying a best-fit model to Shimizu's empirical work on aerial shells,[2] resulting in:

$$C_D = -0.0921 \text{ h } D + 0.9283$$

where D =effective presented diameter of projectile to airflow [mm]

Shimizu's C_D values are most likely on the low side; he used Japanese shells which were most likely of better quality than those of Chinese manufacture, which represent the majority of shells used worldwide today.

C_D for comets is more difficult to predict, as a comet in flight is a deflagrating cylinder that is inherently unstable. For simplicity's sake, the C_D of comets was taken to approximate that of an aerial shell of similar diameter.

Estimated Shell Mass

An approximate value of mass, m, for aerial shells with diameters of 2 in (50 mm) to 12 in (300 mm) was determined by applying best fit to values from various sources:[2,3]

$$m = 205.25 d^{2.7029}$$

The user can enter the mass of the aerial shell in question if this is known; otherwise the program will use the estimated value.

Correction for Comet Mass Consumption

Unlike aerial shells, which are assumed to remain intact during flight, an allowance must be made for the consumption of the burning comet in flight. If the effect of pressure on burning rate is ignored (that is, burning rate remains constant), and surface burning of a cylindrical comet is assumed, the mass of the comet m after elapsed time t can be calculated using:

$$m = \frac{\pi \rho_P}{4} \left(d_0 - 2rt \right)^2 \left(l_0 - 2rt \right)$$

Table 1. *Typical dimensional and burning rate parameters for a 2 in (50 mm) roman candle comet.*[4]

Parameter	Value
m	0.068 kg
ρ_P	1860 kg m^{-3}
d_0	0.045 m
l_0	0.023 m
r	0.00143 m s^{-1}

where: ρ_P = density of comet [kg m^{-3}]
d_0 = initial diameter of comet [m]
l_0 = initial thickness of comet [m]
r = linear burning rate of comet composition [m s^{-1}]

Typical values for these parameters for 2 in (50 mm) roman candles are shown in Table 1. These values for density ρP and burning rate r should be reasonably accurate when applied to all solid black-powder or flash powder effects (including comets and stars), and these values are used by default in SHELLCALC©. The user has the option of inputting a different comet burn time if this is known; in this instance, the program will alter r to achieve the required total burn time.

Effective Comet Diameter

As a comet is consumed during flight, its effective diameter reduces, thereby reducing the effective presented area of the comet. SHELLCALC© uses the following formula to achieve an approximation of the effective presented diameter, d:

$$d = d_0 - 2rt$$

Correction for Wind

SHELLCALC© permits the user to input wind direction and speed relative to the direction of aim of the mortar or Roman candle. The program requires the user to input a wind bearing relative to the direction of aim as shown in Figure 4. For example, a headwind has a relative bearing of 0°, and a wind from the right has a bearing of 90°.

Based on the wind direction and speed input by the user, SHELLCALC© resolves the velocity vectors in the x and y axes and adjusts the values of V, $\dot{x}$ and $\dot{y}$ in the relevant point mass equations.

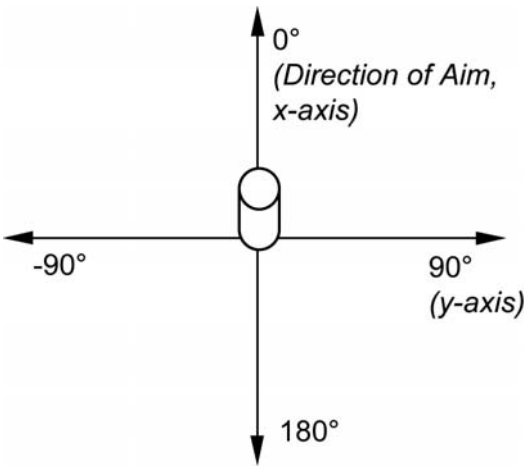

Figure 5. *Relative wind bearings used in SHELLCALC©.*

Correction for Mortar/Roman Candle Angle

When the mortar or roman candle is set at an angle other than vertical, the user can nominate the appropriate angle from vertical. Based on this angle, SHELLCALC© calculates the mortar elevation θ (refer Figure 1), resolves the velocity vectors in the x and z axes and adjusts the values of $\dot{x}$ and $\dot{z}$ in the relevant point mass equations.

Correction for Terrain

Terrain affects actual wind speed at ground level. If turbulence and other anomalies are ignored, a good estimate of wind speed w for a given height above ground level z can be estimated if the AS/NZS 1170.2 terrain category is known.[5] The value of w for terrain category 2 (open spaces and water) is:

$$w = w_0(0.1036\ln(z+1) + 0.8731)$$

where w_0 = wind speed out of ground effect [ms^{-1}].

Similarly, the value of w for terrain category 3 (sports grounds and built-up areas) is:

$$w = w_0(0.139\ln(z+1) + 0.7503)$$

Based on user input, SHELLCALC© corrects V using the appropriate equation. If the user does not nominate a terrain category, the program ignores terrain effects on V.

Correction for Air Density

As air density ρ changes with altitude, SHELLCALC© calculates ρ at each 0.1 second increment and uses this value in the relevant point mass equations. Air density at a given altitude ($z + z_0$) is calculated according to the following equation:

$$\rho = \rho_0 e^{-0.0001065(z+z_0)}$$

where: ρ_0 = density of air at sea level [kg m^{-3}]
z_0 = elevation of launch site above sea level [m]

Program Output

Once the user inputs all data, SHELLCALC© will provide both numerical (Figure 6) and graphical (Figures 7, 8 and 9) outputs. The graphical outputs are Excel charts, and so may be copied to other applications for inclusion in reports or presentations.

Shell Burst Diameters

Shellcalc© also displays the typical burst diameter of shells at either the time selected by the user, of if this parameter is not entered, at the apex of the shell's flight. The values for typical shell burst diameters are taken from work on Japanese Shell Break Radii7 and are a mathematical close fit to the typical values cited in that paper (Figure 10). However, the authors noted that the maximum observed break radii can exceed the typical values by a significant amount, and that shells from different suppliers, and shells comprising different effects may also deviate significantly from the "typical" values. The user is cautioned to consider the graphical output as illustrative only.

Output

Max Downrange Carry	38 m
Max Height	236 m
Max Crossrange Carry	0 m
Approx Burst Diameter	150 m
Time at All Burnt	6.0 s
Height at All Burnt	235 m
Comet Mass	1217 g

Figure 6. *Numerical output for aerial shell prediction.*

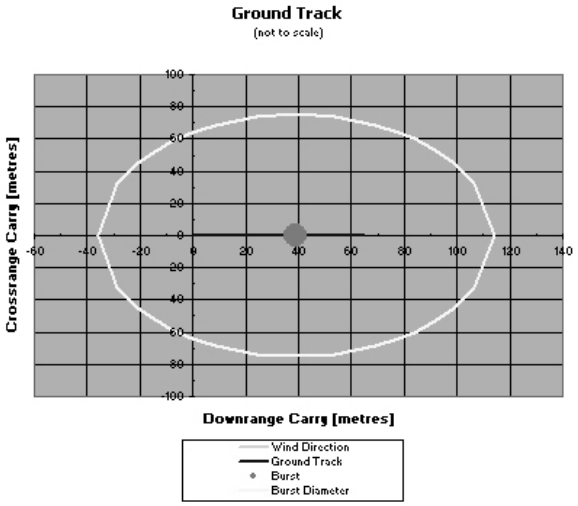

Figure 7. *Ground track of aerial shell showing location of shell burst and approximate shell burst size*

Shell Drift

Firework shells are subject to several mechanisms to account for the observed shell drift, even in completely still conditions. Such factors include shell spin (Magnus effect) and shell balloting due to the fit of the shell in a mortar and the mortar length. SHELLCALC© uses shell balloting data from Norton[7] to attempt to factor in, albeit in a crude way, the observed deviations. SHELLCALC© allows the user to select three values related to this effect,

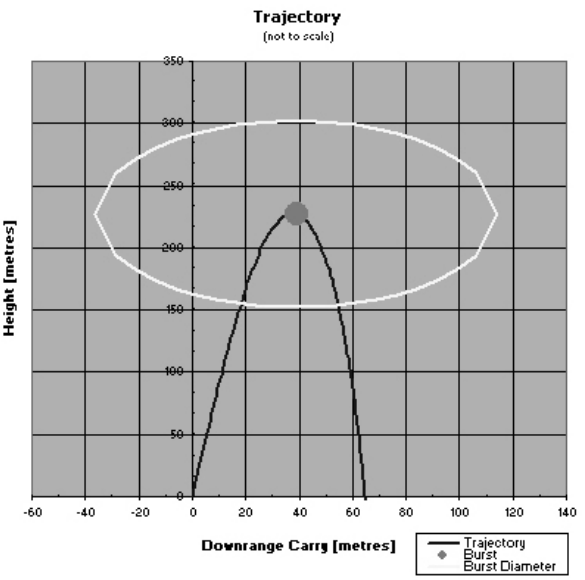

Figure 8. *Trajectory of aerial shell showing location and approximate shell burst size.*

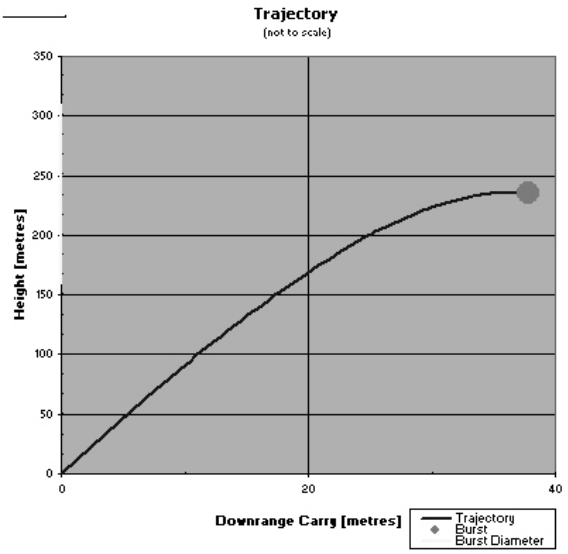

Figure 9. *Trajectory of comet showing location of "burn out".*

and to incorporate this into the final output values and graphs.

None – shell drift parameters are ignored

Typical – an average value of shell deviation from Norton is used (approx. 2° deviation)

Maximum – the largest value of shell deviation calculated by Norton is used (approx. 5° deviation)

The user should note that shell drifts are due to many factors, and the incorporation of this parameter into SHELLCALC© is largely to prevent the program calculating that in still conditions, where a shell is fired vertically, that it would necessarily return to earth exactly at the point of firing. It is also useful to use this parameter when estimating "worst case" scenarios, for instance angled mortars, significant tailwind, maximum shell drift and

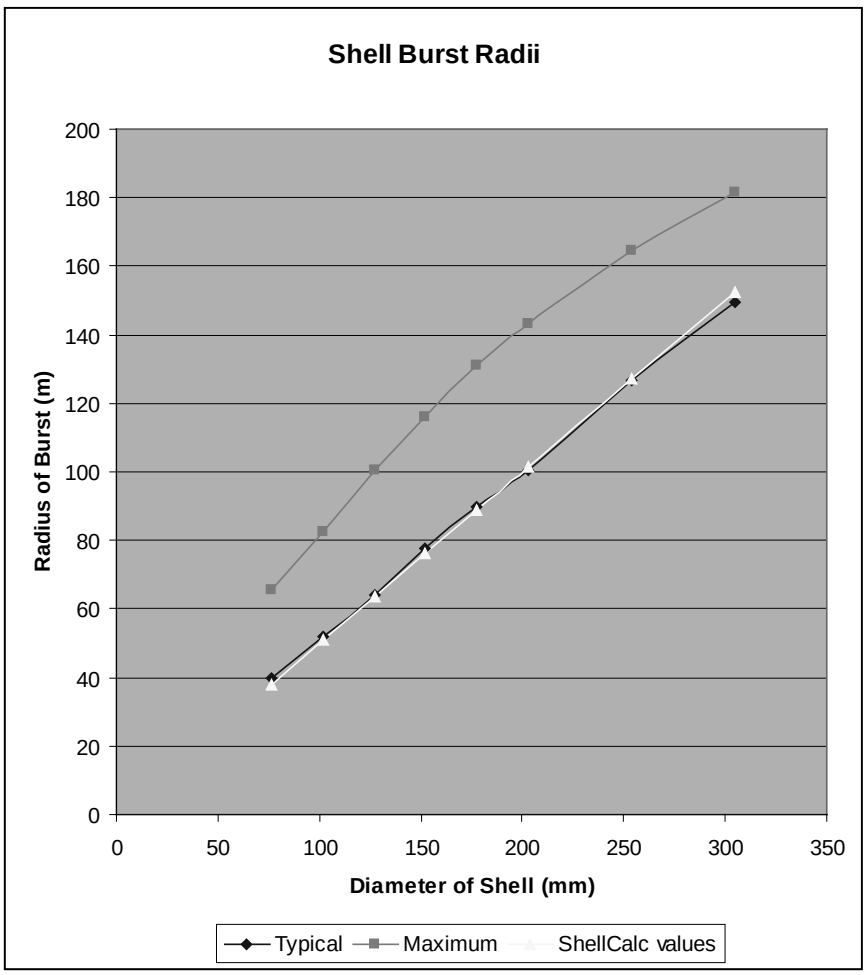

Figure 10. *Typical, Maximum and SHELLCALC© values for burst radius as function of shell diameter used in SHELLCALC© calculations.*

shell bursting at ground level. The extent of shell balloting depends on the shell–mortar clearance and to the effective length of the mortar and in general better shell–mortar fit and longer mortars decrease this effect.

Agreement with Observation

Based on the authors' observation and Shimizu's work,[2] the predictions made by SHELLCALC© are close to the actual behaviour of aerial shells and Roman candle comets. As SHELLCALC© is still a basic program with limited accuracy, the authors would appreciate any feedback on improvements.

References

1 Aeromechanical Systems Group, *Basic External Ballistics Lecture Notes*, Royal Military College of Science, Shrivenham, UK, 1992.

2 T. Shimizu (translated by A. Schuman), *Fireworks From a Physical Standpoint – Part III*, Pyrotechnica Publications, 1985.

3 J. B. Harradine, *Chemical and Physical Analysis of Roman Candles, Other Types of Fireworks and Their Residues*, Explosives Inspectorate, Department of Natural Resources and Mines, Brisbane, 2001.

4 J. B. Harradine, *Dynamic Testing of Roman Candles and Other Types of Fireworks, Safety and Health Division*, Department of Natural Resources and Mines, Brisbane, 2001.

5 Standards Australia, *AS/NZS 1170.2:2002: Structural design actions - Wind actions*, 2002.

6 K. L. and B. J. Kosanke, *Pyrotechnics Guild International Bulletin*, No. 59 (1988), p. 104.

7 Randall K. Norton, *Journal of Pyrotechnics*, Issue 13, 2001, p. 31.

Note

SHELLCALC© is a freeware program and is designed to run on Microsoft® Excel 95 or later.Copies and updates may be obtained directly from the download section of the Journal of Pyrotechnics Website:

http://www.jpyro.com/downloads/shellcalc/

Reaction propagation between fireworks shells and compositions confined in steel pipes

E. Contestabile and B. von Rosen

Canadian Explosive Research Lab
555 Booth St.Ottawa, Ontario K1A 0G1
Canada

Abstract: *This study presents the experimental results on the ignition of linear arrays of fireworks articles and bulk stars and describes their propensity to mass explode. Star and report shells, roman candles, and bulk cylindrical and spherical stars were functioned in steel pipes through initiation with a small black powder charge or an explosives booster. Continuous velocity of detonation probes was used to monitor the rate of reaction among the pyrotechnic components and the resultant fragmentation of the steel pipe was used to rate the violence of the reaction. All pipes fragmented and the measured reaction rate ranged from 170 to 870 m* s^{-1}*. Based on fragmentation, the violence of reaction increased from the star shells, to the roman candles, to the report shells, and then to the bulk stars.*

Keywords: *explosion, steel, mortars, fragments, reports*

Introduction

In an attempt to determine the reaction rate within a pile of fireworks, tests were performed with pyrotechnic composition and firework shells confined in steel pipes. The justification and applicability of such tests including unconfined burns and height-to-detonation tests were presented previously.[1] Fundamentally, the intent of the tests was to confine the samples to such an extent that maximum reaction rates would be achieved.

In a recent series of trials,[2] attempts were made to determine the shell-to-shell reaction rate with report and star shells. The 76, 102, and 127 mm shells were placed, in contact, end-to-end, in 3 m long Schedule 40, open-ended, steel pipes of corresponding nominal inside diameters of 3, 4, and 5 inches. A commercial explosive booster was used as initiator. It was found that complete, shell-to-shell communication within the pipe did not occur. Although most of the shells usually exploded, live and video observations indicated that some shells were ejected intact and/or burning from both ends of the pipes. Except for the small fragments produced by the booster, pipe fragments were large and fragmentation was very localized.

It was found that the commercially available coaxial-cable-type velocity of detonation (VoD) probe used to monitor the reaction rate over the length of the pipe was not sufficiently sensitive to detect all reactions/explosions. The records obtained indicated reactions/explosions occurring along the length of probe from which reaction rates could be determined. An example of such a record is shown in Fig. 1. It does not show a staircase-shaped trace as would be expected from the discrete amounts of energetic material in each shell exploding at the shell location. Such a trace, as explained in reference 2 could have been produced by non-sequential explosions of shells coupled with possible shell movement within the pipe. Non-sequential explosions would generate poor reaction rate records that could be used to determine average reaction rate values over the length of the pipe. On the other hand, had the shells been in motion within the pipe when they exploded, then the reaction rate calculated would be incorrect. The values of the reaction rate for the shells tested in the 3 m long pipe configuration ranged from 35 to 750 m s^{-1}.

Other researchers (Link *et al*.,[3] Downs,[4] Kennedy,[5] Kosanke *et al*.[6]) investigated the Bray Park accident (May 20, 2000, in Australia) where 50 mm roman candles placed in steel tubes exploded and ruptured the steel tubes. The investigators experimentally reproduced the accident and through modeling considered scenarios where the pyrotechnic

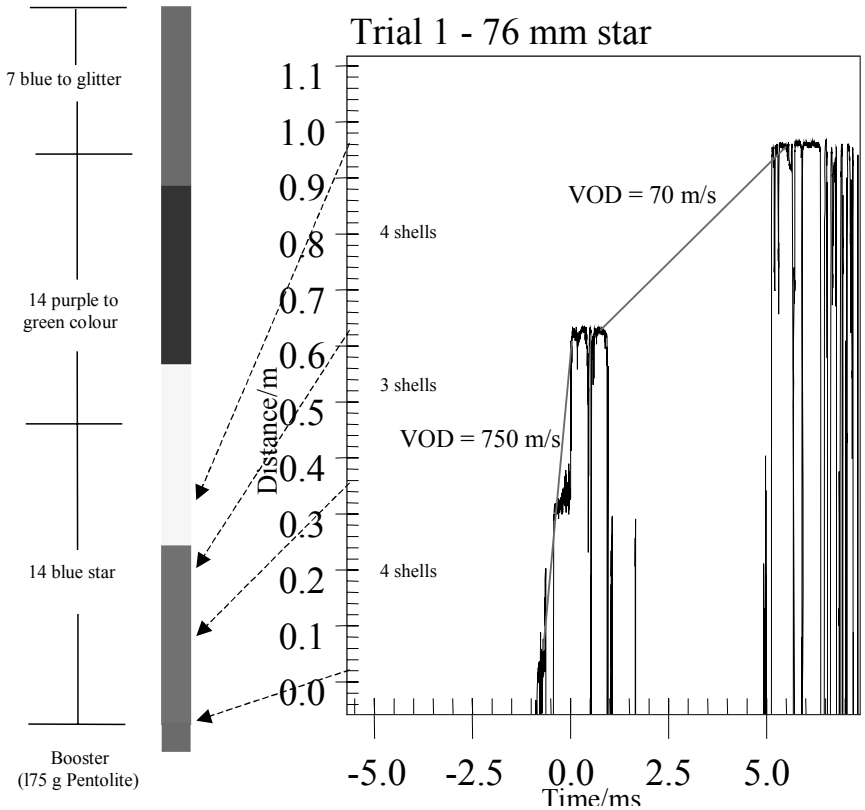

Figure 1. *Example of reaction rate record for 35, 76 mm star shells loaded in a steel pipe*

material either reacted instantaneously as a constant volume event or the roman candle's discrete pyrotechnic material exploded sequentially, in an effort to predict pipe rupture. The conclusion was that an ignition caused a deflagration-to-detonation transition (DDT) in one of the comet charges of the roman candle, which in turn initiated the rest of the energetic material of the roman candle by a shock-to-detonation transition process. The ability of an ignition-to-deflagration-to-detonation crossover was facilitated by the very sensitive and reactive nature of the comet composition and the confining effect of the steel pipe. A finite element code used to model the process predicted that pressures exerted on the pipe wall from detonating comet charges exceeded 500 MPa.

On a related topic, Kosanke and Kosanke[7,8] explain shell malfunctions in mortars, flowerpots, muzzle breaks, in-mortar "detonations" or, using the more acceptable term, violent in-mortar explosion (VIME). The term VIME, usually associated with firework mortar bursts, is used because it is usually unknown whether a detonation actually occurred. The authors suggest that the malfunctions can be due to the high pressure from the lift charge causing shell-casing failure, structural damage of the timing fuse (fuse driven into shell casing), and/or premature ignition through inertial setback. Flame from the lift charge then spreads through the damaged shell pyrotechnic components, accelerating due to the confining effect of the mortar and ambient pressure loading from the lift charge being consumed. Andoh and Kubota[9] have proven similar behaviour with solid propellants drilled with different size holes and subjected to ignitions at pressures ranging from ambient to seven atmospheres. They showed that flame penetration and propagation rates increased with open-ended holes. The flame paths within stars in fireworks shells can be considered as being open-ended holes.

As a reference to mortar bursts, Takishita *et al*.[10] report that bursting 82 mm star shells, can project individual stars at speeds of 70 m s^{-1}, and that a pressure of 5.6 MPa is reached in 3 ms within the shell and causes the shell to burst. This magnitude of pressure can quite easily rupture paper and plastic fireworks mortars. On the other hand, Takishita *et al*.[11] also report the time required for communication between the acceptor shell and a donor shell, both contained in a cardboard container, as 5 s. This is ignition and shell explosion through the time delay element (normal function) and not ignition through structural deformation or rupture of the shell. In reference 11, Takishita *et al*. conclude that the "heat transfer process by the hot gases and/or by the hot fragments plays a dominant role on the prevention of accidental bursts of shells. It is suggested that ignition prevention caps be placed on the end of each delay fuse of the shells." This is plausible in low confinement scenarios and deserves further investigation beyond the few tests performed by Takishita *et al*. to investigate mitigation methods for preventing communication. Then, Takishita *et al*.[11] qualify their proposed ignition and corresponding mitigation method by stating that "No mechanical damage is suffered by neighboring shells as long as each shell is separated physically by a paper barrier when an accidental burst of a shell occurs."

This paper presents and discusses a series of tests where the same report shells and similar star shells to those used in the study with the 3 m long pipes,[2] roman candles, and bulk fireworks stars were loaded in 1 m long Schedule 40 steel pipes capped at one or both ends. This configuration was designed to restrain the shells and prevent them from moving during their initiation and communication process.

Since the performance of the tests presented herein, similar pipe tests have been carried out under the CHAF[12] program in Europe. At this time not all the data have been analyzed but some information and results are given in Work Reports WP5, WP6 and WP7, which are available from their web site.[12] Their pipe test configuration is referred to as the 1D (one-dimensional) test. Initiation was through the use of a report shell initiated with an electric match. The shells were instrumented with trigger wires that "sensed" the shell bursting. The pipes were also fitted with piezo-type pressure transducers, which recorded the pressure profile within the steel pipe. The wall thickness of these pipes was twice that of the pipes used in this study and the CHAF program reports no pipes as bursting. Therefore, no fragments were produced.

Figure 2. *Array of fireworks shells on cardboard (Test 1)*

Experimental Set-up

Four series of tests were performed, the first with star shells (35 g burst charge and 60 g stars), the second with report shells (35 g burst), the third with roman candles, and the fourth with bulk fireworks stars contained in 76 mm (nominal 3 inch Schedule 40) steel pipe, 90 cm long. In the first and second series of tests, 76 mm shells, with their lift charge removed, were rolled in a single layer of single-sided corrugated cardboard (Fig. 2). A continuous velocity of detonation probe (VoD) was placed in one of the corrugations. The assembly was then inserted into a steel pipe that was sealed on one or both ends with cast iron pipe caps. In this configuration, with the cardboard packaging fitting snugly against the inside surface of the pipe, the void volume consisted mainly of that between the shells in the linear array (Fig. 2) and it was estimated to be in the range of 25–30%. Note that the void volume refers only to that between the pyrotechnic packaging and the confines of the steel pipe. It does not, for example, include the voids among the stars or that among components within a roman candle tube.

As indicated in Fig. 3, a hole was drilled in the wall of the pipe for the purpose of inserting initiator wires in the tests where the pipe was capped at both ends. In this configuration, initiation of the samples was either with a 175 g Pentolite booster initiated with detonating cord or with approximately 15 g of 5FA black powder initiated with an electric match. In the tests where the pipe was only capped at one end, the initiator was placed at the open end. A 4 mm hole was drilled in the cap

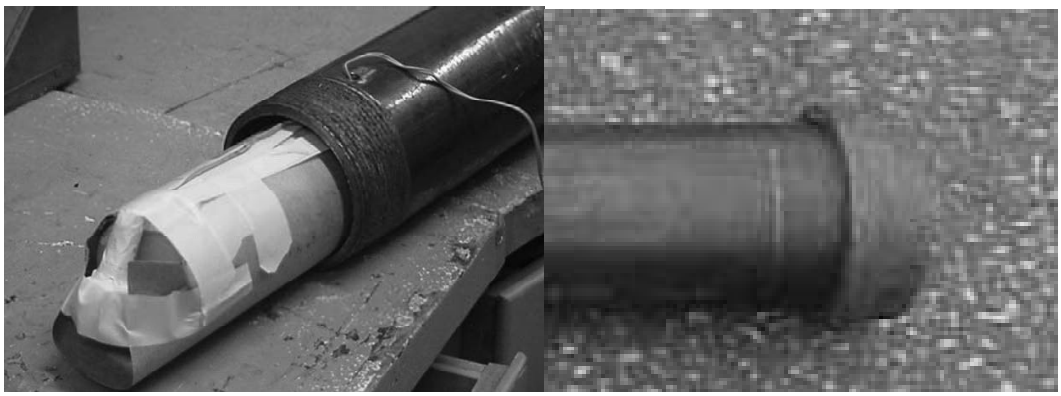

Figure 3. *VoD probe signal wires and capped-end of pipe*

located at the end opposite to the initiator end of the pipe to accommodate the VoD probe.

In the third series of tests, candles were inserted in Schedule 40 pipes. In the first test, an eight-shot, blue star candle was used. It contained approximately 120 g of pyrotechnic composition in the form of the black powder lift charges and stars. The stars were housed in plastic shells. The 30 mm candle, with an outside diameter of approximately 38 mm was inserted into a nominal 2 inch pipe (outside diameter 6.05 cm, wall thickness 3.8 mm, burst pressure approximately 60 MPa[13]), with a nominal inside diameter of 5.26 cm. No additional packaging was used. Therefore there was a 7.3 mm air gap between the candle and pipe. The candle was 850 mm long and assuming that only 60% of the candle length is filled and the remainder forms the muzzle end, the candle occupies a volume of approximately 580 cm^3. The candle was placed in a 92 cm long pipe having an internal volume of approximately 2000 cm^3. Then the void volume within the pipe is 70%. If only the length of pipe equal to the length of candle containing composition is considered, then the void volume within that length of candle and pipe is approximately 50%.

In the second test, an eight-shot, two-colour, 60 mm candle containing approximately 430 g of energetic materials (lift charge and stars) was used. The stars were contained in a spherical paper shell slightly smaller in diameter than the candle inside diameter. The 1000 mm long candle, with an outside diameter of approximately 71 mm was placed inside a nominal 3 inch pipe (outside diameter 88.9 mm, wall thickness 5.6 mm, burst pressure approximately 45 MPa[14]), whose inside diameter was 77.7 mm. Again, with only 60% of the candle length being filled and the remainder forming the muzzle end, the candle occupies a volume of approximately 2.4×10^6 mm^3. Therefore there was a 3.4 mm air gap between the candle and pipe. The steel pipe was 1150 mm long, with a volume of 5.4×10^6 mm^3, so that the void volume was approximately 55% of the total pipe volume. If only the length of pipe equal to the length of candle containing composition is considered, then the void volume in that length is approximately 15%.

In the fourth series of tests, red stars removed from fireworks shells were placed inside a cylindrical tube, formed with two layers of kraft paper. A VoD probe was inserted between the layers of kraft paper and the assembly was placed inside the steel pipe. Two tests were performed with spherical stars and one with cylindrical stars. The components of this configuration, with the pipe capped at only one end, are shown in Fig. 4. Initiation of the samples was with a 175 g Pentolite booster initiated with detonating cord placed at the open end

Figure 4. *Components of fireworks star tests*

of the pipe. The booster was placed tightly against the package of stars so as to minimize the void volume between the kraft paper tube and steel pipe, estimated to be approximately 5%. Note that the void volume among the stars is approximately 20%, less than the theoretical 25% for equal size spheres, correcting for the fact that the stars are approximately of the same diameter.

During the test program it was found that the commercially available copper VoD probes were too rugged and were not responding. Therefore, trials were also performed with custom-made aluminum VoD probes. The pipes were prepared and then hung inside a blast chamber where they were initiated via an electric firing system. Testing inside the chamber allowed recovery of the fragments but prevented video recording.

Figure 5. *Test 1: 8 star shells*

Figure 6. *Test 2: 8 star shells*

Test Results

Two methods of initiation were used in these tests, a booster initiated with a short length of detonating cord and a small amount of black powder ignited with an electric match. The small booster will itself contribute to fragmentation more than the black powder charge, but its fragmentation effect will be limited to a very short distance of the initiated end of the pipe. Comments relating to fragments will refer to those produced over the whole length of the pipes.

Figures 5, 6, 8, 9, and 11 to 15 show the fragmentation of the pipes resulting from the various configurations. Only two rate-of-reaction traces were obtained and they are shown in Figs. 7 and 10. Table 2 summarizes the results and quantifies the fragmentation.

Except for Tests 2 and 5, the damage to all pipes was substantial. Fragmentation of the pipes with star shells resulted in quite different results when initiated with a booster than with the black powder charge, with the booster initiation resulting in more than twice the number of fragments.

In Test 1 with the star shells, the pipe suffered damage mostly at the initiated end and the far end. A section approximately 10 cm long remained undamaged. The pipe in Test 2 was capped at both ends and as a result, even though initiation was with a black powder charge (inside pipe), the initiating end suffered localized damage. A rate-of-propagation was recorded in Test 2 with the continuous copper VoD probe indicating a rate of approximately 160 m s^{-1}.

Tests with the report shells, Tests 3 and 4 produced 3 to 4 times more fragments than those from the star shells. The interesting occurrence with these two tests is that Test 3 with a pipe capped at one end and with booster initiation resulted in about 25% fewer fragments than the pipe in Test 4, which was capped at both ends but was initiated with a black powder charge. Both pipes suffered similar damage with the additional number of fragments in Test 4 being primarily due to the fragmentation of the second cap. Note that this result indicates that the two different initiation methods resulted in the same type of response from the shells. A reaction rate trace was obtained for Test 4, where a continuous aluminum VoD probe was used. The measured rate ranged from 700 m s^{-1} to 870 m s^{-1}. This coincides with the upper range of values determined from the 3 m long pipe tests reported in reference 2.

The third series of tests, Tests 5 and 6, was performed with roman candles. One was an eight-shot candle, 30 mm by 850 mm long and the other was an eight-shot candle, 60 mm by 1000 mm long.

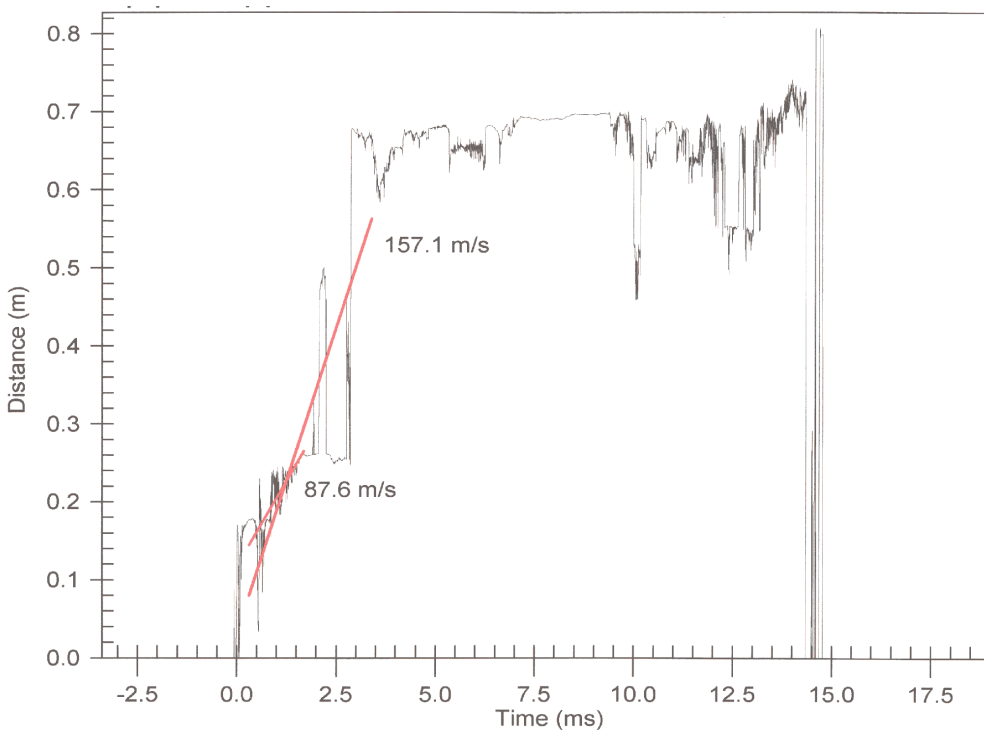

Figure 7. *Record from Test 2 Average rate of propagation 157 m s^{-1}*

Figure 8. *Test 3: report shells (booster initiated)*

Figure 9. *Test 4: report shells (15 g black powder initiated)*

Both tests made use of pipes capped at one end and both candles were initiated with a booster. The smaller, 30 mm candle was the only sample tested in a smaller diameter steel pipe (2 inch Schedule 40), in an attempt to keep the void volume low. It still had the highest void volume of all the tests at approximately 70% while the volume over the length of the candle containing energetic material was only approximately 50%. This combined with the relatively low mass of energetic material per unit length resulted in very low fragmentation of the pipe, as low as the star shells initiated with the black powder charge. The larger candle was tested in a pipe with a welded base, instead of a threaded cap, to better simulate the Bray Park accident set-up. With a void volume of approximately 55% and slightly higher energetic material per unit length, the resulting explosion caused fragmentation equivalent to that of the star shells initiated with a booster. Again, note that the void volume over the length of the candle containing energetic mate-

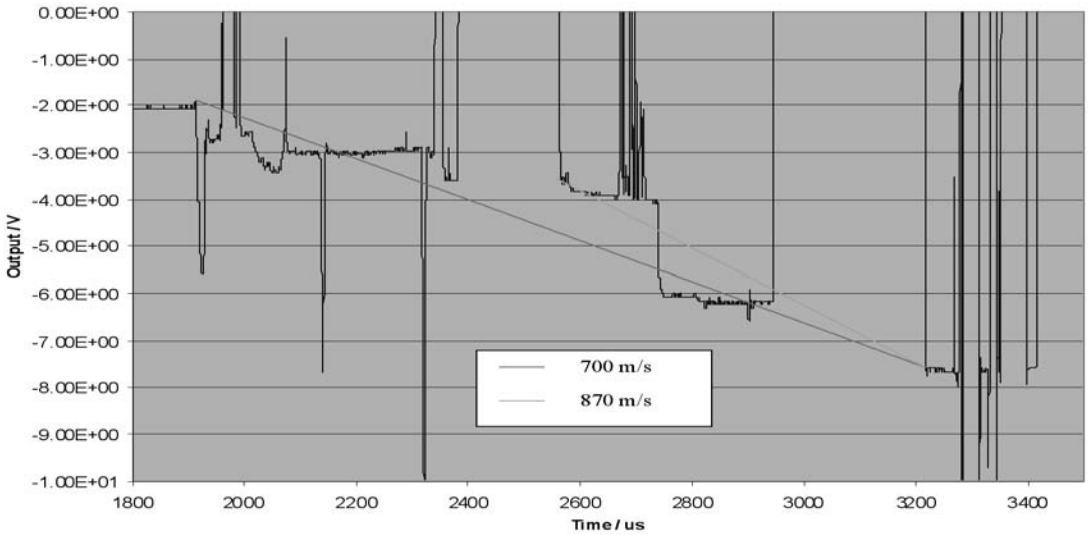

Figure 10. *Record from Test 4 - Average rate of propagation 700 m s^{-1}, Maximum rate of propagation 870 m s^{-1}*

Figure 11. *Test 5: One 30 mm Ø × 85 cm roman candle*

rial was only approximately 15%. The capped end of the pipe was undamaged because it housed the top, empty part of the roman candle. Both candles were totally consumed in these tests but no rates of propagation were obtained, as the VoD probes did not respond.

The last series of tests was with bulk stars. Considering the extent of fragmentation, the highest of all the trials, it was surprising not to obtain a response from the VoD probes. The high fragmentation was obviously due to high energetic material (star composition) mass per 10 cm length (250 g) but even at this loading density, less than twice the number of fragments were produced than

Figure 12. *Test 6: One 60 mm Ø × 100 cm roman candle*

those caused by the report shells which had an energetic material (flash composition) mass values per 10 cm length of only 40 g. No large distinction was noted in fragmentation caused by the cylindrical and spherical stars.

Figure 13. *Test 7: Loose cylindrical red stars 12 mm Ø × 19 mm (2.6 kg)*

Figure 14. *Test 8: Loose spherical 12 mm Ø red stars (2.8 kg)*

Figure 15. *Test 9: Loose spherical 12 mm Ø red stars (2.6 kg)*

Discussion

Possible Ignition/Reaction Propagation Mechanisms

There are essentially five probable reaction propagation mechanisms for fireworks confined in a steel pipe. In these tests, the initiation stimulus is either from an explosive booster or a quantity of black powder. This stimulus fractures part of the initiating end of the pipe and the first and possibly the second shell thereby igniting their contents either through shock, mechanical, and/or flame initiation. The following five possibilities then exist:

1. Failure: the contents of the shell(s) do not explode en masse, in which case the pipe will not be damaged. It is possible that other shells further along the column ignite (out of sequence ignition) and burn (see scenario 5), resulting in the jetting of flame or ejection of shells from the open end of the pipe as seen in the 3 m long pipe tests and possibly causing some damage to the pipe.

2. Detonation: this is typical of high explosives where a supersonic pressure wave (shock) travels through an energetic material. The pressure generated by the shock causes the rapid reaction of the materials (pyrotechnics) behind the shock front. This reaction generates its own pressure wave, which coalesces with the shock front, thereby maintaining it. Detonation would be expected to occur promptly after initiation of the stimulus.

3. Shock initiation: the contents of the shells explode and the adjacent shell is sufficiently shock sensitive that it too explodes. This process repeats along the linear array of shells in the pipe until all shells are consumed. Reference 8 suggests that conditions can exist for hot spot initiation through adiabatic compression of entrained air bubbles (voids) within the star composition. Another possibility is that of shear band heating. High pressures, as those from the detonation of the booster, acting on dislocations, imperfections or microcavities within the star composition, can generate shear slip planes with associated shear band heating.[15,16] Ignition points, either due to hot spots or shear banding, will then cause an increase in pressure through coalescence of the shocks from each site and can result in a transition to an explosion/detonation. This initiation-to-explosion process was identified as the cause of the catastrophic

Table 2 – Test results (Nominal 3" diameter, Schedule 40 steel pipes)

Test	No. of Capped Ends	Sample Type	Sample Mass /kg	Sample Size /mm	No.	Initiator	VoD Probe Type	Number of Fragments > 1 kg	Number of Fragments < 1 kg	Number of Fragments Total
1	1	SS	0.095	76	8	Booster	C	3	13	16
2	2	SS	0.095	76	8	EM+BP	C	1	5	6
3	1	RS	0.035	76	12	Booster	A	7	31	38
4	2	RS	0.035	76	12	EM+BP	A	5	43	48
5*	1	RC	0.15	30Nx850	1	Booster	C	4	3	7
6**	1	RC	0.43	60Nx1000	1	Booster	C	12	20	32
7	1	CBS	2.6	12Nx19	---	Booster	C	10	51	61
8	1	SBS	2.8	12 N	---	Booster	C	8	59	67
9	1	SBS	2.6	12 N	---	Booster	C	7	65	72

* – Nominal 2" diameter, Schedule 40 steel pipe, ** – 115 mm long pipe with one end sealed with a welded steel plate

EM – Electric Match, BP – Black powder, C – Copper VoD probe, A – Aluminum VoD probe, RS – Report shell, SS – Star shell, RC – Roman candle, SBS – Spherical bulk stars, CBS – Cylindrical bulk stars

propellant explosion that resulted in the death of 26 people on the USS Iowa in 1989.[17] The propellant exploded when it was being rammed into the gun. Interestingly, it was found that the propellant grains were only sensitive to this type of initiation when sheared across the extrusion axis. The CHAF[12] program included the gap sensitivity of flash composition. It was found that the flash composition could be initiated with pressures ranging from 350 to 400 MPa.

4. Deflagration-to-detonation transition (DDT): the contents of the fireworks articles behave more like a propellant confined in light casing, their reaction rate is related to the local pressure. The high pressures generated by the booster will cause ignition and structurally damage the stars. In so doing, the flame is exposed to very large surface areas of the star composition so that convective heating can quickly accelerate, thereby increasing the pressure and continued flame progression under the confinement provided by the pipe. As the local pressure increases due to the production of reaction products, the reaction rate increases until either the pipe bursts or the pressure reaches a critical value causing the reaction to transition to detonation. References 5, 8 and 9 support this argument. The voids found among the stars in the pipe can be envisaged as being similar to those among propellant grains of the same form. In Reference 18, Bernecker *et al*. indicate that the stages of a DDT mechanism for porous charges are; 1. Pre-ignition, 2. Ignition/conductive burning, 3. Convective burning, 4. Compressive ("Hot spot") burning, 5. Shock formation, 6. Compressive burning, 7. Detonation.

5. Normal function: the flame from the booster or black powder channels around the shells igniting them through their normal initiation train. In this scenario, the shells are expected to be ejected from the open end of the pipe in a sequential fashion. With the pipe closed at both ends, this mode of ignition could result in a mass explosion, as the burning rate of the delay fuses would increase under the pressure built-up. An individual shell could also function first, possibly causing the explosion of the remaining shells. Pipe rupture would be expected in either case. As with the previous work with the 3 m long pipes,[2] results indicate that the sequence of ignitions within a linear array of shells is not clear. Shell movement, flame channeling between shells and the pipe wall, and pipe break-up can result in scenarios where a second or third shell ahead of the linear array ignites before the first. High-speed video of tests in the CHAF[12] program, where shells were placed in plastic tubes, also indicate that flame channeling was occurring and shells were exploding out of sequence.

In reality the effects observed in the tests involve a combination of these mechanisms. For example, with the use of a booster, the first few shells could be overdriven and respond as if they were shock initiated. However, they may not release sufficient

energy for this type of reaction to continue the entire length of the pipe. On the other hand, the initial shock would likely cause some or all of the remaining shells to rupture exposing energetic material to flames. As a result, a large quantity of propellant may ignite nearly simultaneously resulting in rapid deflagration of the remaining material.

Without a means of directly recording the sequence of events inside a pipe, such as with flash X-ray or neutron radiography, the mechanism of reaction propagation inside the pipe must be interpreted indirectly. One possibility is through the number and size of the fragments produced. Typically, detonation inside a pipe results in small fragments with sharp, jagged, brittle-like edges, while an explosion/deflagration results in large fragments without the sharp edges. Thus, in the five scenarios described above, the fragments resulting from a failing reaction would include small fragments near the ignition end of the pipe, but the opposite end of the pipe would be essentially undamaged. Scenario 2 (detonation) would produce a large quantity of small fragments. Scenario 3 (shock initiation) would produce small fragments at the ignition end, larger longitudinal fragments in the middle and possible smaller fragments at the end if transition to detonation occurs. Scenario 4 (deflagration) would result in a few large fragments. Finally, Scenario 5 (normal function) could result in just small fragments at the initiating end if shells are ejected or small fragments at the initiating end and larger fragments from the remainder of the pipe if all the shells were to explode simultaneously.

These above explanations between the size of fragments and the reaction rate are not straightforward for fireworks articles but are complicated by the fact that the energetics in fireworks are rarely directly in contact with the pipe wall. They are decoupled, by air and blast attenuating material (packaging) between the energetics and the wall. The formation of fragments will depend on the distance separating the article from the pipe wall and packaging material.

A comparison of the number of fragments and the shape of the fragments produced in Tests 1 to 8 (Fig. 5, 6, 8, 9, 11–15) shows three different modes of response. The star shells and the small roman candle produced just a few very large fragments indicating a response similar to scenario 1 or 5 (Failure and Normal Function). As an example, in Test 2, only the centre of the cap was punched out. The pipe suffered no other damage. Again, this could only happen if flames from the original shell(s) explosions by-passed other shells to initiate shells along the column closer to the remaining capped end of the pipe. The explosion of a shell close to the cap would do damage to the cap and drive the remaining shells back toward the open end of the pipe, possibly initiating them in the process. The fact that pressure could be relieved from both ends would reduce the damage to the pipe. High-speed video of similar trials reported in Reference 2 indicated flame and shell ejection from both ends of the 3 m long pipes, and the pipes suffering little or no damage.

The larger roman candle and the report shells produced significantly more fragments, and if one disregards the brittle pipe caps, the fragments are primarily large longitudinal strips. The rate of propagation recorded for one of the report shell tests was six times higher than that recorded for a star shell test, 870 m s^{-1} *vs*. 150 m s^{-1}. Researchers in the CHAF[12] program found a similar trend between report shells and star shells recording propagation rates of 200 to 300 m s^{-1} for 55 mm report shells and 90 m s^{-1} (5 shells were consumed in 5 ms) for star shells. Based on the propagation rate and the size and number of fragments, the response of the larger roman candle and the report shells correspond most closely with the propagation mechanism proposed as Scenario 4 (Deflagration). The bulk stars on the other hand, produced many relatively small fragments more closely resembling Scenario 2 (Detonation), but the lack of the sharp jagged edges typical of those produced by a high explosive in contact with metal indicate that the reaction was not a detonation. Thus it is more likely that the propagation mechanism is that discussed in Scenario 3 (Shock initiation) or 4 (Deflagration initiation), and that the large number of fragments are the result from the large mass of energetic material in these tests, the large surface area exposed to flame, and the fact that the energetic material was coupled to the wall of the pipe.

The disparity in the number of fragments produced by the two roman candles demonstrates the effect of confinement on the reaction rate of energetic materials. The estimated void volume was 50%

for the smaller candle and 15% for the larger candle. In both tests a high explosive booster provided the initial stimulus. The larger candle produced 38 fragments while the smaller one produced only 7 fragments. An even more graphic example occurred in the Bray Park accident where a roman candle was placed in a relatively tight fitting steel mortar. Because of the tight fit the void volume was very low and thus there was a high level of confinement. The initial stimulus was provided by the normal ignition of the article, and in spite of this low energy ignition the roman candle is believed to have made the transition to detonation due to a very energetic composition.

The void volume, reactivity and the energy output of the compositions determine whether an ignition-to-explosion process will proceed to adjacent fireworks articles or composition. The maximum pressure of 5.6 MPa, measured by Takishita *et al*.[8] on the surface of a star shell exploding in free air, can be easily increased by providing confinement at the shell surface. This was noted in the CHAF[13] program where pressures for shells confined in steel pipes reached a maximum of 7.7 MPa. Pressures six to eight times higher must have been developed locally in the pipe tests reported herein to rupture the pipes which had burst pressures of 45 and 60 MPa for the nominal 2 and 3 inch schedule 40 steel pipes, respectively. Furthermore, steel is typically 20% stronger under dynamic loading than under static loading, as such it is possible that the pressure could have been 20% higher. Link[3] reports that pressure levels between 35-40 MPa would have been required to rupture the pipes (76 mm OD, 3.6 mm wall, 500 mm long) of the Bray Park accident. Calculation from reference 11 using static loads results in a 25 MPa pressure to rupture the pipe.

Conclusions

The intent of this test program was to determine the mechanism by which the reaction resulting from the ignition of a single fireworks article propagates to adjacent articles and results in a mass explosion. Because the testing of large masses of fireworks is prohibitively expensive, pipes where used simulate the confining effect of a large mass of fireworks.

It was found that the mechanism of propagation of a reaction inside the pipe was highly dependent on the packing configuration within the pipe. Parameters such as composition, packing density, ullage, area of contact between shells, strength and shock attenuating properties of packaging material, and confinement all play a substantial role in determine the rate of reaction. Because the design of a fireworks article is specific to each manufacturer there can be a great variation between the types of materials, the geometry and the composition in fireworks of the same type of article manufactured by different companies. This makes it very difficult to draw general conclusions from specific test results.

In this program, two or possibly three different levels of reaction violence were observed. The star shells and the small roman candle produced very few fragments, indicating that the reaction failed to propagate fully within the pipe while the pipe was still intact. This type of slow propagation was designated either a “Failure” (to propagate) or as propagation by “Normal Function”. The other tests resulted in many more fragments, indicating a more complete reaction of the articles in the pipe before the pipe ruptured. This faster reaction propagation was attributed to a process involving first the damaging of the articles and exposing of the energetic material (in the case of bulk stars the material was already exposed) and then a rapid deflagration of the energetic material. This process was designated as “Deflagration”. There was no evidence of a detonation in any of the tests. All pipes fragmented and the measured reaction rate ranged from 170 to 870 m s^{-1}. Based on fragmentation, the violence of reaction increased from the star shells, to the roman candles, to the report shells, and then to the bulk stars.

There are insufficient data here to prove that detonation is not possible in a mass of fireworks. Before this can be demonstrated further work would be required, particularly in the areas of the effect of confinement and packing density.

Acknowledgements

The author wishes to acknowledge the D. Wilson and R. Guilbeault for performing the CERL tests.

References

1 E. Contestabile, "Applying Explosives Testing Techniques to Obtain Insight into the Explosion Phenomenon of Piles of Fireworks", *Journal of Pyrotechnics*, Issue 14, 2001.

2 E. Contestabile, R. Guilbeault, D. Wilson and B. von Rosen, "Fireworks Shells Subjected to a Modified Height-To-Detonation Test", *Journal of Pyrotechnics*, Issue 20, 2004.

3 Link, R.A., G. Delbridge, and D. V. Ritzel, "Computational Modeling of a Steel Tube Subjected to Internal Fireworks Explosion", 7th International Symposium on Fireworks, Valencia, Spain, 2003.

4 G. Downs (editor), *Investigation Report - Bray Park Fireworks Tragedy*, Queensland Government, Department of Natural Resources and Mines, 2001

5 D. L. Kennedy, *Bray Park Investigation: Explosive and Propellant Behaviour (Revision 2)*, Orica Explosives, March 2002.

6 K. L. Kosanke, B. J. Kosanke, G. Downs and J. Harradine, "Roman Candle Accident: Comet Characteristics", *Fireworks News, Fireworks Business News*, Issue 225, 2002.

7 K. L. Kosanke and B. J. Kosanke, "Hypothesis Explaining Muzzle Breaks", Proceedings of the Second International Symposium on Fireworks, Vancouver, Canada, 1994.

8 K. L. Kosanke and B. J. Kosanke, "Hypotheses Regarding Star Shell Detonations", *Journal of Pyrotechnics*, Issue 14, 2001.

9 E. Andoh and N. Kubota, "Flame Penetration into Solid Propellant Holes", *Propellants and Explosives*, Vol. 6, 1981.

10 Y. Takishita, et al., "Experimental Studies on Spherical Burst - Aerial Shells", Proceedings of the 5th International Symposium on Fireworks, Naples, Italy, 2000.

11 Y. Takishita, et al., "Safety Characterization on Burst - Aerial Shells", Proceedings of the 5th International Symposium on Fireworks, Naples, Italy, 2000.

Thermodynamic and Spectroscopic Analysis of a Simple Lilac Flame Composition

B. T. Sturman[a] and K. L. Kosanke[b]

[a] 6 Corowa Court, Mount Waverley, Victoria 3149, Australia
[b] PyroLabs, Inc., Whitewater, CO, USA

Abstract: *A simple lilac flame composition consisting of 80% potassium nitrate and 20% shellac was investigated by emission spectroscopy and thermodynamic modeling. The flame from the burning composition had a reddish-pink core with a brighter pale lilac outer envelope. The core of the flame is presumably close to the equilibrium conditions predicted by thermodynamic modeling. The calculated equilibrium flame temperature is 1526 K; seven gases (CO, H_2O, N_2, CO_2, H_2, KOH, K) and one liquid (K_2CO_3) account for 99.7% of the molecules in the core of the flame. Of these, liquid potassium carbonate (mole fraction 9.6%) is expected to emit a continuous spectrum while atomic potassium (mole fraction 2.5%) imparts a red colour from the resonance doublet (766.491 and 769.897 nm), which is considerably broadened by self-absorption. The outer flame envelope is presumably a diffusion flame in which flammable gases from the core burn in entrained air. The maximum adiabatic temperature of such a flame was calculated as 1723 K; seven gases (N_2, CO_2, H_2O, KOH, K, Ar, $K_2O_2H_2$) account for 99.8% of the molecules in the outer flame envelope. The emission spectrum of atomic potassium superimposed on a continuous spectrum arising from the combining of atomic potassium with OH radicals to form gaseous KOH is responsible for the lilac colour of laboratory flames containing potassium and is the likely cause of the lilac colour of the outer regions of this pyrotechnic flame. The article includes a brief tutorial outline of some relevant aspects of the atomic spectroscopy of potassium.*

Keywords: *lilac flame colour, potassium nitrate, shellac, thermodynamic modeling, visible spectrum*

Introduction

Potassium nitrate, potassium perchlorate and potassium chlorate are very widely used in pyrotechnics as oxidizers. One of the advantages of potassium salts is that in most compositions they contribute little colour to the flame. It is well known, however, that potassium compounds emit visible light in laboratory flames[1] and it is to be expected that they would have some effect on the colour of pyrotechnic flames. Webster[2] studied the effect of potassium salts in magnesium-fueled flares and noted that visible emission from potassium may be part of the reason that high purity colours are not obtained from signal flares that incorporate a potassium salt as an oxidizer. Jennings-White[3] noted that mixtures of potassium perchlorate or potassium chlorate with shellac burn with white or off-white flames respectively, but a mixture of potassium nitrate and shellac burns with a lilac flame and has been used as a composition for a coloured lance. In 1980 Winokur[4] presented a comprehensive review of pyrotechnic mixtures for producing purple fire and listed a very simple composition for a violet lance: 80% potassium nitrate and 20% shellac. The source was an Italian work[5] published in 1845 (which the authors have not seen).

Recently Jennings-White[6] observed for the potassium nitrate and shellac composition that

"...close examination of the flame shows the red is in the interior of the flame, with lilac on the outside. I had some observers look at this from a greater distance with a strontium pink comparison. The consensus was that the flames were clearly similar pink, but the potassium (nitrate) one had a bluish fringe."

The authors decided to attempt to provide an explanation for these observations.

Background

1. Possible Sources of the Flame Colour

Flames emit light by several processes including:

1. Emission of continuous spectra by incandes-

cent solids or liquids
2. Emission of line spectra by atoms
3. Emission of band spectra by molecules
4. Emission of continuous spectra by chemiluminescent recombination reactions.

Band emission from molecules is an extremely important source of pyrotechnic colour,[7] but does not appear to be relevant in the case of the lilac flame being discussed.

It is well known that potassium salts impart a lilac colour to laboratory flames. The colour is attributable to the combination of the following:[1a,8,9a]

1. Atomic emission from potassium. Possible lines include the pair of resonance lines at the far red extreme of the visible spectrum (at 766.491 and 769.897 nm) and another pair at the violet end of the spectrum (at 404.414 and 404.721 nm).
2. Continuum emission, extending from about 570 to 340 nm[9a] and peaking in the violet around 400 nm,[1a] arising from the chemiluminescent combination of atomic potassium with hydroxyl (OH) radicals to form gaseous potassium hydroxide.[10]

2. Tutorial Outline of Relevant Aspects of the Atomic Spectroscopy of Potassium[1,11,12]

According to the quantum theory, electrons in an atom occupy regions of space around the atomic nucleus called *orbitals*. Different arrangements of electrons in orbitals correspond to different energy states of the atom. In atoms having more than one electron (such as the potassium atom) most of those electrons occupy very stable orbitals and do not participate in the electron rearrangements associated with chemical reactions or with interactions of atoms with light. Such changes involve rearrangements of only the outermost electrons, which are the most loosely bound. The potassium atom has only one electron that is not locked up in a highly stable inner orbital. That outer electron can occupy many different orbitals, but only the lowest energy one is stable. An electron in that orbital can stay there forever. If the atom gains energy, for example by colliding with another atom, the outer electron can move into another orbital that corresponds to a higher energy state, but it cannot remain there indefinitely. Most commonly, the atom will lose energy in the same way it gained it – in a collision with another atom. Even if the atom were completely isolated, however, quantum theory predicts that the electron will eventually return to the stable orbital. The time that any one atom remains in a higher energy state is unpredictable, but the average time (referring to a large number of such atoms) is known and is called the *radiative lifetime* of the energy state. When an atom spontaneously changes from a higher energy state to a lower one, the excess energy is emitted as light. The energy difference (ΔE) between the two states corresponds to the energy of one photon of the emitted light (E_p). The wavelength of the emitted light (λ) is related to the photon energy by the Planck equation,

$$\Delta E = E_p = h\nu = hc/\lambda \qquad (1)$$

where energy is expressed in joules (J), h is Planck's constant (6.626×10^{-34} J s), ν is the frequency (s^{-1}) of the emitted light, c is the velocity of light (2.998×10^8 m s^{-1}) and λ is the wavelength in metres. Similarly, the opposite process can take place, wherein the atom can absorb a light photon having an energy E_p that corresponds to the difference ΔE between two energy states of the outermost electron; in this process the electron temporarily moves from a lower energy state to a higher one.

Figure 1 shows some of the energy states of the potassium atom, together with some of the energy transitions giving rise to the emission lines discussed in this article. Not all lines are labeled, and not all possible lines are shown. Energy states above the lowest one are called *excited states* and atoms in such states are said to be *excited*. The lowest energy state is called the *ground state*. Emission lines that result from transitions from excited states to the ground state are called *resonance lines*. The four resonance lines indicated in Figure 1 are the most intense potassium emission lines in flames.[1a]

Most potassium atoms in a flame will be in the ground state. Consequently, whenever potassium atoms are present in a flame, photons having energies corresponding to potassium resonance lines can be absorbed when they pass through the flame.

In Figure 1, the columns labeled 'S, P, D' indicate families of atomic energy states that differ from each other in the shape of the electronic orbitals.

According to quantum selection rules, electrons can participate in transitions where they move between S and P states, and between P and D states, but not between S and D states or between states having the same label (such as between S and S states). By convention, the superscript before the letter is one more than the number of unpaired electrons in an atom in that energy state. A potassium atom has one unpaired electron, so the superscript is 2. It is read as "doublet", for the historical reason that spectral lines associated with atoms having one unpaired electron often occur in pairs that are called "doublets". The subscript after the letter indicates the *total angular momentum* of the energy state, which depends on whether the angular momentum associated with the spin of the unpaired electron adds to, or subtracts from, the angular momentum associated with the motion of the electron around the nucleus of the atom (the electron's *orbital angular momentum*). The electronic energy states in each family are labeled with lower case letters indicating the shape of the orbital preceded with a number (the *principal quantum number*), which increases with increasing energy. In some cases, there are pairs of electronic energy states (e.g. $4p_{1/2}$, $4p_{3/2}$) that have the same principal quantum number and are labeled with the same letter, but have different angular momenta as a result of electron spin. The energy differences between the atomic energy states (e.g. $4^2P_{1/2}$, $4^2P_{3/2}$) are very small in the potassium atom. In Figure 1 these energy differences have been exaggerated for clarity – if shown to scale the difference would be lost in the thickness of the line. Electronic transitions from these energy states result in the characteristic "doublets" in the potassium spectrum (e.g. 766.491 and 769.897 nm). The energy state diagram, Figure 1, is based on data from the NIST *Handbook of Basic Atomic Spectroscopic Data*.[8]

The measurement of the intensity of resonance lines emitted from laboratory flames has long been used for the determination of potassium concentration in analytical samples by flame emission spectrometry.[9] The success of this analytical method requires that the number of potassium atoms

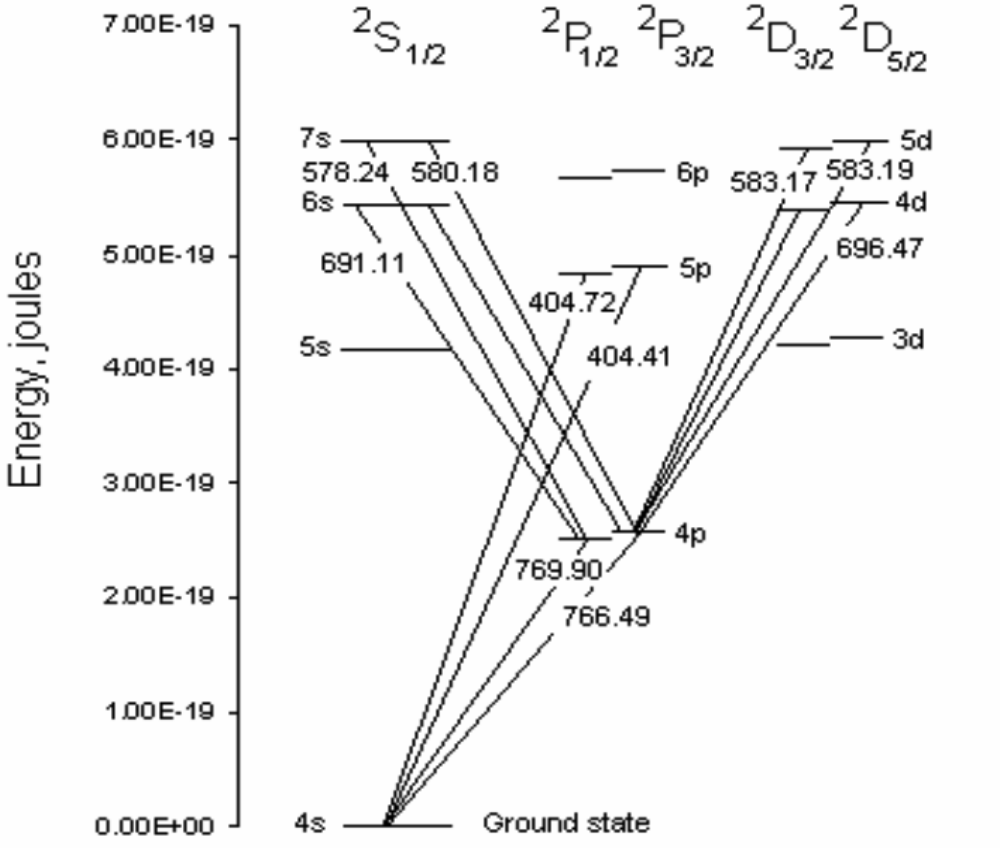

Figure 1. *A simplified diagram of electronic states (energy levels) in the potassium atom.*

in the path through the flame of the light being measured is so low that a photon emitted by one atom will have a high probability of escaping from the flame rather than being re-absorbed by another atom. Such a flame is described as being *optically thin*.

The gases in a flame can often be considered as being in *local thermodynamic equilibrium*. This means, amongst other things, that the number of potassium atoms in a particular excited state (n) is related to the total number of free potassium atoms (n_t) by the *Boltzmann equation*

$$n = n_t \frac{g}{Z} e^{-\Delta E / kT} \qquad (2)$$

where g is the *statistical weight* of the excited state, Z is the *partition function* of the potassium atom (2 at the temperatures of interest), e is the base of natural logarithms (2.718…), ΔE is the *excitation energy* (the energy difference in joules between the excited state and the ground state), k is *Boltzmann's constant* (1.38×10^{-23} J atom^{-1} K^{-1}) and T is the absolute temperature (K). If the number of excited atoms is consistent with the Boltzmann equation, the excitation process is described as *thermal* or *collisional* excitation.

In some flames, particularly in relatively cool flames or in the primary reaction zone of normal flames, the number of atoms in a particular high energy state sometimes greatly exceeds that predicted by the Boltzmann equation. In these circumstances the formation of excited atoms is attributed to *chemiluminescence*.[13,14] Several different chemiluminescent processes have been described.[13,14] In all of them a population of excited atoms or molecules arises as a result of energy released in the formation of chemical bonds being transferred directly to electrons in an atom or molecule, causing the most loosely-bound electron in that atom or molecule to move to a higher energy state.

Irrespective of the mechanism that produces the excited species, the intensity of emission (I), expressed as photons per second, is simply

$$I = n / t \qquad (3)$$

where n is the average number of excited atoms and t is the radiative lifetime. (To convert from photons per second to joules per second, one multiplies by the photon energy E_p; see equation 1.)

The maximum temperature calculated for the air–propane flame by thermodynamic modeling is 2275 K. The expected thermally excited emissions from potassium atoms at this temperature are shown in Table 1. The intensity of the 766.49 nm line has been arbitrarily set to 100,000 and the intensities of the other lines have been normalized to this value.

As shown in Table 1 the two deep red lines are very intense and the two violet lines are much less so. Both pairs of lines lie in regions of the spectrum to which the human eye is not particularly sensitive, but they have been known for a long time and are shown in some of the very early drawings of flame spectra.[15] Kirchhoff and Bunsen[16] referred to the pair of deep red lines as "Ka α" and the pair of violet lines as "Ka β". (The symbol "Ka" indicated potassium.) The prism spectroscope used by these researchers was evidently unable to resolve each pair of lines into their two components. Kirchhoff and Bunsen[16] reported another very weak red line in the potassium flame. This line coincided with Fraunhofer line B. It was visible from a "highly intense flame" and described as "not very characteristic". It can be identified with an unresolved group of five lines (696.47, 694.42, 693.88, 693.63, and 691.11 nm), arising from transitions

Table 1. *Spectroscopic Parameters of Potassium Resonance Lines and their Relative Intensities.*

Wavelength (nm)	Excitation Energy (J)	Statistical Weight of Excited State	Lifetime of Excited State (s)	Normalized Relative Intensity[(a)]
404.41	4.91×10^{-19}	4	1.16×10^{-6}	2.7
404.72	4.91×10^{-19}	2	1.07×10^{-6}	1.5
766.49	2.59×10^{-19}	4	2.67×10^{-8}	100000

[(a)] Intensities were calculated in joules per second per unit atom concentration, assuming thermal excitation at 2275 K, and then normalized to 100,000.

between excited states.[8] The coincidence of these red potassium lines with Fraunhofer line B is of no significance; Fraunhofer line B arises from absorption of sunlight by oxygen in the air.[17] Two of the lines from this group of potassium lines are identified in Figure 1. These red lines are of comparable intensity to the other potassium lines at the high temperatures prevailing in the electric arc,[8] but would be very weak in flames.

When Shimizu[18a] described the flame spectrum of potassium he did not mention the deep red resonance lines and described the violet lines as "intense". He wrote "The lines are very strong, but they are in the ultraviolet, at the outer edge of the eye's visibility, and have no color influence". Shimizu's assessment of the intensity of the violet lines is certainly valid, given that he was comparing them to some faint yellow and green potassium lines arising from transitions between excited states that would be very sparsely populated at flame temperatures. Compared to the deep red lines, however, the violet lines are extremely weak. The literature suggests, however, that in some flames the violet lines are not always as weak as would be expected from calculations that assume thermal excitation. For example, referring to the use of these lines in flame photometry, Dean[9a] states that "the sensitivity of the violet doublet is one tenth the sensitivity of the red doublet". This is very different from the ratio of 2.8×10^{-5} calculated in Table 1. The issue is clouded by the fact that the detectors used in flame photometry vary greatly in sensitivity across the wavelength range,[9b] but this variation is not sufficient to account for the difference in the ratios of the calculated and reported intensities of the two doublets. The implication is that the violet doublet can be excited by chemiluminescence in some laboratory flames. An example is given by Alkemade,[19] but the enhancement over thermal excitation was not large. Whatever the excitation mechanism, the intensity of the violet doublet is always very much less than that of the red doublet. If the colour of the potassium flame were attributable solely to a combination of the deep red and violet lines, the flame would be red. Clearly there is another contributor to the colour of the potassium flame that changes the colour from red to lilac.

It has long been known that the distinctive lilac colour of the potassium flame is easily masked by the yellow light from sodium and that this can be overcome by viewing the flame through blue cobalt glass. This glass transmits almost no light between about 500 and 700 nm but transmits quite efficiently at each of the extreme ends of the visible spectrum. The potassium flame, when seen through blue cobalt glass, is not lilac but purplish-red; when seen through green glass it is bluish-green.[20] Green glass transmits blue, green and yellow light but absorbs light at each of the ends of the visible spectrum. Accordingly the lilac colour of the potassium flame must result from a combination of the red light expected from the potassium resonance lines and light that is largely absorbed by blue cobalt glass but largely transmitted by green glass. That light is attributable to a continuum in the flame spectrum of potassium. This continuum has been known for a long time. It was described by Kirchhoff and Bunsen,[16] who wrote "In the flame the volatile potassium compounds give a very long continuous spectrum with only two characteristic lines…", and was subsequently studied by other spectroscopists.[21,22a,10] It was once thought to originate from the recombination of electrons and potassium ions,[22a] but in 1958 James and Sugden[10] demonstrated that it was the result of the combination of hydroxyl radicals and potassium atoms to form gaseous potassium hydroxide. Shimizu[18a] mentioned this continuum, attributing it to the potassium atom and noting that "it does tend to whiten the flame and interfere with other flame colors".

The pale lilac colour of laboratory flames that are coloured by a vaporized potassium salt can thus be attributed to a combination of the deep red resonance lines from atomic potassium with the potassium hydroxide recombination continuum. The violet potassium resonance lines contribute very little to the colour, being much less intense than the red lines and the continuum. The fact that the continuum is a substantial contributor to the colour accounts for the pale, washed-out appearance of the lilac flame.

The observation of a lilac colour in a pyrotechnic flame containing potassium salts is consistent with observations of laboratory flames into which potassium has been introduced, and provides the explanation of the lilac colour of the outer regions of the flame from the potassium nitrate–shellac composition. The pink colour of the core, however,

was not so readily explained.

The discussion so far implies that each spectral line consists of photons having exactly the same energy, corresponding to exactly the difference between two atomic energy levels. In reality, the photons in each line have a range of energies and the emission "lines" might be better described as "peaks". While each line (peak) has its maximum at the photon energy (or wavelength) predicted from the energy of the corresponding atomic transition, it tails away on either side. There are several factors that contribute to this *line broadening*.[12a] In flames, the dominant effect operating at low concentrations of emitting/absorbing atoms is the collision of excited atoms with other atoms and molecules.[12a] At higher atom concentrations emission lines can become extremely broad. When there is a relatively high concentration of emitting/absorbing atoms in the source, a photon emitted by one excited atom is very likely to be absorbed by another ground state atom. The chance of a photon being re-absorbed depends on its energy; a photon having an energy corresponding to the maximum of the emission line will have a much greater chance of being absorbed than a photon having energy that is slightly greater, or slightly less, than the maximum. The resulting excited state atom will then either transfer its extra energy to another atom or molecule in a collision or re-emit a photon. If the re-emission occurs after a collision, it is very likely that the energy of the emitted photon will be slightly different from that of the photon that was absorbed. Accordingly that emitted photon is likely not to correspond to the energy corresponding to the maximum of the emission line (peak). At these higher atom concentrations, this process occurs many times before a photon finally escapes from the flame. The result of these many emissions and re-absorptions before photons eventually manage to escape from the flame is greatly to broaden the energy distribution of those emitted photons. Such a flame is described as *optically thick*. The characteristics of spectral lines from atoms in optically thick sources are well documented in the literature.[11a, 12a, 23]

The emission of light from an optically thick source can be thought of as intermediate between what happens in optically thin sources and in a *black body*. A black body is an object in which matter (atoms) and electromagnetic radiation (including light) are in thermal equilibrium. The rate of emission of radiation by atoms exactly equals the rate of absorption by other atoms. For such perfect equilibrium, all emitted radiation is reabsorbed and no light leaves the object, which is why the object ("body") is called "black". An ideal black body can be approximated by the inside of a hollow object, so well insulated that there is no exchange of energy between the object and the outside world. The only way the spectrum of such an object can be viewed is to make a tiny hole in it, a hole so small that the effect on the equilibrium between atoms and radiation is not significantly disturbed by the slight loss of radiation through the hole. The spectrum of such an object is continuous, and the relationship between light intensity and wavelength at any given temperature can be calculated theoretically from the fact that radiation and matter are in thermal equilibrium.[11b, 12b]

Recall that for an optically thin source a photon emitted by an atom in the source has a high probability of leaving the source without ever interacting with another atom. In contrast, a photon emitted by an atom in an optically thick source is highly likely to be absorbed by another atom as just described, but photons do eventually escape. Photons having energies corresponding to the theoretical maximum of the emission line are more likely to be absorbed than photons having energies away from the maximum. Eventually, if the concentration of emitting and absorbing atoms becomes sufficiently high, the rate of absorption at the peak's maximum approaches the rate of emission. In other words, the photons having energy corresponding to the line's maximum are close to being in equilibrium with the atoms. For photons of that energy, the source then behaves like a black body. The intensity of the emitted light at the line's maximum approaches the intensity of light of that same wavelength that would be predicted for a black body at the same temperature as the source. Accordingly, at a given temperature, as the concentration of atoms of the emitting element increases, the intensity at the centre of the emission line only increases until it reaches the intensity that would be emitted at that wavelength by a black body at the same temperature. Thereafter, it is only the intensity of light having wavelengths on either side of the maximum that continues to increase with increasing concentration of emitting

atoms. The result is that as the concentration of emitting atoms increases, the radiation from the emission line is spread over an increasingly wide region of the spectrum on either side of the line's maximum. This line broadening process is described as *self-absorption*.

Douda[24–28] has shown that the light from sodium nitrate–magnesium flares arises predominantly from sodium resonance lines that have been broadened by self-absorption. Such a substantially broadened line may be referred to as a *resonance line continuum*. Douda also demonstrated that in these flares, the light emitted by sodium atoms in the core of the flame is re-absorbed by sodium atoms in the cooler outer regions of the flame, resulting in a distinct dip in the centre of the broadened emission line where there would otherwise be a maximum. This is called *self-reversal* of the emission line. Of greater relevance to the discussion of lilac flame is the observation by Douda *et al.*[25] of broadened self-reversed potassium resonance lines in the spectra of potassium nitrate–magnesium flares.

The fact that self-absorption and self-reversal of sodium lines can transform the familiar amber-yellow sodium flame into the yellowish-white of the sodium nitrate–magnesium flare, coupled with the observation by Douda and his colleagues[25] of similar processes in potassium nitrate–magnesium flares, led the authors to consider whether the same mechanisms, applying to the deep red potassium lines, could account for the pink core of the potassium nitrate–shellac flame.

Experimental

The spectroscopic measurements were made using three slightly different configurations. However, each used an Ocean Optics CHEM-2000 spectrometer. The first configuration was one in which solutions are aspirated into a propane–air flame. This apparatus is sketched in Figure 2 and was previously described more completely.[29] The other two configurations were used to record spectra from burning pellets of pyrotechnic composition and tiny specially made tubes of lance composition. In these latter two configurations, the flame burner in Figure 2 is replaced with a holder for 6 mm (1/4 inch) diameter test pellets or 6 mm (1/4 inch) diameter lance. In one of these configurations, a fish-eye lens was used so as to fully integrate the light emitted from the entire area of the flame. In the other configuration the lens was removed and a collimator used to limit light collection to a spot no more than approximately 5 mm in diameter. In this way, and by carefully positioning the flame source and by collecting data for only a fraction of a second, light could be collected from a relatively small portion of the flickering flame.

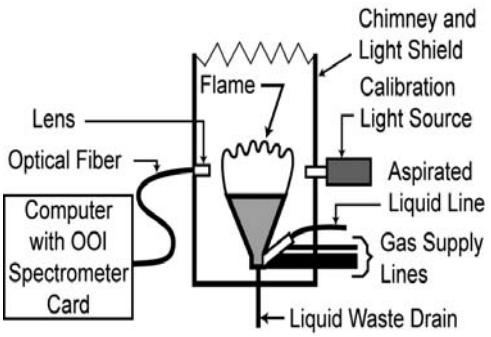

Figure 2. *Illustration of the apparatus for taking spectral data from solutions of interest.*

The potassium nitrate (KNO_3) used in this study (purchased from Service Chemical, USA) and the shellac (purchased from William Zinzer & Co., USA) were each of a grade normally used in the fireworks industry. The raw flame spectrum of potassium nitrate was obtained using the test configuration shown in Figure 2 with a 0.1 molar solution in distilled water. The spectrum was first corrected by subtracting a background flame spectrum (distilled water only) taken under the same measurement conditions as used for the potassium nitrate test solution. Then the background corrected spectrum was corrected for the wavelength dependent response function of the detector.[29] The final result is the potassium nitrate spectrum shown in Figure 3. For comparison purposes, the flame spectrum of a 0.1 M solution of analytical reagent grade potassium nitrate (Mallinckrodt, USA) is presented in Figure 4.

The 80% KNO_3 and 20% shellac lilac test composition was prepared by first thoroughly mixing the two components using a mortar and pestle. Then the composition was divided in two portions; one for use in making bound test pellets and the other for loading into the lance tubes. To make the bound

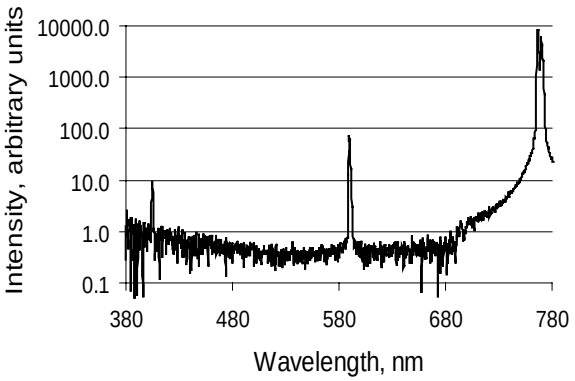

Figure 3. *Spectrum of a solution of technical grade potassium nitrate aspirated into an air–propane flame, corrected for instrument background and detector response.*

pellets, sufficient denatured ethanol was added to make a pliable mass. This dampened composition was then compacted into a series of 6 mm (0.25 inch) diameter and approximately 20 mm (0.8 inch) long test pellets. The test pellets were first allowed to air dry at approximately 20 ºC (68 ºF) for a day and were then raised to approximately 50 ºC (122 ºF) for approximately 1 hour. Figure 5 is a photograph of a burning test pellet, in which the brighter and lighter outer flame envelope is readily apparent.

The raw flame spectra of the test pellets were obtained by burning them in a darkened area using the test configuration described above using the fish-eye light collecting lens, which integrated the light from the entire flame. The raw spectra

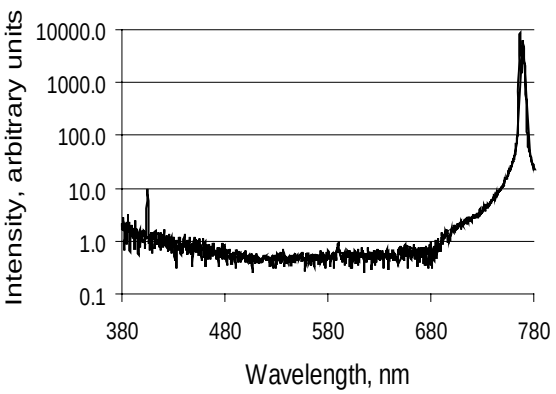

Figure 4. *Spectrum of a solution of analytical reagent grade potassium nitrate aspirated into an air–propane flame, corrected for instrument background and detector response.*

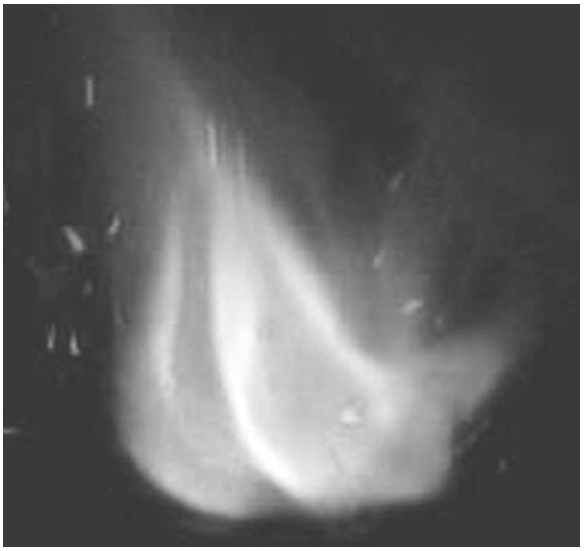

Figure 5. *A photograph of a burning pellet of the lilac composition showing the brighter and lighter outer flame envelope.*

were corrected for instrument background (dark current) and then corrected for the instrument response function.[29] The final result is the spectrum shown in Figure 6.

Using the un-dampened portion of the lilac flame composition, a series of lances was prepared. The lance tubes were specially made using just two wraps of thin tissue paper. This was done so as to limit the interfering effect of the burning lance tube. The lance tubes were 6 mm (1/4 inch) in diameter and approximately 25 mm (1 inch) long. The composition was carefully loaded using the traditional rod and funnel method. The spectra of the lances were recorded using the instrument

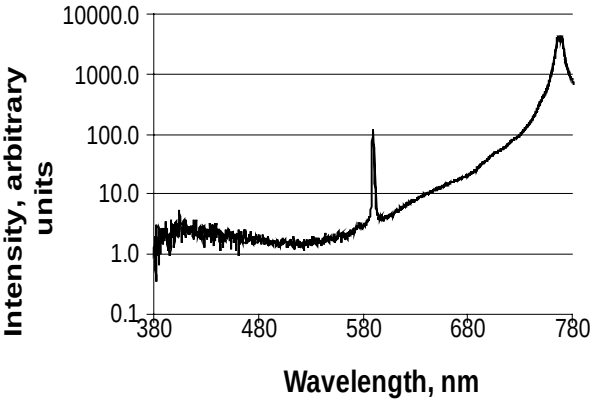

Figure 6. *Spectrum of the flame of a burning pellet of 80% potassium nitrate and 20% shellac mixture, corrected for instrument background and detector response.*

configuration described above using the collimator. By properly positioning the burning lance in front of the collimator, it was possible to collect spectra somewhat selectively concentrating on the emissions from either the inner or outer portions of the flame envelope. Lances were used for these measurements because they produced a more steady flame, which facilitated the collection of spectra from the two regions of interest within the flame. Nonetheless, the movement of the flame was still sufficient to require that the data collection intervals be kept to only 0.1 second to aid in limiting the light acquired from other portions of the flame. (The burning pellets of composition flickered greatly, which facilitated the taking of a photograph more clearly showing the difference between the inner and outer flame envelope, see Figure 5.)

The spectra collected from the inner and outer parts of the flame, corrected as described above, were smoothed with a 9-point moving average to remove some of the "noise" resulting from the low light intensity in this mode of measurement. Finally the intensity data points in each spectrum were normalized to the maximum value in that spectrum. The use of normalized intensities allows the different line widths in the spectra to be seen more clearly. Furthermore, the colour of the flame depends on the relative intensity of the various spectral features, not their absolute intensity.

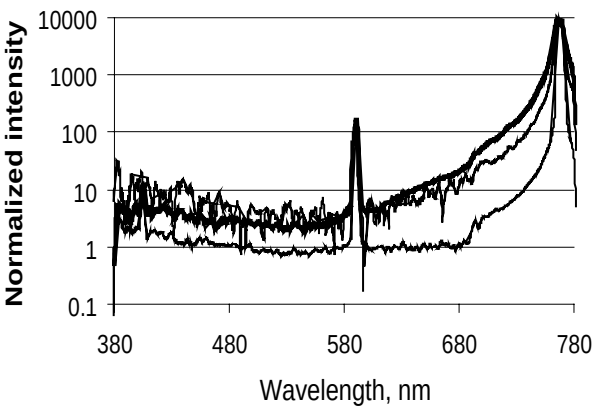

Figure 7. *Spectra of the inner and outer parts of the flame of a burning lance made with 80% KNO_3 and 20% shellac. Bold trace: Inner part of the flame. Upper non-bold trace: Outer part of the flame. Lower non-bold trace: technical grade KNO_3 solution aspirated into the air–propane flame.*

Results are presented in Figure 7. The data used to generate the spectrum of technical grade KNO_3 in the air–propane flame shown in Figure 3 were reprocessed in the same way and the resulting spectrum is included in Figure 7 for comparison.

Additional spectra were derived from each of the test technical grade potassium nitrate and test composition spectra produced as described above. The purpose was an attempt to quantify the effect of the sodium impurities present in the raw chemical ingredients. This was accomplished by simply stripping out the sodium peaks from the two corrected test spectra. Finally, all spectra were converted to their CIE colour values using a program provided by Will Meyerriecks.[30] These results are presented and discussed below.

Results and Discussion

1. Flame Spectra

The visible spectrum of the technical grade KNO_3 solution aspirated into the air–propane flame is presented as Figure 3. Note that the intensity scale is logarithmic. The most prominent feature is the partially resolved pair of deep red potassium resonance lines. The yellow line (actually an unresolved pair of lines at 589.0 nm and 589.6 nm) from sodium impurities is also obvious. The (unresolved) pair of violet potassium resonance lines can be discerned, but, as expected, its intensity is very low. The continuous spectrum is evident by the offset of the spectrum from the 0.1 unit intensity line in Figure 3. Figure 4 presents the corresponding spectrum of analytical reagent grade KNO_3 solution aspirated into the air–propane flame. The obvious difference between this spectrum and that of the technical grade material is the very much lower intensity of the yellow sodium line.

Figure 6 presents the visible spectrum of the flame from the burning of a bound pellet of the 80% KNO_3–20% shellac mixture. The spatial resolution of the apparatus used as configured and the dynamic flickering of the flame did not allow the separation of the spectrum of the reddish-pink core from that of the lilac outer regions of the flame. The pair of deep red potassium resonance lines is again the dominant feature of the spectrum The extent to which these lines have broadened and extend well into the shorter wavelengths of the red

region of the spectrum to which the eye is more sensitive, can be seen by comparing Figure 6 with Figures 3 and 4. This broadening is attributed to self-absorption caused by a high concentration of potassium atoms in the flame. The sodium line is evident, as expected. The unresolved pair of weak violet potassium lines cannot be discerned above the background noise. It is clear from Figure 6 that the continuum is greatly increased in intensity compared to that in Figure 3. This is attributable to two sources: (a) potassium– hydroxyl recombination, as expected for a flame containing potassium, hydrogen and oxygen, and (b) possibly from particles of solid or liquid suspended in the flame.

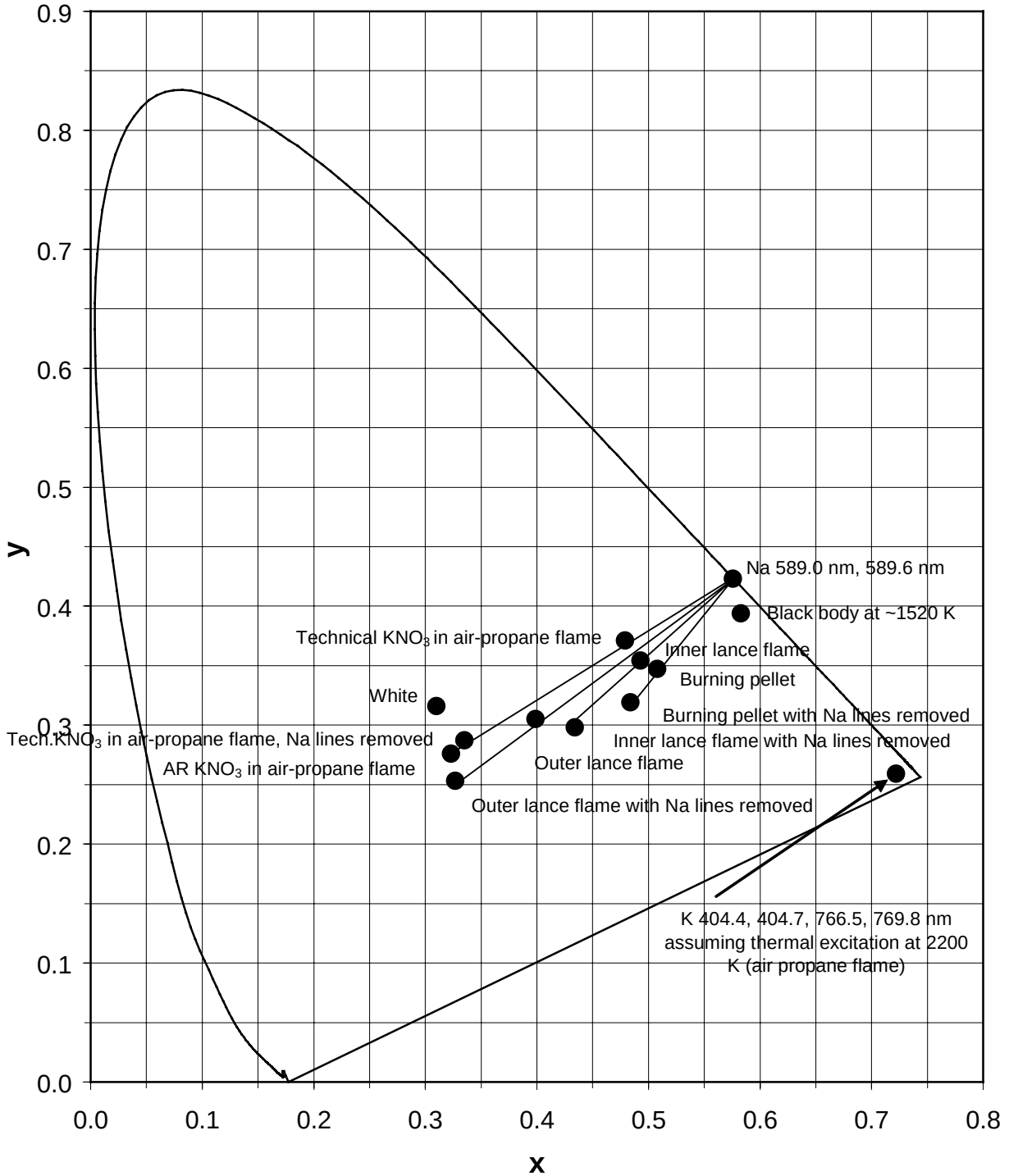

Figure 8. *CIE chromaticity diagram showing the positions of the various flame colours, plotted from the coordinates in Table 2.*

Table 2. *CIE x and y Coordinates Calculated From the Spectra, and their Corresponding Colours.*

Spectrum or Spectral Feature	CIE *x*	CIE *y*	Colour
Analytical reagent KNO_3 in air–propane flame	0.323	0.276	Pale reddish-purple
Technical KNO_3 in air–propane flame	0.479	0.371	Pink
Technical KNO_3 in air–propane flame, Na resonance lines removed	0.335	0.287	Pale reddish-purple
Burning pellet of 80% KNO_3, 20% shellac	0.507	0.348	Pink
Burning pellet of 80% KNO_3, 20% shellac, Na resonance lines removed	0.484	0.319	Pink
Inner core of lilac lance flame	0.493	0.354	Orange-pink
Inner core of lilac lance flame, Na resonance lines removed	0.434	0.298	Pink
Outer envelope of lilac lance flame	0.399	0.305	Pink
Outer envelope of lilac lance flame, Na resonance lines removed	0.327	0.253	Pale reddish-purple
Potassium resonance lines from air–propane flame (calculated relative intensities, assuming thermal excitation at 2200 K)	0.722	0.259	Red
Sodium resonance lines	0.569	0.430	Yellowish-orange
Black body at ~1520 K[12b]	0.583	0.394	Orange

There was no attempt to calculate the contribution of the latter, but there would presumably be a considerable effect from the rather high concentration of molten potassium carbonate in the flame. The spectrum of a black body at ~1500 K would peak in the infrared, with sufficient "tailing" into the visible to make the body appear yellowish-orange. Flame particles are likely to be very small, with the result that the "black body" spectrum would be shifted to shorter wavelengths, making the emitted light whiter.[31]

Figure 7 presents spectra attempting to concentrate on the inner and outer parts of the lance flame, collected using the collimated light collection configuration. Because of the limited special resolution and the motion of the flame, it is likely that spectra of the edge of the flame included at least part of that from the inner flame. Further, the inner part of the flame had to be viewed through the outer part. Thus it must be expected that the both spectra are, to a significant extent, mixtures of the emissions from both the inner and outer regions of the flame, Nonetheless, there are distinct differences in the spectra from the inner and outer parts of the flame. (As expected, most of the spectra collected were of intermediate character to the two presented in Figure 7.)

The spectrum of the inner part of the flame is similar to that of the burning pellet (Figure 6). The most notable difference is that the unresolved violet resonance line pair is clearly visible, but is still of low intensity. The spectrum of the outer part of the flame is different is several ways: the pair of red potassium lines is less broad, the continuum in the shorter wavelength region is relatively more intense and the pair of violet lines is not discernible above the background noise. The spectrum of potassium nitrate in the air–propane flame is different from either of the lance flame spectra, with the pair of red lines being less broad, the continuum much less intense and the unresolved violet lines distinctly more intense. The wavelength resolution of the spectrometer used in this work was not sufficient to show whether or not self-reversal of the potassium resonance lines was present.

2. CIE Chromaticity Diagram

Table 2 shows the CIE *x* and *y* coordinates (using the 1931 2º Chromaticity Diagram) of some relevant spectra and spectral features. Some of these colour coordinates are plotted on a CIE chromaticity diagram in Figure 8. The colours indicated on the diagram for the KNO_3 in the propane gas flame and for the lilac flame composition are consistent with observations, bearing in mind that the CIE descriptions cover quite a broad range of perceived hues. The CIE results and visual observations both find the inner part of the flame to be "redder" than the outer part. The results for the colours expected when the sodium lines were removed from the experimental spectra indicate that there would be a definite improvement in the colour of the lilac flame if there were less sodium present.

3. Thermodynamic Modeling

It seemed obvious that the colour of the flame from the potassium nitrate–shellac composition was attributable to potassium, but no data for the composition and temperature of the flame were available to support this. Thermodynamic modeling was used to obtain an indication of the potassium concentration in the flame and the flame temperature. It was assumed that at the core of the flame the temperature and composition were close to those expected at thermodynamic equilibrium. Moving away from the core, the effects of entrained air would presumably be increasingly significant.

Thermodynamic modeling was done using the NASA-CEA program.[32,33] The combustion was modeled at a pressure of 1 bar. The required inputs were the quantities of the reactants (relative weight), their chemical composition and their enthalpies of formation. The enthalpy of formation and chemical composition of potassium nitrate are included in the database that forms part of the NASA-CEA program. The data for shellac were taken from Meyerriecks.[34] The empirical formula was $C_6H_{9.5}O_{1.6}$ and the enthalpy of formation was −440 kilojoules per gram formula weight. As noted by Meyerriecks[34] this enthalpy value is subject to considerable uncertainty; the results of the modeling must therefore be regarded as semi-quantitative. Furthermore, no account of energy loss from the flame by radiation was considered. Despite these limitations it was thought that thermodynamic modeling would provide a useful basis for an explanation of the spectrum of the flame from the burning composition.

The output of the program included the equilibrium temperature and the mole fractions of the combustion products. The number of significant figures in the values reported in this paper does not indicate the uncertainty in the values, as no at-

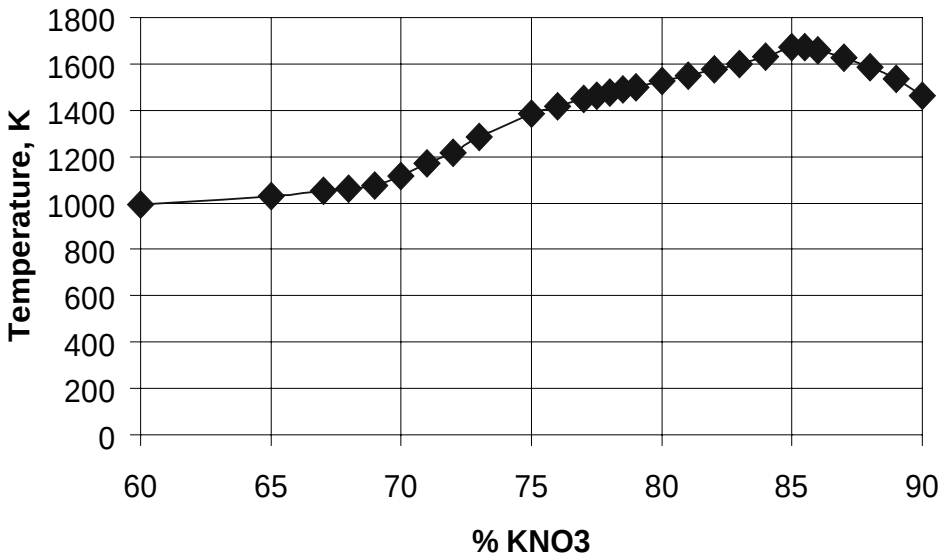

Figure 9. *Equilibrium flame temperatures for the combustion of binary mixtures of potassium nitrate and shellac.*

tempt was made to estimate the uncertainties. The aim was only to produce a plausible, consistent account of the flame colour. This certainly required an indication of the flame temperature and composition, but a fully detailed quantitative analysis was not necessary and probably not possible. The program took ionization effects into account but these turned out to be insignificant. No species are included in the output unless they are present at mole fractions greater than 5×10^{-6},[29] and no ions were reported in the output of the program.

A plot of equilibrium adiabatic temperature predicted for the combustion of a series binary mixtures of potassium nitrate and shellac is shown in Figure 9. For the 80% KNO_3 and 20% shellac mixture, the predicted flame temperature is 1526 K and the maximum temperature is predicted to be reached by a mixture of 85% KNO_3 and 15% shellac. The equilibrium composition of the flame gases from these binary mixtures, each at their predicted flame temperature, is shown in Figure 10. The 80% KNO_3 and 20% shellac mixture is close to that producing the greatest concentration of atomic potassium in the flame. As indicated in Figure 10, the maximum atomic potassium concentration occurs at about 83% KNO_3.

Figure 11 shows the major components of the flame gases for the 80% KNO_3 and 20% shellac mixture. Of these, carbon monoxide (CO), hyrdrogen (H_2) and potassium (K) are expected to burn in the air, forming a diffusion flame around the flame core. Modeling such a flame is difficult because there are two competing factors operating: (a) the reaction of combustible gases with air, which tends to heat the flame, and (b) the cooling of the flame gases by the loss of heat into the surrounding cold air.

The maximum possible temperature of the diffu-

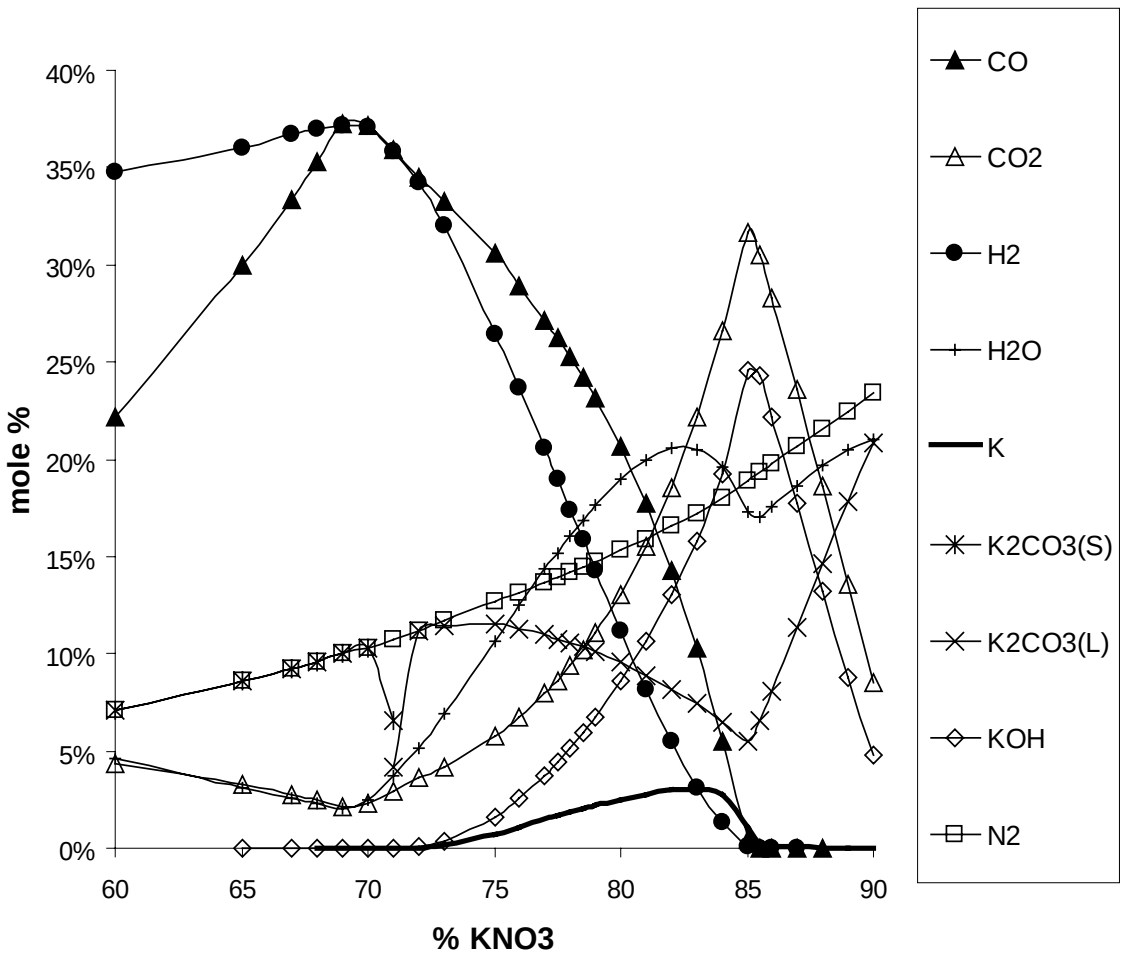

Figure 10. *Equilibrium flame compositions for binary mixtures of potassium nitrate and shellac. Trace components (<1%) have been deleted for clarity.*

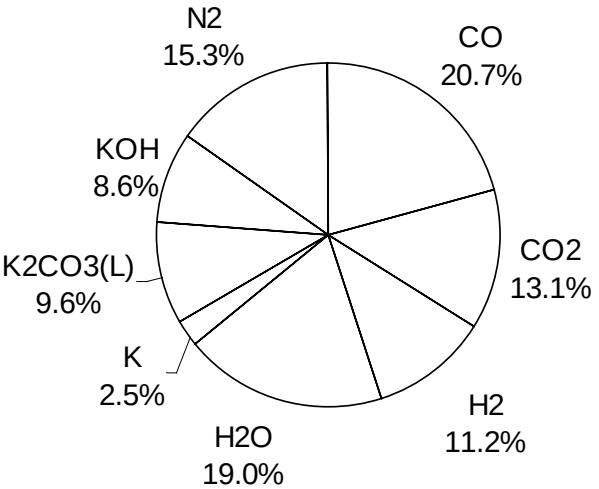

Figure 11. *Equilibrium composition of the flame of 80% KNO_3 and 20% shellac mixture (1526 K).*

sion flame was calculated by modeling the combustion of the 80% KNO_3 and 20% shellac mixture in varying amounts of air. The maximum temperature (1723 K) occurred with a mixture of 50.66% KNO_3, 12.66% shellac and 36.68% air by mass and produced the products shown in Figure 12. As shown in Figure 12 there is still a significant concentration of atomic potassium in the diffusion flame, but the number of potassium atoms per unit volume (2.2×10^{16} atoms cm^{-3}) is only approximately 18% of that calculated to be present in the flame core (1.2×10^{17} atoms cm^{-3}). Concentrations of the various species in atoms or

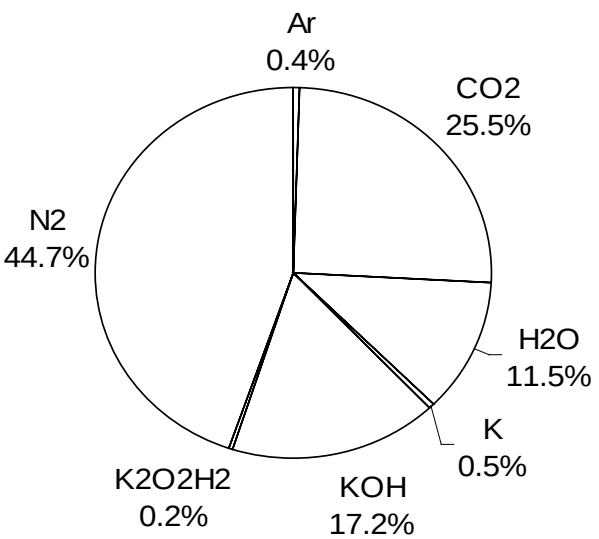

Figure 12. *Equilibrium composition of the flame of 80% KNO_3 and 20% shellac mixture with sufficient entrained air to reach the maximum adiabatic flame temperature (1723 K).*

molecules per cubic centimetre were calculated from the mole fractions and the molar volume at the flame temperature and a pressure of 1 bar, as found from the ideal gas law. The calculated concentrations of potassium atoms in the diffusion flame and in the flame core were of a similar magnitude to the concentration calculated by Douda and Bair[26] for sodium atoms in the flame of a sodium nitrate–magnesium ($NaNO_3$–Mg) flare (4×10^{17} atoms cm^{-3}).

Despite the substantial decrease in the concentration of potassium atoms in the diffusion flame, the intensity of the deep red resonance lines is expected to be similar to (approximately 0.75 times) that from the core. This is because the diffusion flame is hotter, with the result that the fraction of potassium atoms excited to emit these lines is approximately 4.1 times greater in the diffusion flame than in the core. However, the lower concentration of ground state potassium atoms in the diffusion flame compared to the core would result in the deep red lines being less subject to broadening by self-absorption. Thus there would be less emission in the shorter wavelengths of the red region of the spectrum, making the diffusion flame appear less red than the core. The same considerations indicate that the violet potassium resonance lines would be approximately 2.7 times more intense in the diffusion flame than in the core, because the fraction of potassium atoms excited to emit these lines is approximately 14 times greater in the hotter diffusion flame.

It was not possible to test all of these predictions with the results of Figure 7, because the sampled volume of the flame was almost certainly not the same for each spectrum. Absolute intensity comparisons are meaningful only if the sampled volume is constant. The possibility of normalizing the intensities to that of the sodium line was rejected because this normalization would be valid only if the temperatures were the same in each part of the flame. Figure 7 does show, however, that the red lines are relatively less broadened, and the short-wavelength continuum relatively more intense, in the outer part of the flame than in the inner part, the standard of comparison being the maximum intensity of the red potassium line in each spectrum.

The calculated concentration of potassium hy-

droxide (KOH) in the diffusion flame (7.2×10^{17} molecules cm^{-3}) is greater than that in the flame core (4.1×10^{17} molecules cm^{-3}). Accordingly, assuming that the chemiluminescent potassium hydroxide emission is proportional to the equilibrium potassium hydroxide concentration, one can predict that the ratio of red potassium emission to the bluish-violet KOH continuum would be less in the diffusion flame than in the core. This would make the diffusion flame appear bluer than the core. Another source of blue light in the diffusion flame could be the blue emission associated with the combustion of carbon monoxide.[22b] (This is the principal source of the familiar blue colour of the outer mantle of flames in which fuels containing carbon are burnt in air or oxygen).

Conclusions

The pink colour of the core of the flame from the 80% KNO_3–20% shellac mixture is attributable to broadening of the deep red potassium resonance lines by self-absorption, which extends the emission into the region of the spectrum to which the eye is more sensitive. The potassium emission is superimposed on a continuum produced by a combination of thermal emission from droplets of molten potassium carbonate suspended in the flame and chemiluminescent emission from potassium–hydroxyl recombination. The lilac colour of the outer regions of the flame presumably arises from the same combination of emission lines from potassium atoms and the potassium–hydroxyl recombination continuum, with very much less thermal emission from liquid droplets. However, (1) the visible intensity of the red potassium emissions is reduced because of less self-absorption broadening of the 766.491 and 769.897 nm resonance lines; and (2) the intensity of the violet chemiluminescent emissions is increased. The result is the lilac colour of the outer (diffusion) flame envelope.

References

1 R. Mavrodineanu and H. Boiteux, *Flame Spectroscopy*, Wiley, New York, 1965, [a] pp. 368–371, [b] pp. 507–508.

2 H. A. Webster III, "Emission From Molecular Species in Pyrotechnic Flames", *Proceedings of the 5th International Pyrotechnics Seminar*, 1976, pp. 551–565.

3 C. Jennings-White, "Nitrate Colors", *Pyrotechnica*, Vol. XV, 1993, pp. 23–28.

4 R. M. Winokur, "Purple Fire", *Pyrotechnica*, Vol.VI, 1980, pp. 21–31.

5 V. Pacini, *Il dilettante di pirotechnicia, ovvero regole da tenersi per lavorare i fuochi d'artificio e colorati (The amateur pyrotechnist, or rules to be observed when working with fireworks and colours),* Campolmi, Florence, 1845 (cited by Winokur, *loc. cit.*).

6 C. Jennings-White, personal communication, 2004.

7 R. F. Barrow and E. F. Caldin, "Some Spectroscopic Observations on Pyrotechnic Flames", *Proceedings of the Physical Society (London)*, 62B, 1949, pp. 32–39.

8 J. E. Sansonetti, W.C. Martin and S.L. Young, *Handbook of Basic Atomic Spectroscopic Data (version 1.1)* [Online]. Available: http://physics.nist.gov/Handbook. National Institute of Standards and Technology, Gaithersburg, Maryland, 2004.

9 J. A. Dean, *Flame Photometry*, McGraw-Hill, New York, 1960, [a] pp.167–173, [b] pp. 82–83.

10 C. J. James and T. M. Sugden, "Photometric investigations of alkali metals in hydrogen flame gases, III: The source of the alkali metal continuum", *Proceedings of the Royal Society of London*, Vol. A248, 1958, pp. 238–247.

11 A. Thorne, U. Litzen and S. Johansson, *Spectrophysics*, Springer-Verlag, Berlin, 1999, [a] pp. 214–217, [b] pp. 164–166.

12 J. D. Ingle, Jr., and S. R. Crouch, *Spectrochemical Analysis*, Prentice Hall, Upper Saddle River, New Jersey, 1988, [a] pp. 209–219, [b] pp. 88–89.

13 T. M. Sugden, "Excited species in flames", *Annual Reviews of Physical Chemistry*, Vol. 13, 1962, pp. 369–390.

14 C. Th. J. Alkemade, Tj. Hollander, W. Snelleman and P. J. Th. Zeegers, *Metal Vapours in Flames*, Pergamon Press, Oxford, 1982, p. 634–652

15 H. E. Roscoe, *On Spectrum Analysis*, Macmillan, London, 1869, frontispiece.

16 G. Kirchhoff and R. Bunsen, "Chemical Analysis by Observation of Spectra", *Annalen der Physik und der Chemie (Poggendorff)*, Vol. 110, 1860, pp. 161–189. English translation available at http://dbhs.wvusd.k12.ca.us/webdocs/Chem-History/Kirchhoff-Bunsen-1860.html

17 *Fact Sheet 5: Absorption Lines in The Solar Spectrum*, Faculty of Pure and Applied Science, York University, available at http://resources.yesican.yorku.ca/trek/scisat/final/grade9/fact_sheet5.html

18 T. Shimizu, *Fireworks from a Physical Standpoint*, transl. A. Schuman, Vol. II, Pyrotechnica Publications, Austin, Texas, 1983, [a] p. 75, [b] p. 114.

19 C. Th. J. Alkemade, in J. A. Dean and T. C. Rains, eds., *Flame Emission and Atomic Absorption Spectrometry*, Vol. 1, Marcel Dekker, New York, 1969, p. 146.

20 R. C. Weast, ed., *CRC Handbook of Chemistry and Physics*, 63rd edn., CRC Press, Boca Raton, Florida, 1982–1983, p. D138.

21 T. N. Panay, "Sur le spectrum continu de potassium dans la flame" ("On the continuous spectrum of potassium in the flame"), *Comptes Rendus de l'Academie des Sciences*, Vol. 204, 1937, pp. 251–253.

22 A. G. Gaydon, *The Spectroscopy of Flames*, Chapman & Hall Ltd, London, 1957, [a] p. 224, [b] pp. 95–101.

23 N. Omenetto, J. D. Winefordner and C. Th. J. Alkemade, "An expression for the atomic fluorescence and thermal-emission intensity under conditions of near saturation and arbitrary self-absorption", *Spectrochimica Acta*, Vol. 30B, 1975, pp. 335–341.

24 B. E. Douda, "Formation of the sodium resonance line continuum", *RDTN No. 95*, Naval Ammunition Depot, Crane, Indiana, 1970.

25 B. E. Douda, R. M. Blunt and E. J. Bair, "Visible radiation from illuminating-flare flames: Strong emission features", *Journal of the Optical Society of America*, Vol. 60, 1970, pp. 1116–1119.

26 B. E. Douda and E. J. Bair, "Visible radiation from illuminating-flare flames: II. Formation of the sodium resonance continuum", *Journal of the Optical Society of America*, Vol. 60, 1970, pp. 1257–1261.

27 B. E. Douda and E. J. Bair, "Radiative transfer model of a pyrotechnic flame", *Journal of Quantitative Spectroscopy and Radiative Transfer*, Vol. 14, 1974, pp. 1091–1105.

28 B. E. Douda and R. J. Exton, "Optically thick line widths in pyrotechnic flares', *Journal of Quantitative Spectroscopy and Radiative Transfer*, Vol. 15, 1975, pp. 615–617.

29 W. Meyerriecks and K. L. Kosanke, "Color values and spectra of the principal emitters in colored flames", *Journal of Pyrotechnics*, Issue 18, 2003, pp. 1– 22.

30 W. Meyerriecks, personal communication, 2003.

31 A. G. Gaydon and H. G Wolfhard, *Flames: Their Structure, Radiation and Temperature*, 2nd edn., Chapman & Hall, London, 1960, p. 231.

32 S. Gordon and B. J. McBride, *Computer Program for Calculation of Complex Chemical Equilbrium Composition and Applications I. Analysis*, NASA Reference Publication 1311, National Aeronautics and Space Administration, Lewis Research Center, Cleveland, Ohio, 1994.

33 B. J. McBride and S. Gordon, *Computer Program for Calculation of Complex Chemical Equilbrium Composition and Applications II. Users Manual and Program Description*, NASA Reference Publication 1311, National Aeronautics and Space Administration, Lewis Research Center, Cleveland, Ohio, 1996.

34 W. Meyerriecks, "Organic fuels: Composition and Formation Enthalpy Part II – Resins, Charcoal, Pitch, Gilsonite and Waxes", *Journal of Pyrotechnics*, Issue 9, 1999, pp. 1–19.

Acknowledgements

The authors are grateful to Dr B. E. Douda, Dr. C. Jennings-White and Dr H. Webster for their reviews of this article, and to Dr J. B. Willis and Mr P. S. Doidge for helpful comments on the spectroscopic section

A Thrust and Impulse Study of Guanidinium Azo-Tetrazolate as a Fuel Additive for Hybrid Rocket Motor

Ann Wright[a], Warfield Teague[a]
M. Keith Hudson[b], Andrew Wright[b], Patrick Foley[b]

[a]Department of Physics and Department of Chemistry, Hendrix College, Conway, AR 72032, USA
[b]Department of Applied Science and the Graduate Institute of Technology
University of Arkansas at Little Rock, Little Rock, AR 72204, USA

Abstract: *Guanidinium azo-tetrazolate (GAT) is an organic salt with a high percentage of nitrogen. GAT was mixed with the standard hybrid rocket fuel, hydroxyl-terminated polybutadiene (HTPB), in concentrations of 15% and 25% by mass. The fuel grains with the GAT additive were fired for 4 seconds with oxygen flows of 0.04, 0.06, 0.08, and 0.10 lbm* s^{-1}.

Physical characteristics of the rocket were measured while firing the GAT fuels. Thrust, internal pressure, fuel mass consumed, oxygen flow rate, nozzle throat diameter, and fuel port radius were measured. Fuel regression rate, specific impulse, total impulse, and average thrust were calculated from the data.

GAT was found to increase the thrust output when added to the standard hybrid rocket fuel, HTPB. 25% GAT fuel produced approximately the same thrust as the 15% GAT fuel. Specific impulse was slightly lower with both 15% and 25% GAT fuels than with plain HTPB fuel.

Standard deviation of thrust was used as a crude measure of amplitude of oscillations during combustion. GAT-added fuels showed a very small decrease in thrust oscillation amplitude.

Keywords: *GAT, rocket, additive, motor*

Introduction

A hybrid rocket is normally powered by a solid fuel over which a gaseous or liquid oxidizer flows. The main benefit of the hybrid rocket is the ability to throttle the rocket by controlling the oxidizer flow. The fuel, usually hydroxyl-terminated polybutadiene (HTPB), is a polymer that will not burn unless a significant amount of oxygen is present. Unlike a solid rocket, the hybrid rocket may be started, stopped and restarted. This feature is especially important in the event of a problem during launch. The hybrid rocket can be shut down quickly by eliminating the oxygen source. A hybrid rocket is safer and has more flexibility than solid rockets. Hybrid rockets are also much less complex than liquid rockets, having one half of the complexity in plumbing.

The hybrid rocket facility at the University of Arkansas at Little Rock (UALR) consists of a labscale hybrid rocket motor, transducers to measure physical properties such as pressure and thrust, a control computer, and a data acquisition computer. The facility was originally built to investigate combustion instabilities and plume diagnostics. A description of the facility and history of the research at the facility may be found in previous papers.[1,2]

The UALR hybrid rocket facility is especially suited to studies of rocket fuels and fuel additives because the fuels are fabricated on site. The UALR hybrid rocket uses a cylindrical fuel grain that is 10 in (25 cm) long with a 2 in (5 cm) outer diameter and a cylindrical port through the center with initial diameter of 0.75 in (19 mm). During combustion, gaseous oxygen flows through the fuel port and over the fuel. When a spark is supplied, the fuel is ignited and burns in the presence of the oxygen. Ignition is accomplished with a plasma generator attached to a standard automobile spark plug. A small burst of propane is used to facilitate ignition.

One useful measure of hybrid rocket fuel performance is regression rate. The regression rate of a fuel is the rate of depletion of the surface of

the fuel grain during combustion. Regression for the cylindrical fuel grains is defined as

$$r = \frac{\left[\left(\sqrt{\frac{m_i - m_f}{\rho \pi l} + r_i^2}\right) - r_i\right]}{t} \quad (1)$$

where r is regression rate, r_i is initial port radius, m_i is initial mass, m_f is final mass, ρ is fuel mass density, l is the length of the fuel grain, and t is the burn time.[7]

The purpose of the experiments was to determine if guanidinium azo-tetrazolate (GAT) increases the performance characteristics (regression rate, thrust, specific impulse, total impulse) of a hybrid rocket when added to HTPB fuel. GAT is an organic salt with a high nitrogen content. It is a highly energetic compound due to the energy stored in the pi bond system.

The GAT used in this project was synthesized at UALR. The process was time consuming and the initial chemical ingredients are expensive. The process contains one step in which a contact explosive, SAT, is created. Care must be taken to prevent air-drying at this step. All other steps of the process are safe. The chemical bond structure of GAT is shown in Figure 1.

Several regression rate studies have been done on guanidinium azo-tetrazolate (GAT).[7,8,10] A preliminary study of the feasibility of using GAT as a fuel additive with HTPB was presented in 1996.[8] The results of that study detailed solutions to problems in casting the fuel grains and the possibility of an increased regression rate. More data was needed to fully describe the properties of the GAT/HTPB fuel mixtures. A complete regression rate study was presented in 1998,[7] verifying that GAT does increase the regression rate when used as an additive to HTPB fuel in Hybrid Rockets. Concentrations of 15%, 20%, 25%, and 30% GAT were tested. The highest regression rate was given by 25% GAT, by mass, fuel concentration. Results of this study are presented in reference 7. The increase in regression rate makes GAT a desirable fuel additive to HTPB. The next step was to determine the effect of the GAT on the average thrust, specific impulse, and total impulse of the motor.

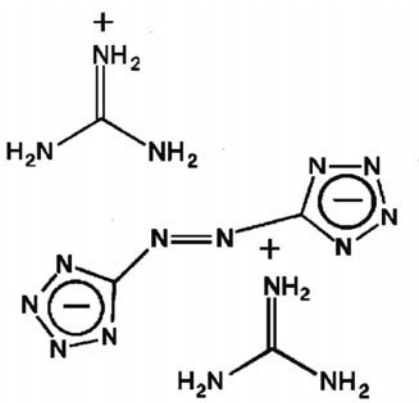

Figure 1. *The chemical structure of guanidinium azo-tetrazolate (GAT).*

The thrust of a rocket, F, is the reaction force experienced by its structure due to the ejection of high-velocity matter.[3] Ideally, the forward momentum of the rocket is equal to the rearward momentum of the ejected gases from the nozzle. Some losses may occur due to gravity effects and air resistance in a flying rocket.

All hybrid rockets are characterized by a rapid oscillation in both pressure and thrust. There are several theories for the cause of these oscillations. One possible cause is the nature of the fuel itself. As the fuel burns, a fuel layer either liquefies or sublimates, mixes with the oxygen, and burns, forming hot gases and a char layer. The char layer is continually sloughed off out of the rocket, revealing a fresh layer of fuel for combustion. This process, called chuffing, happens many times per second. The chuffing may be a significant cause of the characteristic pressure and thrust oscillations that are seen in all hybrid rocket combustion.[3–6] Another potential source for the oscillations is the oxidizer feed line. As combustion occurs in the motor, the chamber pressure increases, reducing the pressure-fed oxidizer flow, which then causes a pressure decrease. A third possible cause of the oscillations is the presence of a swirling motion of the hot gases inside the combustion chamber. This swirling motion has been imaged in the UALR hybrid rocket.[2] If hybrid rockets are to be employed to lift valuable cargo or human passengers into orbit, these pressure oscillations must be better understood so that they may be

minimized or eliminated. The motivation for the measurements detailed in this paper is to be able to measure the thrust oscillations more accurately. With a better measurement of the amplitude and frequency composition of the oscillations, a more complete understanding of the underlying cause may be possible.

From the thrust measurement, specific and total impulse may be calculated. Total impulse, I_T, is defined as the thrust force integrated over the burning time.

$$I_T = \int F dt \qquad (2)$$

where F is thrust force, and t is time.

Specific impulse, I_S, is the total impulse per unit mass of propellant consumed. Since hybrid rockets use a solid fuel and a gaseous oxidizer, mass flux of both the fuel and oxidizer must be taken into account.

$$I_S = \frac{\overline{F}}{\dot{m}_o + \dot{m}_f} \qquad (3)$$

where $\overline{F}$ is the average thrust, $\dot{m}_o$ is the time rate of change of the oxidizer mass, and $\dot{m}_f$ is the time rate of change of fuel mass.

Experimental

The hybrid rocket fuel grains were cast in paper phenolic cylinders 10 in (25 cm) in length, with a 2 in (5 cm) outer (fuel) diameter and an initial port diameter of 0.75 in (19 mm). Standard fuel grains were prepared with 85% HTPB and 15% PAPI diisocyanate used as the curative agent. Additional sets of fuel grains were formed with 15% and 25% GAT by mass added to the standard HTPB and PAPI fuel mixture.

The fuel grains were fired in the UALR hybrid rocket. The gaseous oxygen flow was varied between 0.04 lbm s^{-1} and 0.12 lbm s^{-1}. The initial and final mass, port radii of the fuel grain, and nozzle diameter were measured for each run. The runs were set for 4 or 5 seconds. However, delays in ignition caused some combustion times to be less than the set time. Pressure data were used to determine the actual length of time between ignition and shut-down.

Because thrust is dependent upon nozzle diameter, care was taken to ensure that the nozzle diameter stayed as constant as possible throughout all of the trial runs. Since the nozzle was made of graphite, exact consistency was impossible due to ablation during the runs. The nozzle opening diameter varied from 0.28 to 0.31 in (7.1 to 7.9 mm) for the entire data sample.

An attempt was made to eliminate the nozzle ablation source of error entirely by using a high-temperature ceramic nozzle. Unfortunately, the ceramic nozzles could not withstand the hostile environment and high stresses. The nozzles shattered unpredictably during firing. Their use was discontinued for safety reasons.

The thrust measurement was made using strain gages mounted on aluminum legs supporting the rocket.[4,5] The flexing beams were made from 2024-T81 aluminum with a yield strength of 65 kpsi. Four strain gages from Measurements Group (CEA-13-125UW-350) were placed on the two beams to form a Wheatstone bridge circuit. A two stage amplification circuit was built to collect the voltage output of the strain gages and produce a voltage between 0 and 10 V. The voltage was sampled by an A/D board at 1000 Hz.[4]

As the rocket is fired, the thrust pushes the rocket away from the plume, causing the aluminum support legs to deflect in a predictable manner. The strain experienced by the support legs is proportional to the force. The strain gage circuit output is a voltage that is proportional to the force causing the deflection. A picture of the thrust sensor is shown in Figure 2.

The thrust detector was calibrated using a hanging weight system. Known weights between 0 to 50 lb were suspended from the rocket using a pulley system to direct the force along the rocket axis. The voltage output of the strain gage conditioning circuit was collected. The calibration curve is shown in Figure 3.

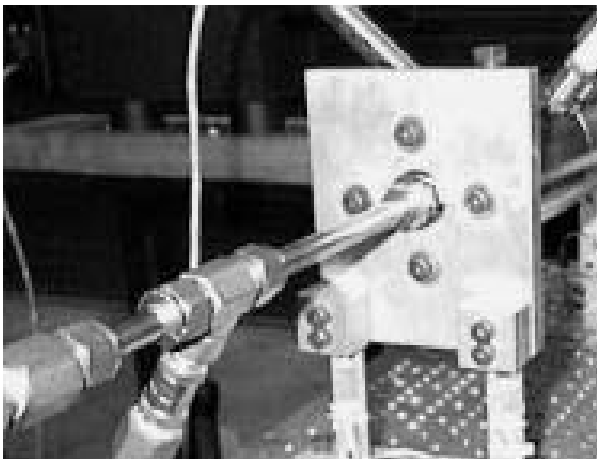

Figure 2. *The UALR hybrid rocket, showing the strain gage thrust sensors on the rear support legs.*

Results and Discussion

The thrust as a function of time was recorded for each data run. A sample plot is shown in Figure 4. The thrust curve is characterized by several features. A small thrust was seen during the initial gas (oxygen and propane) flow from 0 to approximately 2 seconds. A sharp increase in thrust indicates the moment of ignition, followed by several seconds of rapid oscillation during the main part of the run. These oscillations are a direct result of the pressure oscillations that are normally seen in hybrid rockets. The run is then shut down as the oxygen is turned off and nitrogen gas is flowed through the rocket to quench the combustion. The flow of nitrogen is responsible for the small non-zero thrust after shutdown.

The average and standard deviation of thrust was determined for a range between the initial start-up and the shutdown of the run. The average thrusts for both the plain HTPB grain and the GAT-added grains are plotted in Figure 5 as a function of oxidizer flow rate. The standard deviations ranged from 1.5 to 2.5 lb of thrust. There was no apparent correlation between the standard deviation of thrust and the fuel content, oxygen flow, or the number of firings on each fuel grain.[6] The amplitude of the oscillations did not increase or decrease with the addition of GAT to the HTPB fuel.

Fuel grains with 15% GAT and 25% GAT show an increase in the thrust output compared to the plain HTPB fuel thrust output, especially at all oxygen flow rates. The 25% GAT fuel does not produce significantly more thrust than the 15% GAT fuel.

Average thrust, total impulse, and specific impulse for each flow rate were determined for each firing run. Total impulse calculations were normalized for a four second run since the actual burn times varied for each run. Results are shown in Tables 1–3.

Results for specific impulse vs. oxygen flow rate are given in Figure 6. Results for total impulse vs. oxygen flow rate are given in Figure 7.

The fuel grains with 15% and 25% GAT show

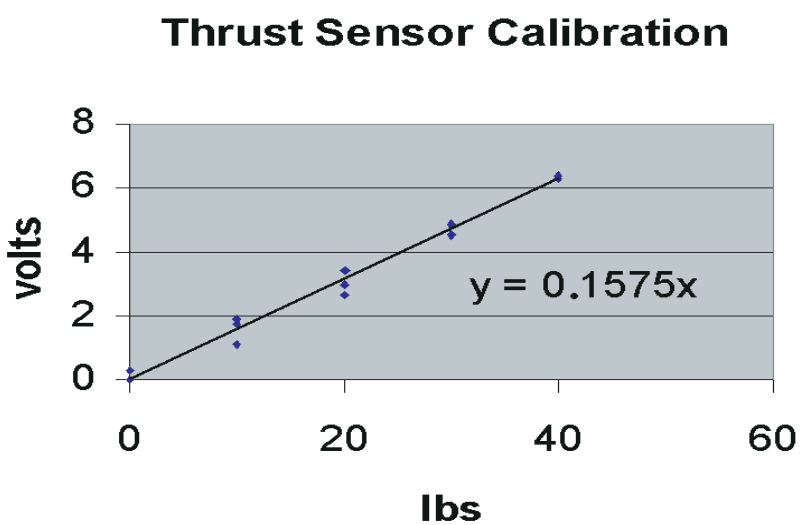

Figure 3. *Calibration curve for the thrust sensor strain gage circuit.*

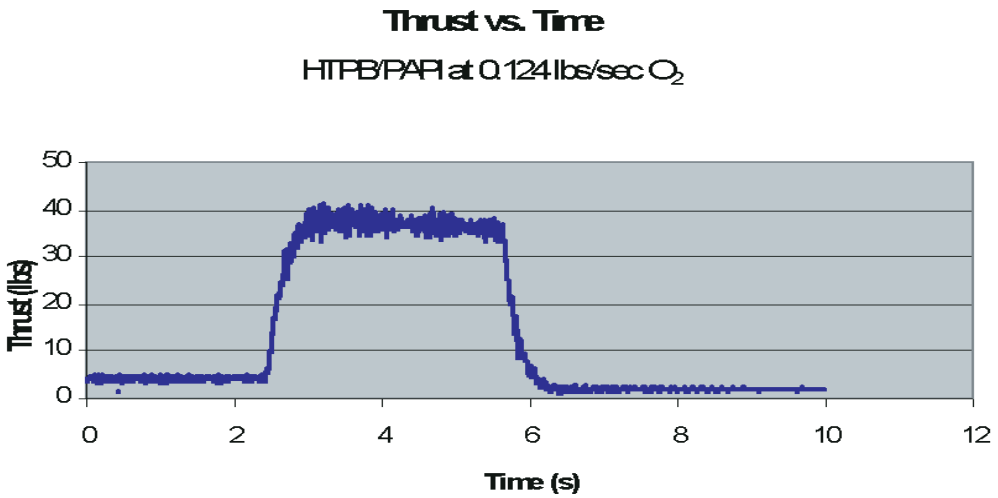

Figure 4. *Thrust as a function of time.*

increased total impulse compared to plain HTPB fuel. The 25% GAT fuel produces more total impulse than the 15% GAT fuel, especially at the higher oxygen flow rates.

Table 1. *Data Summary for Plain HTPB*

O_2 flow/lbm s^{-1}	*F*/lbf	I_T/lbf s	I_S/s
0.049	15.55	45.92	182.29
0.064	21.87	70.12	211.45
0.082	27.69	80.45	228.42

Table 2. *Data Summary for 15% GAT*

O_2 flow/lbm s^{-1}	*F*/lbf	I_T/lbf s	I_S/s
0.048	18.42	54.14	181.34
0.065	25.47	72.18	204.96
0.082	33.78	99.39	214.99

Table 3. *Data Summary for 25% GAT*

O_2 flow/lbm s^{-1}	*F*/lbf	I_T/lbf s	I_S/s
0.044	15.56	45.37	164.23
0.059	22.14	64.48	203.09
0.075	27.55	80.39	198.31
0.099	39.00	105.18	230.81

The 15% and 25% GAT fuels show a slight decrease in specific impulse. Specific impulse is the average thrust divided by the rates of fuel consumption (see equation 3). Since the average thrust of the GAT-added fuels has increased, the rate of fuel consumption must have also increased, which is consistent with the larger regression rates found previously.[7] Ideally, a fuel additive would increase the average thrust more than increasing fuel regression rate (assuming the oxygen flow rates are unchanged), thereby increasing the specific impulse. In this study, the increase in thrust due to the addition of GAT comes at the price of faster fuel consumption and a decreased specific impulse.

The addition of GAT to the standard hybrid rocket fuel, HTPB, increases the regression rate and therefore the performance of the fuel.[3] Regression rates in general are increased not only by degradation of the fuel molecules, but also by the release of energy by the azo-compounds during combustion. In addition, this compound breaks down into more reactive radicals with higher volume per unit mass. These factors contribute to a faster pyrolysis of HTPB and overall pyrolysis of the fuel.[7]

The synthesis of GAT is very time consuming, moderately expensive, and technically complex. Therefore, commercial use of GAT is unlikely at this time. In addition, environmental impact from combustion products need to be considered before using GAT in large scale hybrid motors. Since

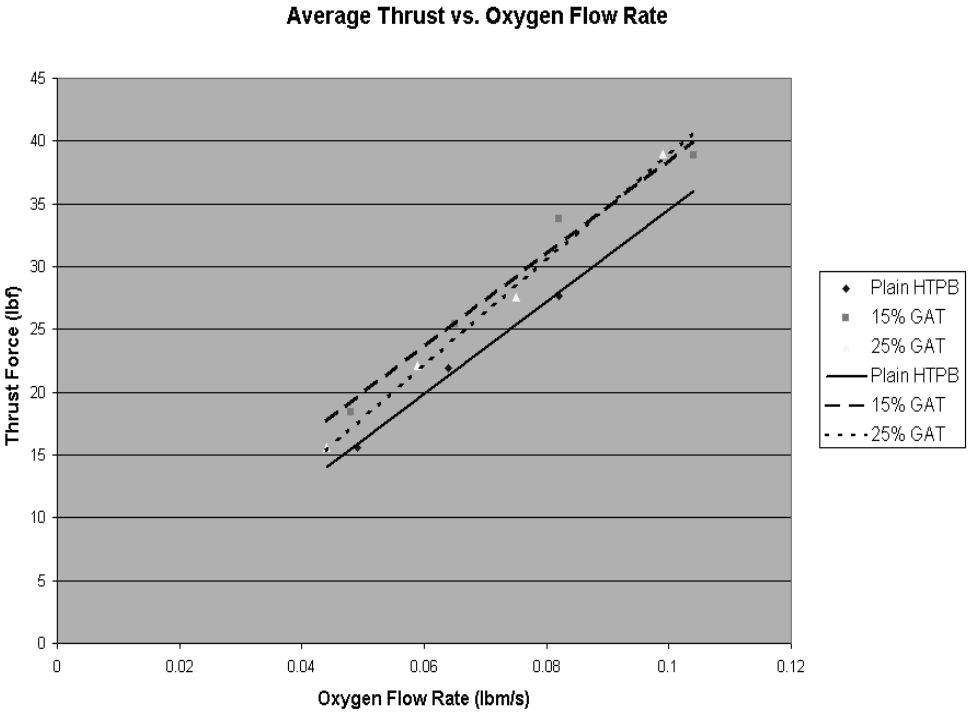

Figure 5. *Average thrust as a function of oxygen flow rate.*

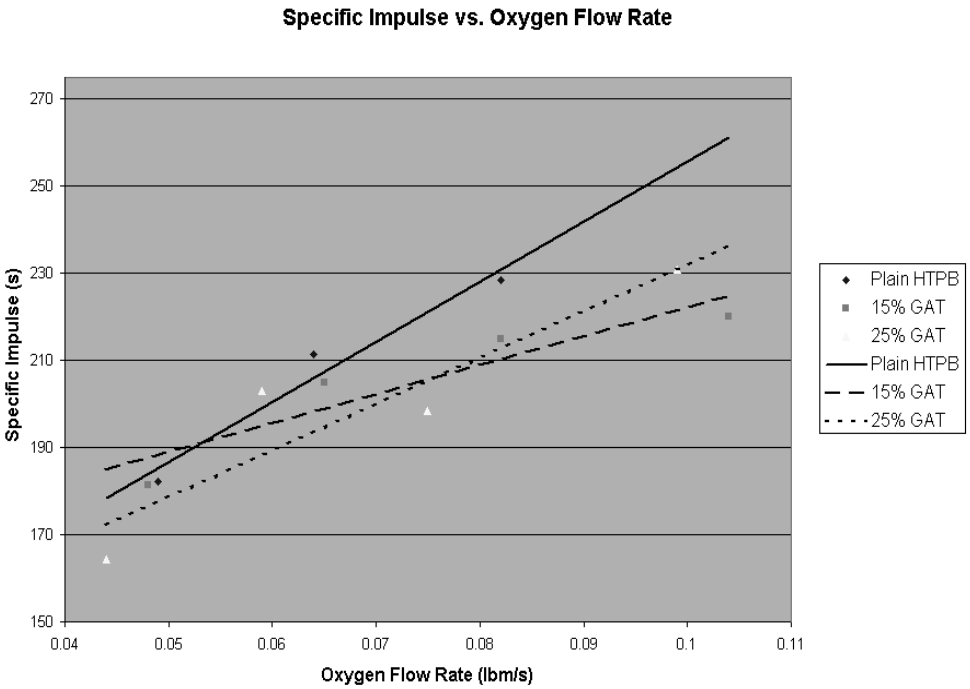

Figure 6. *Specific impulse as a function of oxygen flow rate.*

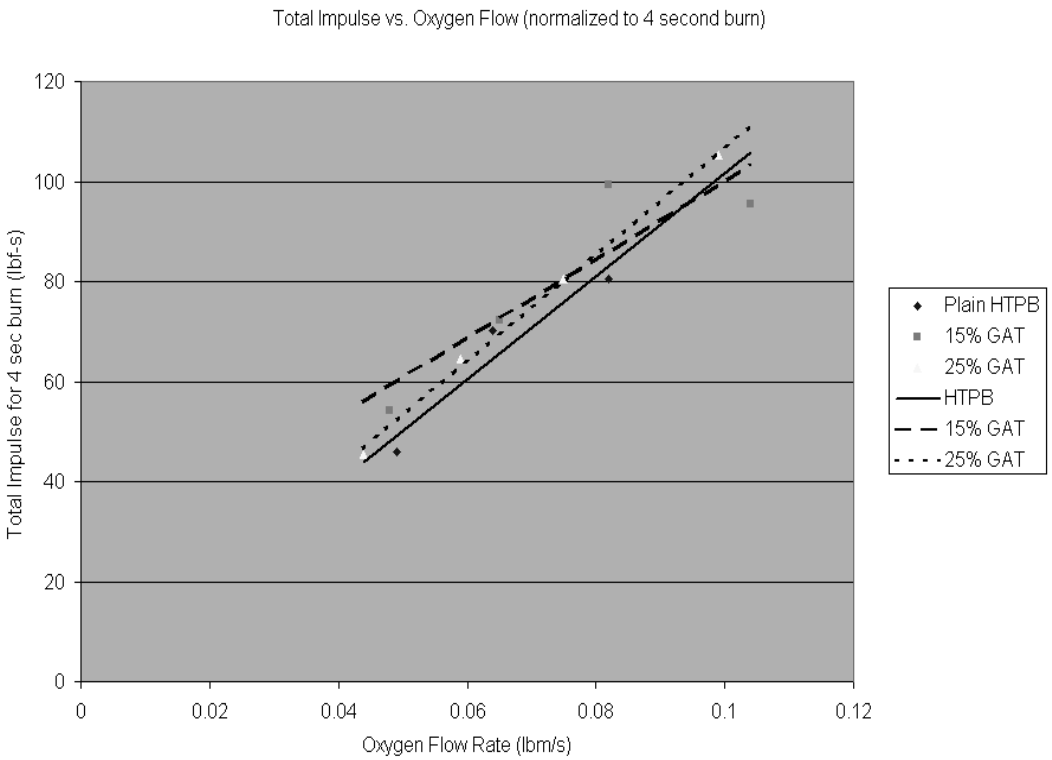

Figure 7. *Total impulse as a function of oxygen flow rate.*

GAT is high in nitrogen content, the formation of nitrous oxide (NO) is a concern because it is known to contribute to the formation of acid rain. Trace amounts of NO in lab-scale hybrid rocket plumes could translate into a significant amount in the plume of a large scale rocket. Spectroscopic analysis of the plume chemistry in the UALR hybrid rocket has found no evidence of NO in the plume.[11,12]

HTPB is the standard hybrid rocket fuel. It has excellent qualities, along with some problems. The main issues are the pressure and thrust oscillations experienced by the rocket during firing. It is thought that these oscillations may be a characteristic of the fuel. We may be able to minimize these oscillations by altering the fuel with a fuel additive. An optimal fuel additive should have the following properties: thrust should be increased, regression rate should increase, specific impulse should remain the same or increase, total impulse should increase, oscillation amplitudes should decrease, and no additional harmful chemicals should be released into the atmosphere via the exhaust. The additive, GAT, in quantities of 15% by mass, is found to have most of these desirable properties. Fuels with 25% added GAT show slightly better performance. However, the increased performance may not justify the added expense of the fuel.

References

1 R. B. Shanks, "A Labscale Hybrid Rocket Motor and Facility for Plume Diagnostics and Combustion Studies", PhD Thesis, Department of Applied Science, University of Arkansas at Little Rock, 1994.

2 A.B. Wright, J. Elsasser, M. K. Hudson, A. M. Wright, "Optical Studies of Combustion Chamber Flame in a Hybrid Rocket Motor", *Journal of Pyrotechnics*, Issue 19, Summer 2004.

3 G. P. Sutton, "Rocket Propulsion Elements, An Introduction to the Engineering of Rockets", 6th edn., 1992, John Wiley and Sons, Inc.

4 M. F. Desrochers, “Instrumentation of a Labscale Hybrid Motor”, Master of Science Thesis, Department of Applied Science, University of Arkansas at Little Rock, May 1997.

5 M. F. Desrochers, “Investigation of Pressure, Plume Flicker, and Thrust in a labscale Hybrid Rocket,” AIAA Paper No. 97-3036, 1997.

6 A.M. Wright et al.,”A Study of the Amplitude of Pressure and Thrust Oscillations in a Lab-Scale Hybrid Rocket”, *Arkansas Academy of Sciences Journal*, vol. 54.

7 M.K. Hudson, A.M. Wright, C. Luchini, P. Wynne, and S. Rooke, “Guanidinium Azo-Tetrazolate (GAT) as a High Performance Hybrid Rocket Fuel Additive”, *Journal of Pyrotechnics,* Issue 19, Summer 2004.

8 C. B. Luchini, P. Wynne, and M. K. Hudson, “Investigation of GAT as a High Regression Rate Hybrid Rocket Fuel,” AIAA Paper No. 96-2592, 1996.A. Wright,

9 A. M. Wright et al., “A Thrust and Impulse Study of Guanidinium Azo-Tetrazolate as an Additive for Hybrid Rocket Fuel”, AIAA Paper No. 99-2538, 1999.

10 A. Wright, “A Hybrid Rocket Regression Rate Study of Guanidinium Azo-Tetrazolate”, AIAA Paper No. 98-3186, 1998.

11 M. W. Teague, “Effect of Energetic Fuel Additives on the Temperature of Hybrid Rocket,” AIAA Paper No. 99-2138, 1999.

12 M. W. Teague, J. R. Welborn, T. M. Felix, M. K. Hudson, and J. Willis, “UV-Vis Absorption as a Diagnostic for NO in Rocket Plumes”, *International Journal of Turbo and Jet Engines*, vol. 13, 1996, 211–215.

Conversion from English to Metric Units

1 lbm = 1 pound mass = 454 gram
1 lbf = 1 pound force= 4.45 N
1” = 1 in = 1 inch = 25.4 mm
1 psi = 1 pound force per square inch = 0.145 kPa

Pressure in a Mortar and Estimation of Muzzle Velocity of Expelled Stars

Dayu Ding, Morimasa Higaki, Yuzo Ooki, and Tadao Yoshida*

Ashikaga Institute of Technology
268-1 Omae-cho, Ashikaga-shi, Tochigi 326-8558, Japan
* To whom all correspondence should be addressed
Tel: +81-284-62-0605, fax: +81-284-62-0976, email: yoshida@ashitech.ac.jp

Abstract: *Firing firework star experiments have been carried out using 20 mm and 25 mm inner diameter steel mortars equipped with two or four pressure transducers, and the pressure profiles were recorded. The relative pressure profiles of the four positions in the mortar changed with the gap ratio between sectional areas of the star and the mortar wall, and with the mass of the lifting charge. The maximum pressure attained decreased and the scatter of observed data increased with an increase of the gap ratio. It was shown by experiment using four pressure transducers that, when the gap ratio is large, the pressures to the rear and front of a star should be corrected for the pressure distribution in the mortar.*

In the first half of the experiment, using two pressure transducers the muzzle velocity of a star was estimated from the pressure profile of the bottom transducer. When the gap between star and mortar wall and the mass of lifting charge were small, the calculated and observed muzzle velocities agreed well. However, in the case of a large gap, the calculated value was larger than the observed one.

In the latter half of the experiment, four pressure transducers were used and it was found that in the case of a large gap the pressure profile from the bottom transducer did not give the real pressures to the rear and front of the star in the mortar. A correction for the difference was tried and the agreement between the observed and calculated values was improved.

Keywords: *fireworks, interior ballistics, pressure profile, muzzle velocity*

Introduction

Firework stars are important elements of aerial fireworks. The burning stars fly into the sky and appeal visually to the spectators. The stars are used in two modes. In one mode, stars are packed in a shell with a bursting charge, and ejected into the sky by the deflagration of the bursting charge followed by bursting of the shell. Aerial shell fireworks are examples. In the other mode, stars are fired directly from mortars on the ground. Roman candles and mines are examples.

In the present work, firing star experiments were carried out using mortars equipped with pressure transducers and a high-speed video camera. The inner pressure profiles and the initial velocities of the expelled stars were recorded, and results were analyzed.

A preliminary study was done by the present authors for the inner pressure profiles in the firing stars.[1] K. L. and B. J. Kosanke[2] and Y. Ooki *et al*.[3] have measured inner pressure profiles in the mortar on aerial shell firing, and estimated the muzzle velocity of the shells from the pressure profile.

Experimental

Materials

Stars for no. 2 to no. 10 shells (no. 2.5 shell corresponds to a 3 inch (75 mm) shell) were supplied by the Sunaga Fireworks Co. Ltd., Ashikaga, and the lifting charge and the electric match were made by the Nippon Kayaku Company. The lifting charge is always the same product in Japan and is a grain black powder with the following standards:

Composition (%): potassium nitrate 74–80, sulfur 8–12, charcoal 10–16.
Size (mm) 0.4–1.2
Density (g cm^{-2}) 1.75–1.85

The particle distribution of the lifting charge was determined by us as follows:

<0.15 mm 0%
0.15–0.3 mm 0.03%
0.3–0.6 mm 23.89%
0.6–1.2 mm 76.07%
1.2–2.5 mm 0.01%
>2.5 mm 0%

Apparatus

The two mortars used for firing stars were made of steel, with inner diameters of 20 mm and 25 mm, and depths of 361 mm and 455 mm, respectively. The two mortars were each equipped with two pressure transducers, at the bottom and middle (2/3 from bottom) of the mortar. In the latter experiment, two pressure transducers were added to the 20 mm inner diameter mortar. The dimensions of the mortars with pressure transducers are shown in Figure 1.

The pressure in the mortar during firing was measured using two or four pressure transducers (Kistler 6041A), charge amplifiers (Kistler 5011) and a digital oscilloscope (Sony Tektronix TDS3012 or Yokokawa DL1640 with four channels). The set-up of the pressure measuring system is shown in Figure 2.

The muzzle velocity of the star was measured using a high-speed video camera (Phantom VR-V4.2) with a frame speed of 1000 frames per second.

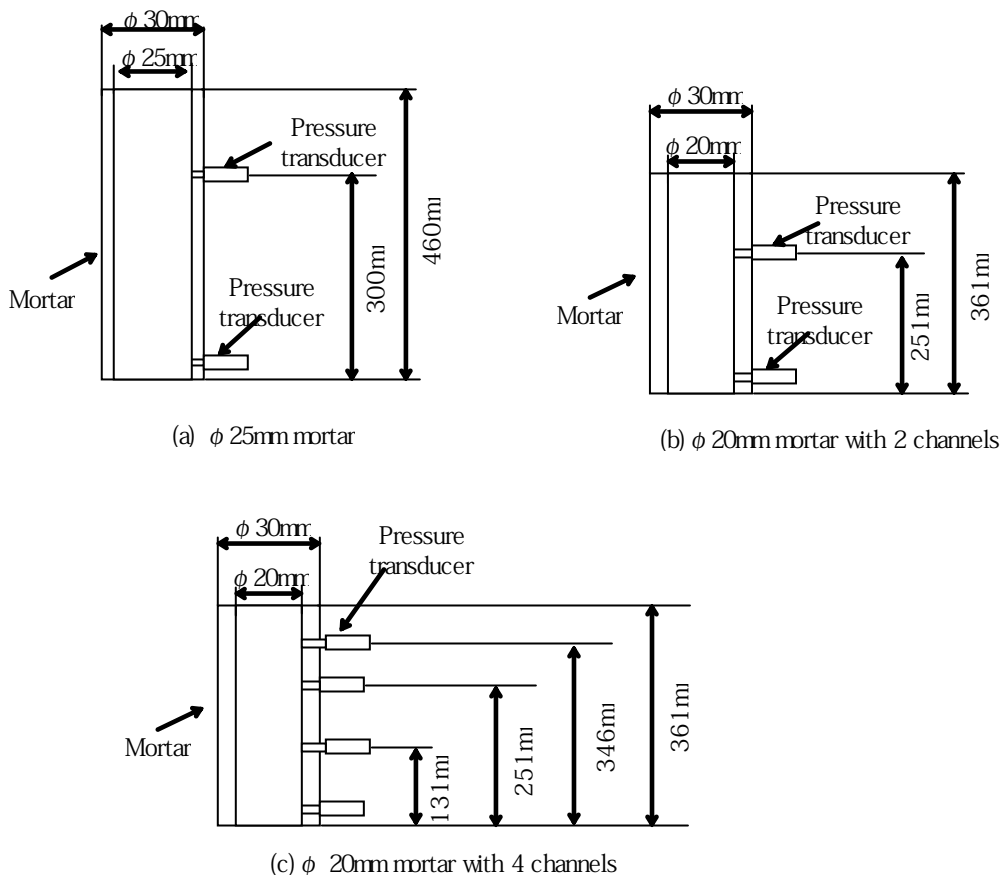

Figure 1. *Mortars and positions of pressure transducers.*

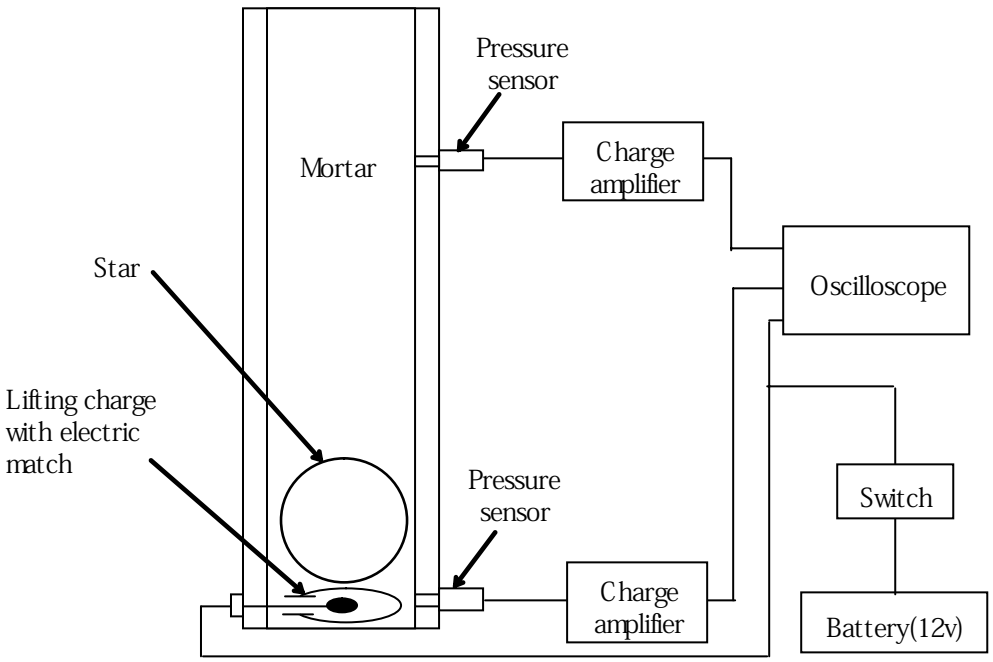

Figure 2. *Setup of the pressure measuring system.*

Procedure

The mortar is set on the ground vertically. The electric match is put in the bottom of the mortar and the lifting charge is poured into the mortar through the muzzle. Then a star is placed on the lifting charge. The electric match is ignited by turning on an electric current. The lifting charge burns, pressure develops and the star moves upwards. The pressure profiles are recorded on an oscilloscope and the initial trajectory of the star in the air is recorded on a high-speed camera. Each frame of the video is reproduced on a video screen and initial velocity of the star is determined.

Results and Discussion

Pressure profile

Examples of the pressure profiles by two pressure transducers in the mortar during shot of the star are shown in Figure 3(a)–(c). Figure 3(a) shows an experimental result with a small lifting charge (LC 0.7 g) and small gap ratio (GR 0.20). Here, the gap ratio is defined as the ratio of the area of the gap between the mortar and the star divided by the area of the mortar.

In the pressure profile at the middle of the mortar, no pressure increase was observed during the first stage of the event. Then, the pressure decreased a little and then increased sharply. The small decrease in pressure may be attributable to the high-speed flow of the combustion gas through the gap between the mortar and the star when the star passed the pressure transducer. The pressures at the bottom and middle transducers decreased sharply after the star left the muzzle. The start time of this sharp decrease at the middle transducer was similar to that at the bottom transducer. This suggests that there is no pressure distribution in the mortar in this case.

Figure 3(b) shows an experiment with a similar GR (0.19) and different LC (2.0 g) compared to Figure 3(a). The pressure at the middle transducer increased a little at first, then decreased a little as in Figure 3(a), and increased sharply. The pressure at the middle transducer after the star passed the transducer was lower than that at the bottom transducer at the same time. This indicates that the pressure behind the star becomes lower higher up, that is, there is a pressure distribution in the space behind the star. The first increase in pressure at the middle transducer shows the pressure increase in front of the star by the combustion gas leaking through the gap between the star and the mortar wall.

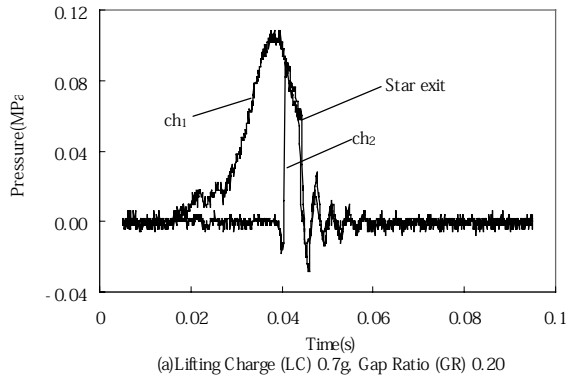

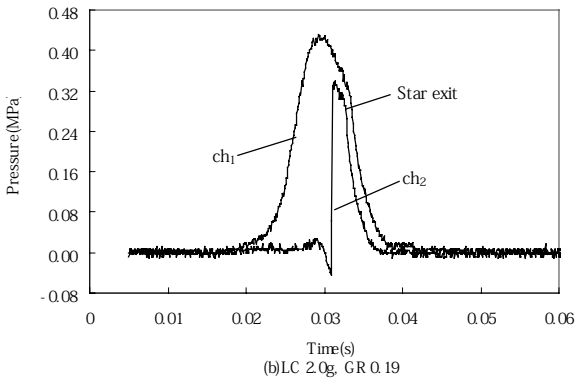

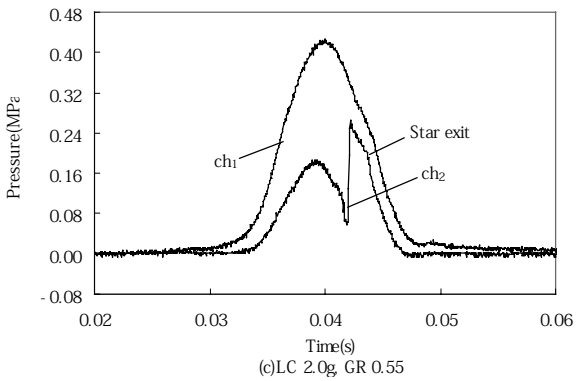

Fig. 3 *(a-c). Pressure profiles at the bottom and middle of the mortar*

The start time of the sharp pressure decrease at the middle transducer in this case was earlier than that at the bottom one. This indicates that the propagation of pressure was delayed more at the bottom than in the middle.

Figure 3(c) shows an experimental result with same LC (2.0 g) and larger GR (0.55) than Figure 3(b). The pressure differences at the bottom and middle transducers increased after the star passed the middle transducer compared to Figure 3(b). This may be attributable to the combustion gas passeing through the larger gap between the mortar wall and the star than the cases in Figures 3(a) and (b).

Reproducibility of the pressure profiles

It is important to know the effect of the mass of the lifting charge, the gap ratio between the mortar wall and the star, etc. on the muzzle velocity of the star. However, it is necessary to know the reproducibility of the data observed under the same condition, in order to understand the relationships correctly.

The following were selected as parameters describing characteristics of the pressure profile: The maximum pressure (P_{1max}), the muzzle pressure (P_{1muz}), the time to maximum pressure (t_{1max}), and the time to muzzle (t_{1muz})by the bottom transducer.

The statistical values of the parameters are listed in Table 1. Here, SD and RSD are standard deviation and relative standard deviation (SD/mean).

Table 1. *Statistical values of P_{1max},P_{1muz},t_{1max} and t_{1muz}.*

GR	*n*	Parameter	Mean	SD	RSD
0.28	6	P_{1max}	533 kPa	68.8 kPa	0.13
		P_{1muz}	521 kPa	67.5 kPa	0.13
		t_{1max}	11.6 ms	1.21 ms	0.10
		t_{1muz}	12.3 ms	1.06 ms	0.09
0.55	5	P_{1max}	295 kPa	79.7 kPa	0.27
		P_{1muz}	212 kPa	38.6 kPa	0.18
		t_{1max}	14.8 ms	2.97 ms	0.20
		t_{1muz}	18.1 ms	2.54 ms	0.14
0.71	5	P_{1max}	253 kPa	65.6 kPa	0.26
		P_{1muz}	102 kPa	74.2 kPa	0.72
		t_{1max}	14.5 ms	3.12 ms	0.21
		t_{1muz}	22.3 ms	4.80 ms	0.21

The scatter of the maximum pressure is larger than that of the time to maximum pressure. The maximum pressure and the time to maximum pressure both decrease with decreasing gap ratio.

Effect of gap ratio

The ratio of the escaped gas from the gap to total combustion gas increases with increasing gap

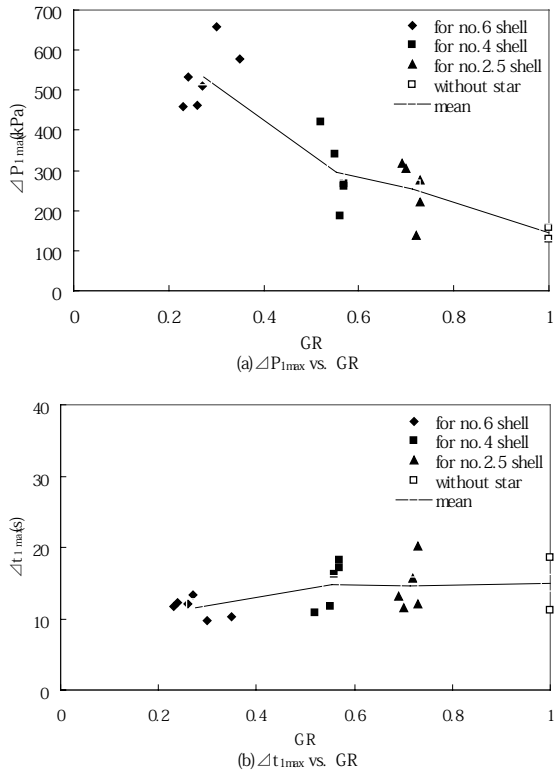

Figure 4(a)–(b). *Plots of P_{1max} and t_{1max} vs. GR.*

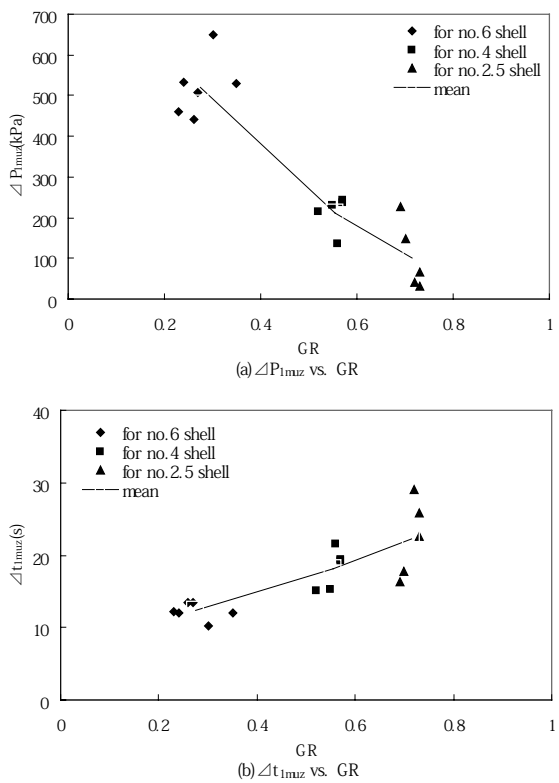

Figure 5(a)–(b). *Plot of P_{1muz} and t_{1muz} vs. GR.*

ratio. Figure 4 shows the plot of P_{1max} and t_{1max} against gap ratio.

The maximum pressure increased with a decrease in the gap ratio. This trend is more noticeable fora smaller gap ratio. The mean values of the time to maximum pressure were similar for GR of 0.55 and 0.71. However, they decreased considerably when the GR was 0.28.

Figure 5 shows a plot of P_{1muz} and t_{1muz} against GR. P_{1muz} decreased monotonously with increasing GR in contrast to the case of P_{1max}. t_{1muz} increased monotonously with increasing GR.

The following changes were observed in the pressure profiles at the bottom transducer of the mortar with 20 mm inner diameter and 361 mm depth using 2.0 g lifting charge, when the gap ratio was changed from 0.28 to 0.71. The star left the muzzle just after the time to maximum pressure when GR was 0.28. On the other hand, in the case of GR = 0.55 the star stayed longer in the mortar after the maximum pressure was attained. When GR was 0.71, the time during which the star stayed in the mortar became longer after the maximum pressure attained.

The following were also observed in the pressure profiles recorded by the middle transducer with the change in GR: no pressure increase was observed before the star passed the transducer when the lifting charge mass and GR were 1.0 g and 0.28, respectively. A pressure increase was observed before the star passed the transducer when the lifting charge and GR were 2.0 g and 0.28, respectively, but the increase was small. With 2.0 g lifting charge and 0.55 GR, the pressure increase before the star passed the transducer was more remarkable and with 0.71 GR much more remarkable.

The pressure increase before the star passed the middle transducer may be attributable to the combustion gas escaping through the gap between the mortar wall and the star. This may be supported by the pressure profiles recorded in the firing experiment using the same mortar without a star (Figure 8).

Effect of the mass of lifting charge

Experiments with different masses of lifting charge were carried out. Though there is some scattering

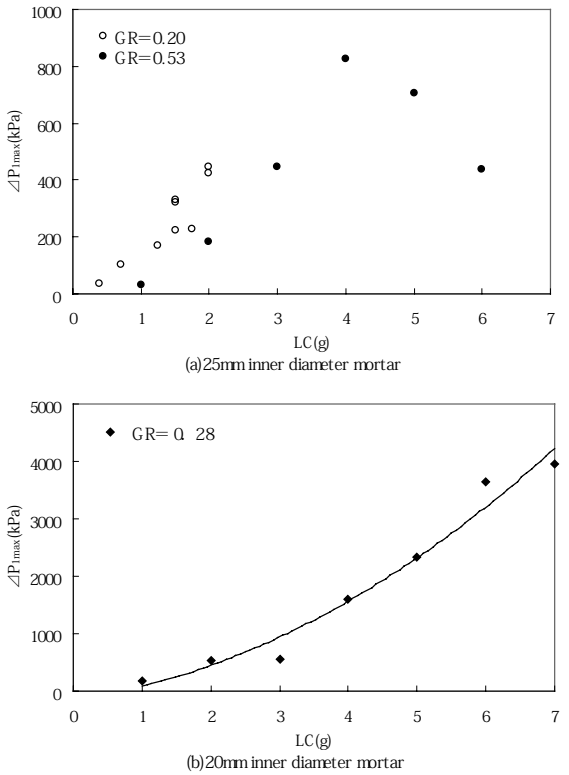

Figure 6. *Plot of P_{1max} vs. LC for (a) 25 mm mortars and (b) 20 mm mortars.*

of the experimental data, the maximum pressure increased with increasing lifting charge. Figure 6 shows the plot of $P_{1\max}$ against the mass of the lifting charge, using the mortars of 20 mm and 25 mm inner diameters.

$P_{1\max}$ increased with increasing mass of lifting charge with one exception. At the moment the reason for the exception is not clear.

Pressure profiles for the real pressures acting on a star using four transducers

It was found that, when the gap ratio became larger, the difference between the bottom and middle pressures became larger. Therefore, we carried out an experiment using a mortar equipped with four pressure transducers. The mortar was a steel tube of 20 mm inner diameter and 361 mm depth. The pressure transducers are situated at 11 mm, 131 mm, 251 mm and 346 mm from the bottom of the mortar (Figure 1). Examples of the recorded pressure profiles are shown in Figure 7.

The pressure profiles of ch1, ch2, ch3 and ch4 were different from each other when GR and LC were 0.71 and 2.0 g, respectively. Here, P_1, P_2, P_3 and P_4 are pressures recorded by ch1, ch2, ch3 and ch4 pressure transducers, respectively.

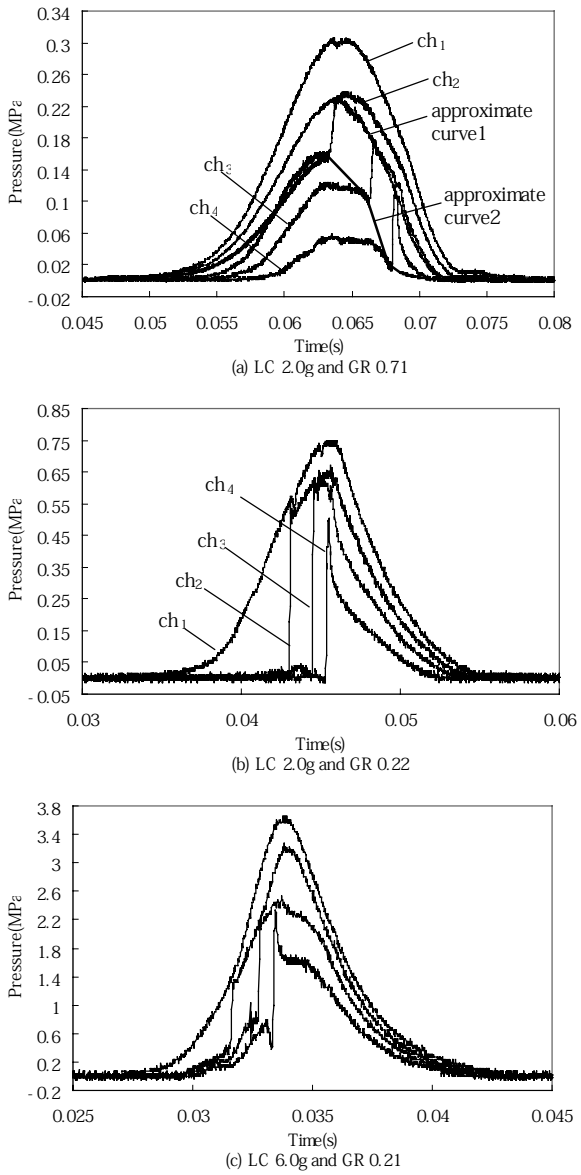

Figure 7. *Examples of the pressure profiles observed by four pressure transducers.*

These profiles may be explained as follows: the pressure P_1 recorded by ch1 reaches a maximum pressure $P_{1\max}$ after $t_{1\max}$ and the muzzle pressure P_{1muz} after t_{1muz}. P_2 recorded by ch2 reaches $P_{2\max}$ after $t_{2\max}$, then P_2 jumps to higher pressure and then reaches P_{2muz} after t_{2muz}. This pressure profile is different from that of ch1. The pressure measured at ch1 is always behind the star, but initially the pressure at ch2 is in front of the star and later behind the star.

These results indicate that the profile of P_1 is not

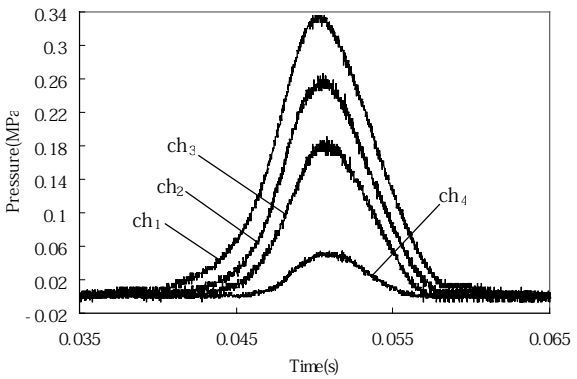

Figure 8. *Pressure profiles of four channels in the mortar on firing with no star.*

necessarily the true pressure profile acting on the rear surface of the star. If the time when the star passes ch2 is t_{ch2}, the real pressure acting on the rear surface of the star is not P_1 but P_2 at t_{ch2}.

Similarly, the real pressure acting on the rear surface of the star is neither P_1 nor P_2 but P_3 at t_{ch3}. The situation is same in ch4. Therefore, the real pressure profile acting on the rear surface of the star is a curve combining P_1, P_2, P_3 and P_4 at t = 0, t_2, t_3 and t_4, respectively. The pressure increases recorded at ch2, ch3 and ch4 before the star passes the respective channel are caused by the pressure in front of the star due to the combustion gas of the lifting charge escaping through the gap between the mortar wall and the star. The pressures decrease in the order: $P_1 > P_2 > P_3 > P_4$. The real pressure acting on the front surface of the star is the pressure at the time just before the sharp increase of pressure in each channel. Therefore, the real pressure profile for the front surface of the star is a curve joining these points. The real driving force is the difference between the above two acting pressures.

The pressure transducer of ch4 is situated near the muzzle of the mortar. The star leaves the muzzle just after it passes the transducer. The onset times of the sharp pressure decrease, t_{muz} , decrease in the order: $t_{1muz} > t_{2muz} > t_{3muz} > t_{4muz}$. The real time when the star passes the muzzle is not t_{1muz}, t_{2muz} or t_{3muz}, but near t_{4muz}.

Effect of the gap ratio GR

In the pressure profiles with GR 0.22–0.27 and LC 2.0 g (Figure 7(b)), the pressure differences of ch1, ch2, ch3 and ch4 are small before the star reaches the respective transducer, compared to the case of GR 0.71 and LC 2.0 g. Furthemore there is nearly no pressure increase in front of the star. This is due to little gas escaping owing to the small gap between the mortar wall and the star. On the other hand, the times of the sharp pressure increases of ch2, ch3 and ch4 decreased when GR was decreased from 0.71 to 0.22–0.27. This may be due to the higher rear gas pressure and higher velocity of the star because of the smaller gap between the mortar wall and the star for lower GR.

We carried out a firing experiment without a star using the mortar with four pressure measuring channels, GR 1.0 and LC 2.0 g. The pressure profiles (Figure 8) look like those of the case where GR = 0.71 and LC = 2.0 g with a star (Figure 7(a)).

Effect of lifting charge mass LC

The pressure profiles (Figure 7(c)) with GR 0.21–0.30 and LC 6.0 g are more different from those (Figure 7(b)) with GR 0.22 and LC 2.0 g, regarding the pressures of all the channels. On the other hand, the times to the sharp pressure increase were shorter than in the case of Figure 7(b). One of the characteristics of the experiment with GR 0.21–0.30 and LC 6.0 g is that the pressure in the mortar remained after the star left the muzzle. This can be seen from the pressure profile of ch4. The pressure of ch4 increases sharply when the star passes near the muzzle. In the experiment with LC 2.0 g, the pressure of ch4 decreased sharply and monotonously. But, in the experiment with LC 6.0 g, the pressure of ch4 decreased initially, but fairly high pressure remained thereafter. This may be due to the continuation of the combustion of lifting charge after the star left the muzzle.

Reproducibility of experiment

Table 2 lists the time to maximum pressure of ch1 t_{1max}, the maximum pressure P_{1max} and their relative standard deviations in the four channel experiments with stars.

In firing stars, the scatter of the times to maximum pressure increased with increasing gap ratio. Regarding the scatter of the maximum pressures, no effect of the gap ratio was observed with LC 2.0 g. With LC 6.0 g, the scatter of both t_{max} and. P_{max} were small.

Table 2. *Time to maximum pressure t_{1max}, maximum pressure P_{1max} and relative standard deviations RSD of the ch1 in star firing*

GR	0.69–0.72	0.22–0.27	0.21–0.30
LC	2.0 g	2.0 g	6.0 g
t_{1max}	12.7 ms	9.32 ms	4.34 ms
RSD	0.28	0.02	0.07
P_{1max}	253 Pa	619 Pa	3704 Pa
RSD	0.30	0.29	0.05

Table 3 shows t_{max}, P_{max} and the relative standard deviations recorded by the four pressure transducers in firing with no stars.

Table 3. *Time to maximum pressure t_{max}, maximum pressure P_{max} and relative standard deviations RSD of the data from all four channels in firing with no star (GR 1.00 and LC 2.0 g)*

ch1	t_{1max}	11.1 ms
	RSD	0.28
	P_{1max}	239 Pa
	RSD	0.43
ch2	t_{2max}	11.38 ms
	RSD	0.28
	P_{2max}	174 Pa
	RSD	0.53
ch3	t_{3max}	11.57 ms
	RSD	0.28
	P_{3max}	119 Pa
	RSD	0.61
ch4	t_{4max}	11.74 ms
	RSD	0.28
	P_{4max}	49 Pa
	RSD	0.83

In the case of firing with no star, the maximum pressures decreased from 239 kPa (ch1) to 49 kPa (ch4), and the relative standard deviation increased from 0.43 (ch1) to 0.83 (ch4). The time to maximum pressure increased slightly from 11.10 ms (ch1) to 11.74 ms (ch4) and the relative standard deviations were 0.28 without change.

Motion of a star in the mortar[3]

The equations of a star in the mortar are expressed as follows:

$$M\frac{\mathrm{d}u}{\mathrm{d}t} = p(t)\times A - Mg \qquad (1)$$

$$\frac{\mathrm{d}Z}{\mathrm{d}t} = u \qquad (2)$$

Here, M, u, A, and Z are mass, motion velocity, maximum cross sectional area, and traveling distance of the star, respectively.

$$A = \frac{\pi D^2}{4} \qquad (3)$$

Here, D is the diameter of the star, and equation (1) can be rewritten as follows:

$$\frac{\mathrm{d}u}{\mathrm{d}t} = \frac{\pi D^2}{4M}\cdot p(t) - g \qquad (4)$$

Here, $p(t)$ is the observed value and substituted into Equation (4).

Equations (3) and (4) are simultaneously solved by numerical calculation, and acceleration du/dt, velocity u and traveling distance Z are obtained.

Observed initial velocity of the star in the air and calculated muzzle velocity

When a star is fired, smoke and flame appear from the muzzle and then the star appears above the smoke. We can only determine initial velocity after the star appears from the smoke. In the same experiment with the pressure measurement, observed initial velocities were compared with calculated muzzle velocities from the pressure profiles in the mortar.

Table 4 and Table 5 list observed initial and calculated muzzle velocities of stars using 25 mm ø and 20 mm ø mortars, respectively.

Figure 9 and 10 show plots of calculated muzzle velocity *vs*. observed initial velocity of stars with 25 mm ø and 20 mm ø mortars, respectively.

In Figure 9 the calculated muzzle velocity agreed fairly well with the observed initial velocity of the star. On the other hand, in Figure 10 it can be

Table 4. *Observed initial and calculated muzzle velocities of stars using 25 mm ø mortar.*

Run no.	Star	Mass/g	Diameter/mm	Lifting charge/g	Gap ratio	Initial velocity/m s^{-1} obs.	cal.
1	no. 10 shell	9.517	22.701	0.40	0.18	27	26
2	no. 10 shell	9.065	22.318	0.70	0.20	57	56
3	no. 10 shell	8.308	22.353	1.25	0.20	77	80
4	no. 10 shell	8.846	22.626	1.50	0.18	86	92
5	no. 10 shell	8.346	21.756	1.50	0.24	103	113
6	no. 10 shell	8.924	22.410	1.50	0.20	106	111
7	no. 10 shell	8.475	22.045	1.75	0.22	91	89
8	no. 10 shell	9.244	22.166	2.00	0.21	117	121
9	no. 10 shell	8.589	22.511	2.00	0.19	117	138

Table 5. *Observed initial and calculated muzzle velocities of stars using 20 mm ø mortar.*

Run no.	Star	Mass/g	Diameter/mm	Lifting charge/ g	Gap ratio	Initial velocity/m s^{-1} obs.	cal.
1	no. shell 6	3.770	16.686	1	0.30	80	86
2	no. shell 6	3.791	17.175	2	0.26	116	
3	no. shell 6	3.742	16.917	3	0.28	131	148
4	no. shell 6	4.084	17.441	4	0.24	167	264
5	no. shell 6	3.310	16.561	5	0.31	145	423
6	no. shell 6	3.847	16.666	6	0.31	190	443
7	no. shell 6	3.705	17.112	7	0.27	195	890
8	no. shell 6	3.908	17.126	2	0.27	119	141
9	no. shell 6	4.002	17.535	2	0.23	138	131
10	no. shell 6	3.520	16.179	2	0.35	134	167
11	no. shell 6	4.070	17.482	2	0.24	121	129
12	no. shell 6	3.751	16.706	2	0.30	126	155
13	no. shell 4	1.868	13.373	2	0.55	93	192
14	no. shell 4	1.838	13.299	2	0.56	83	149
15	no. shell 4	1.836	13.160	2	0.57	104	142
16	no. shell 4	1.984	13.813	2	0.52	104	236
17	no. shell 4	1.813	13.161	2	0.57	90	149
18	no. shell 2.5	0.893	10.342	2	0.73	65	215
19	no. shell 2.5	0.847	10.508	2	0.72	40	187
20	no. shell 2.5	0.898	10.418	2	0.73	39	249
21	no. shell 2.5	1.070	11.088	2	0.69	90	206
22	no. shell 2.5	1.026	10.966	2	0.70	79	251

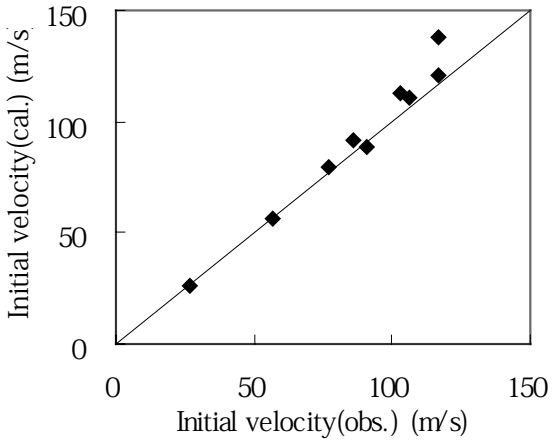

Figure 9. *Plot of calculated muzzle velocity vs. observed initial velocity of star with 25 mm ø mortar.*

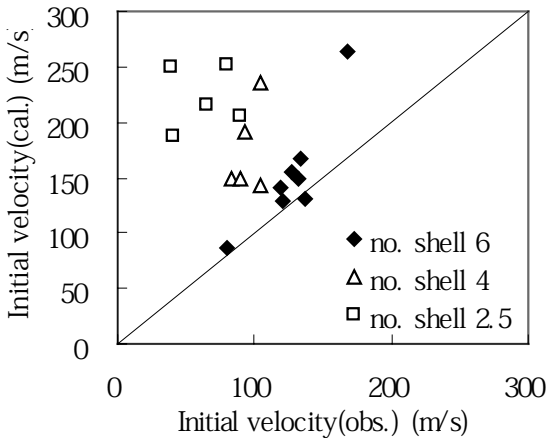

Figure 10. *Plot of calculated muzzle velocity vs. observed initial velocity of star with 20 mm ø mortar.*

seen that the calculated values deviate more from the observed one with the smaller star and more lifting charge.

Correlation of the muzzle velocity of star with the mass of lifting charge

The relationships between the initial velocity of stars and the mass of lifting charges are shown in Figure 11 and Figure 12. Generally, the initial velocity of star increases with the increasing mass of lifting charge, but the increase in the initial velocity weakened when the mass of lifting charge exceeded 2 g.

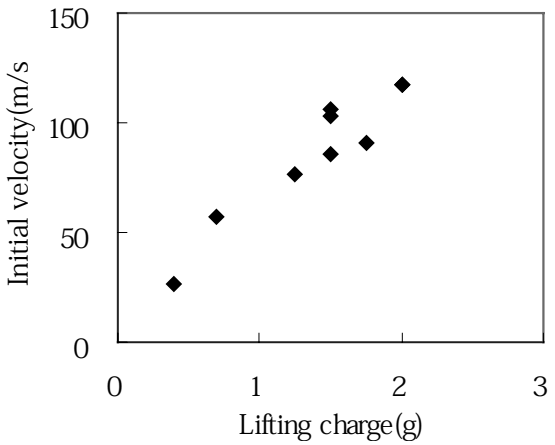

Figure 11. *Plot of the initial velocity vs. the mass of lifting charge with the 25 mm ø mortar and the stars for no.10 shell.*

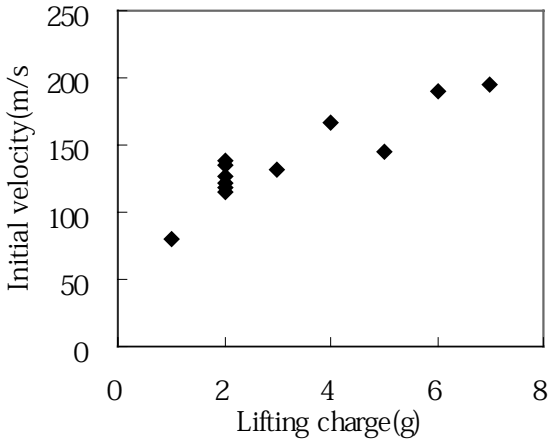

Figure 12. *Plot of initial velocity vs. the mass of lifting charge with the 20 mm ø mortar and the stars for no.6 shell.*

Effect of the gap ratio on the initial velocity of star

Figure 13 shows the plot of the initial velocity of a star against the gap ratio. It was found that the observed initial velocity decreased and the scatter of the initial velocity increased with increasing gap ratio.

Estimation of the muzzle velocity of star considering the pressure distribution in the mortar

The calculated muzzle velocities of the stars with and without correction for the pressure distribution in the mortar are listed in Table 6. The corrected

Table 6. *Observed initial and calculated muzzle velocities of stars using the 20mmφ mortar with 4 pressure transducers*

Stars				Calculated muzzle velocity/ m s^{-1}		
Mass/g	Diameter/mm	Lifting charge/g	Gap ratio	Without correction	With correction	Measured muzzle velocity/m s^{-1}
0.986	10.682	2.0	0.71	254	66	78
4.780	17.696	2.0	0.22	146	136	129
4.757	17.696	2.0	0.22	169	154	135
4.199	17.067	2.0	0.27	145	115	114
4.699	17.553	2.0	0.23	155	134	135
4.155	17.737	6.0	0.21	414	255	233
3.916	17.420	6.0	0.24	361	227	209
3.607	17.041	6.0	0.27	422	249	213
3.644	16.737	6.0	0.30	394	219	209
3.632	16.795	6.0	0.29	388	221	200

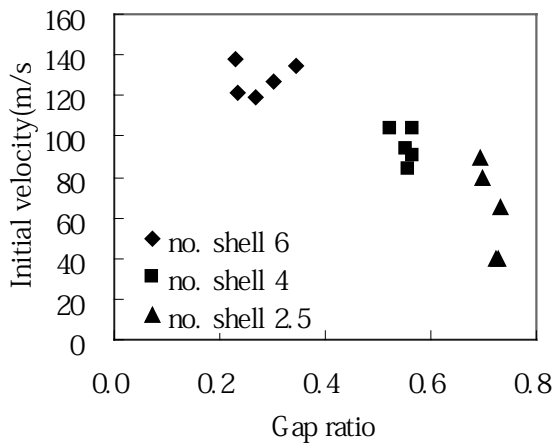

Figure 13. *Plot of initial velocity vs. GR.*

calculated values are in better agreement with the observed initial velocities than the values without correction when the gap ratio was large. In the case of small gap ratio and small mass of lifting charge, the difference between the calculated muzzle and observed initial velocities is small and the effect of the pressure distribution is also small. Therefore, the muzzle velocity of the star is estimated most accurately from the pressure profile at the bottom of the mortar when the gap ratio and the mass of lifting charge are small.

Acknowledgment

The authors wish to gratefully acknowledge the experimental assistance of Sunagaga Fireworks Company, Showarika Company, and the undergraduate students of Higaki Laboratory: Arima, Ariga, Kashiwa and Hukazawa.

References

1 D. Ding, M. Higaki and T. Yoshida, "Burning and Air Resistance of Fireworks Stars", *Science and Technology of Energetic Materials*, in press.

2 K. L. Kosanke and B. J. Kosanke, "Peak In-Mortar Aerial Shell Accelerations", *Journal of Pyrotechnics*, Issue 10, 1999, p. 56.

3 Y. Ooki, D. Ding, M. Higaki, and T. Yoshida, "Interior Pressure in the Mortar and Motion of a No. 3 Shell in a Fireworks Shot", *Journal of Pyrotechnics*, Issue 22, 2005, pp. 3–8.

Notes on chlorinated rubber and some other chlorine donors

Barry T. Sturman

6 Corowa Court, Mount Waverley, Victoria 3149, Australia

Abstract: *A brief review is given of the history and technology of chlorinated rubber. The empirical formula is approximately $(C_{10}H_{11}Cl_7)_n$, corresponding to 65.4% Cl. The structure is complex, and includes partially chlorinated cyclohexane rings. All the Cl is released as HCl on pyrolysis. The enthalpy of formation was estimated from the reported heat of combustion as −395 kJ mol^{-1}. For comparison, the enthalpy of formation of solid polyvinyl chloride $(C_2H_3Cl)_n$ was reported to be −94.6 kJ mol^{-1} and that of solid polyvinylidene chloride $(C_2H_2Cl_2)_n$ was reported to be −100.4 kJ mol^{-1}.*

Keywords: *chlorinated rubber, Parlon, enthalpy of formation, chlorine donors, PVC, polyvinyl chloride, polyvinylidene chloride.*

Introduction

Thermodynamic modelling of the combustion of pyrotechnic mixtures is hindered by the lack of information on the enthalpy of formation of some commonly used ingredients.

In an effort to find values for the enthalpy of formation of various chlorine donors, the writer found some information on chlorinated rubber that may be of interest. This information includes the heat of combustion, which permits the enthalpy of formation of this important chlorine donor to be estimated.

Discussion

Natural rubber is poly(2-methyl-1,3 butadiene), $(C_5H_8)_n$, also called polyisoprene.[1] Chlorination of rubber was studied as long ago as 1888, but commercial production did not start until 1918.[2]. By the early 1930s it was being made by ICI in the UK (brand name "Alloprene") and by several German firms (brand names "Pergut", "Tegofan", "Tornesit").[2] In 1945 the Hercules Powder Co. of Wilmington, Delaware (later Hercules, Inc.) began marketing an improved version of "Tornesit" in the United States as "Parlon".[2]

The original use of chlorinated rubber was as a lacquer for the protection of chemical plant.[2] Later, it became an important ingredient in a wide range of corrosion-resistant and wear-resistant paints and wood finishes.[2] It is also used in adhesives and in printing inks. The first mention that the writer could find of its use as a chlorine donor in pyrotechnics was in a report by Eppig, who lists it as one of the materials tested by German researchers during the Second World War "in an effort to obtain a chlorine carrier which would be more effective than polyvinyl chloride" in green light compositions for military signaling. The report indicates that it was considered less effective than a chlorinated polyvinyl chloride containing about 63% chlorine.[4] Chlorinated rubber is mentioned in Lancaster's 1972 book.[3] Ellern refers to "Parlon" in his 1968 book[5] but says that it is "chlorinated polyisopropylene", that it contains 67% Cl, and that is apparently not used as a chlorine donor. Lancaster points out that Parlon, (chlorinated rubber), is not the same as "Parlon P, which is chlorinated polypropylene, and which is not used as a colour intensifier".[3] Parker says that "chlorinated polypropylene in most respects resembles chlorinated rubber",[2] but current commercial grades (such as "Superchlon" made by Nippon Paper Industries of Tokyo, Japan) contain only 20-40% Cl.[6] This probably explains why it is not used as a colour intensifier. If there ever were a grade that contained 67% Cl, as stated by Ellern,[5] there seems no obvious reason why it would not have been a useful chlorine donor.

Chlorinated rubber was one of the chlorine donors studied by Shimizu in his 1979 article on blue and purple flames,[7] and he mentions it in his 1981 book.[8] In 1981 Fish[9] discussed the use of chlorinated rubber in metal-fuelled coloured flame compositions.

It is unfortunate that the name "Parlon", a

trademark that evidently referred to two different products (chlorinated natural rubber and chlorinated polypropylene),[4] should have become the common name for chlorinated rubber in the firework literature. The US National Institute for Occupational Safety and Health lists 38 synonyms for chlorinated rubber.[10] It would be better to follow Dr Shimizu's example and use the term "chlorinated isoprene rubber"[8] or just "chlorinated rubber".

The chlorine content of chlorinated rubber is in the range 65–68%, but is usually specified as ">65%". Various grades are available, differing principally in the viscosities of their solutions in toluene and presumably corresponding to different chain lengths in the polymer.

Chlorinated rubber was made by passing chlorine into a solution of natural rubber in carbon tetrachloride (tetrachloromethane, CCl_4).[2] Both ICI and Hercules have stopped making chlorinated rubber, possibly because of concern about the use of CCl_4 and the presence of low concentrations of CCl_4 in the product. Carbon tetrachloride is carcinogenic to various laboratory mammals and is classified by the US Environmental Protection Agency as a "probable human carcinogen".[11] Residual CCl_4 in chlorinated rubber is liberated when the product is dissolved, so appropriate care has to be taken. Chlorinated rubber is still made by Bayer MaterialScience AG at Dormagen, Germany ("Pergut")[12] and by Rishiroop Rubber (International) Limited of Mumbai, India ("Chlorub"),[13] to name just two manufacturers. The CCl_4 content of the Pergut brand chlorinated rubber manufactured by Bayer is no more than 0.005%.[12]

Chlorinated rubber is soluble in many solvents "including aromatic hydrocarbons, chlorinated hydrocarbons, ketones higher than acetone and some alcoholic ethers. It is not soluble in water, simple alcohols or aliphatic hydrocarbons".[2]

According to Dodson and McNeill[14] "chlorinated rubber may have a very complicated structure with many variations". The empirical formula given by Dodson and McNeill is $C_{10}H_4Cl_7$ (65.4% Cl).[14] This formula corresponds to 66.7% Cl, not 65.4%, and is obviously a typographical error. The formula corresponding to 65.4% Cl is $C_{10}H_{11}Cl_7$, and this is the formula given by Bloomfield.[15] Fish [9] gives the empirical formula as $C_5H_6Cl_4$, corresponding to a chlorine content of 68.2%.

Parker[2] notes that there is evidence that the structure contains partially chlorinated cyclohexane rings – the chlorination process involves cyclization of parts of the polyisoprene chain as well as substitution and addition at double bonds. If only the latter two processes were involved, the empirical formula would be $C_5H_{10-x}Cl_x$. The formula given by Fish[9] corresponds to this formula with $x = 4$.

Dodson and McNeill[14] studied the thermal decomposition of Alloprene chlorinated rubber and found that the major volatile product was hydrogen chloride. Five sevenths of the total available HCl "is lost with great ease, and complete dehydrochlorination is very much easier than in poly (vinylidene chloride)".

In a temperature programmed thermogravimetric analysis experiment 95% of the total chlorine was lost as HCl below 400 °C. All the chlorine was lost as HCl, accompanied by hydrogen, methane and ethylene, leaving a "carbonaceous residue". These authors also studied the thermal degradation of polyvinylchloride (PVC) and polyvinylidene chloride. PVC lost all its chlorine as HCl between 250 and 300 °C. Polyvinylidene chloride very readily lost half of its chlorine as HCl, but loss of the remaining HCl required high temperatures. Polyvinylidene chloride is the only one of the three polymers that contains equal numbers of Cl and H atoms and evolves only HCl on pyrolysis.[16] The others have an excess of H that is lost as "tar" and as simple gases such as H_2, CH_4 and C_2H_4.[16] Dr Shimizu[7] found that both PVC and chlorinated rubber can function as fuel in pyrotechnic mixtures when $KClO_4$ is the oxidizer, but the burning times for the fastest-burning chlorinated rubber mixtures were roughly twice as long as those of the corresponding PVC mixtures, showing that PVC was the better fuel.

No information about the enthalpy of formation of chlorinated rubber could be found, but values for PVC and polyvinylidene chloride were reported by Sinke and Stull from their measurements of the heats of combustion.[17] The calorimetric measurements required special precautions to prevent attack of the calorimeter by the products of combustion and to ensure that all the chlorine

Table 1. *Chlorine content, chemical formulas heats of combustion and enthalpy of formation of three chlorine donors.*

Material	Common/Trade Names	Chlorine Content (% by Mass)	Empirical Formula	Heat of combustion/ MJ kg^{-1}	Enthalpy of Formation/kJ mol^{-1}
Chlorinated natural rubber	Parlon, Alloprene, Chlororub, Pergut	65–68, typically 65.4	$(C_{10}H_{11}Cl_7)_n$ approximately	13.91 ± ?[18]	−395 ±? see text
Polyvinyl chloride	PVC	56.7	$(C_2H_3Cl)_n$	18.31 ±0.03[17]	−94.6 ±1.3[17]
Polyvinylidene chloride	Saran	73.1	$(C_2H_2Cl_2)_n$	10.52 ±0.03[17]	−100.4 ±1.7[17]

was converted to aqueous HCl of known concentration.[17] Similar precautions would be needed to obtain reliable values for chlorinated rubber. Barton et al. reported the heat of combustion of Alloprene,[18] but it is not clear from their report that they took the precautions specified by Sinke and Stull.[17] The value for the heat of formation of chlorinated rubber was calculated by the writer from the heat of combustion given by Barton et al[18], following the procedure given by Sinke and Stull[17] and using their values for the heats of formation of the combustion products. In view of the uncertainty about the method followed in the determination of the heat of combustion, this estimate of the enthalpy of formation is very much less reliable than the results for the other two chlorine donors, but none the less should be useful for thermodynamic modeling of the combustion of pyrotechnic mixtures containing chlorinated rubber. Data for the three chlorine donors are summarized in Table 1.

Acknowledgement

I am grateful to Rutger Webb for constructive criticism of an earlier version of this article and for his kind provision of References 4 and 18.

References

1 C. T. Greenwood and E.A. Milne, *Natural High Polymers*, Oliver and Boyd, Edinburgh, 1968, p. 82.

2 H. E. Parker, "Chlorinated Rubber", Chapter 5 in R.R. Myers and J. S. Long, eds, *Film-Forming Compositions*, Marcel Dekker, Inc., vol. 1, New York, 1967, pp. 129–210.

3 R. Lancaster, T. Shimizu, R.E.A. Butler and R.G. Hall, *Fireworks Principles and Practice*, Chemical Publishing Co., NY, 1972, p. 34.

4 H. Eppig, *The Chemical Composition of German Pyrotechnic Colored Signal Items, Combined Intelligence Objectives Sub Committee*, H. M. Stationery Office, London, 1945, p. 6.

5 H. Ellern, *Military and Civilian Pyrotechnics*, Chemical Publishing Co., Inc., NY, 1968, p. 125.

6 http://www.np-g.com/e/news/news01081501.html

7 T. Shimizu, "Studies on blue and purple flame compositions made with potassium perchlorate", *Pyrotechnica*, vol. VI, 1980, pp. 5–21.

8 T. Shimizu, *Fireworks – The Art, Science and Technique*, published by T. Shimizu, distributed by Maruzen Co., Tokyo, 1981, pp. 148–149.

9 T. Fish, “Green and other colored flame metal fuel compositions using Parlon”, *Pyrotechnica VII*, (1981) pp 25-37.

10 http://www.cdc.gov/niosh/rtecs/vl6f1a62.html

11 U.S. Environmental Protection Agency. *Integrated Risk Information System (IRIS) on Carbon tetrachloride*. National Center for Environmental Assessment, Office of Research and Development, Washington, DC. 1999. http://www.epa.gov/iris/subst/0020.htm

12 http://www.bayer-ls.com/ls/lswebcms.nsf/id/ABE9563E498BC1B2C12569620050312F

13 http://www.rishiroop.com/

14 B. Dodson and I. C. McNeill, “Thermal degradation of chlorinated rubber: evidence for an alternative cyclic structure for chlorinated rubber”, *Journal of Polymer Science*, Polymer Chemistry Edition, vol. 12 (1974) pp 2305-2315.

15 G. F. Bloomfield, “Rubber, polyisoprenes, and allied compounds. Part IV. The relative tendencies towards substitutive and additive reaction during chlorination”, *Journal of the Chemical Society,* (1943) pp 289-296.

16 J. B. Gilbert, J. J. Kipling, B. McEnaney and J. N. Sherwood, “Carbonization of polymers I – thermogravimetric analysis”, *Polymer*, vol. 3 (1962) pp 1-10.

17 G. C. Sinke and D. R. Stull, “Heats of combustion of some organic compounds containing chlorine”, *Journal of Physical Chemistry*, vol. 62 (1958) pp 397-401.

18 T. J. Barton, T. T. Griffiths, E. L. Charsley and J. Rumsey, “The influence of binders in pyrotechnic reactions. I. Magnesium -oxidant systems”, *Proceedings of the 9th International Pyrotechnics Seminar*, Colorado Springs, Colorado USA (1984), pp 723-759.

An Introduction to the European CHAF Project

D. Chapman

Health and Safety Laboratory, Harpur Hill, Buxton, Derbyshire, SK17 9JN, UK

Abstract: *The CHAF* project was instigated following a series of accidents in large-scale storage of fireworks, by far the most serious being that at Enschede in the Netherlands. The project aims to quantify and suggest means to control the hazards associated with large-scale fireworks storage by small-, medium- and large-scale investigations on a series of well-defined fireworks. Additionally, it is hoped that correlations will be found between the small- and/or medium-scale tests results and those obtained in large-scale trials, and that these will lead to better test methods to predict mass storage hazards. Reports from the individual activities undertaken in the workpackages are posted on a dedicated web site www.chaf.info as they are delivered.*

Keywords: *CHAF, fireworks, accidents, storage*

Introduction

A large number of fireworks accidents occur each year and some of these have recently been reviewed.[1] Press reports of accidents cover those occurring during fireworks use (either professional display or private use) and also accidents in manufacture, storage and transport. The CHAF project[2] was instigated as a European initiative following a number of incidents associated with the large-scale storage of fireworks culminating in that at Enschede[3] in the Netherlands. The majority of fireworks accidents occur in Asia and South and Central America while a lesser number are reported in Europe, North America and Australasia. Many of the accidents not associated with fireworks use occur at manufacturing sites and it is quite possible that the initial fire or explosion occurring during the manufacturing process will propagate to the stored fireworks and that these will produce the major contribution to the overall damage.

Accidents at storage sites have included: Stourbridge (1996), Uffculme[4,5] (1998), Enschede[3] (2000), Carmel[6] (2002), and Kolding[7] (2005). In all these incidents relatively minor initial fires propagated to bulk storage and resulted in major damage and in the case of Enschede, multiple deaths. The CHAF project is part of the European response to such incidents.

Background

In the mid 1990s the UK Health and Safety Executive commissioned large-scale trials[8] which consisted of ISO containers of fireworks initiated by an external fire. External fire had been the mode of ignition in several fireworks incidents in the UK. A mixed load of "shop goods" fireworks‡ as available at that time was found to be unlikely to result in any major hazard. The fireworks burned slowly or smouldered and when the door of the container was opened some 18 hours later the fireworks re-ignited and continued to burn slowly. On the other hand, 125 mm star shells gave a massive fireball but did not give a mass explosion. A mixed load of display and consumer fireworks give effects between the two, forcing the door to open and throwing fireworks out of the front of the container. While these trials were being conducted, but before the work was published, the Uffculme incident occurred. Investigation[9] of this incident revealed that fireworks returned from a display were fused together and were being separated in the storage area by cutting the fuse with scissors. Both actions were contrary to the company's safety

** CHAF is derived from the project title: Quantification and Control of the Hazards Associated with the Transport and Storage of Fireworks*

‡ Shop goods fireworks are those available for sale to the general public and are also termed consumer fireworks. In the UK this is very often in the form of fireworks selection boxes containing a mix of Roman candles, fountains, mines, wheels and possibly rockets, all of limited size.

procedures. This led to the ignition of one or more shells which spread through the stored fireworks, causing a large explosion that devastated the site. While a fireball resulted from the star shell trials, this did not fully account for the extent of the damage and additional United Nations (UN) Test series 6(a) and 6(b) trials[10] were therefore undertaken on a series of flash-containing fireworks to find limits where mass explosion (UN 1.1G events) occur. This work is ongoing and results are provided to the UN technical committee responsible for fireworks classification.

While this testing was in progress, the major incident at Enschede occurred. This was initially a fire at a fireworks storage site that developed into three explosions resulting in the death of 22 persons and injuries to 947.[11] Again, fireworks in mass storage had produced a mass explosion. One of the responses to this incident was a European initiative to investigate large-scale initiation of fireworks and better means of predicting the effects of such fireworks in storage and transport situations.

The CHAF programme

European collaborative programmes are part funded by the European Commission (EC) and matched funding is provided by the participating nations via their internal funding mechanisms. This particular consortium consists of Bundesanstalt für Materialforschung und -prüfung (BAM) in Germany, Nederlandse Organisatie voor toegepast-natuurwetenschappelijk onderzoek (TNO) in Holland and the Health and Safety Laboratory (HSL) in the UK. Typically, these programmes are divided into "workpackages" dealing with different aspects of the work. In the CHAF project there are 10 such workpackages. These each have a series of deliverables; public deliverables are available on the CHAF web site (www.chaf.info) as they are presented to the EC.

Workpackage 1 – Management and Coordination

This is the overall management task for the project, monitoring and reporting to the EC. Formal progress reports are made on a 6-monthly basis. This includes coordination and progress meetings between the partners. Additionally, the coordinator for the project is responsible for other EC related communications. This workpackage runs throughout the project.

Workpackage 2 – Critical Review Panel

A "half-way" review where a mixture of regulators and fireworks company representatives reviewed the work and made recommendations on the remainder of the programme.

Workpackage 3 – Transfer of information

The communication within the project and to the outside world is covered by this workpackage. This includes maintaining the CHAF website, communicating with outside bodies (UN, International group of scientific experts on the explosion risks of unstable substances, IGUS), writing scientific papers to disseminate the findings. This workpackage runs throughout the programme. Additionally, an International Fireworks Symposium will be held in Berlin in April 2006 at which the results from the CHAF project will form a key part.

Workpackage 4 – Literature review

This workpackage is divided into four areas:

1. an overview of fireworks types and compositions, based on the types covered in the European standards for fireworks EN14035 parts 1-37,
2. an assessment of research on reaction mechanisms taking place in fireworks and between adjacent fireworks articles,
3. a summary of legislation on storage and transport of fireworks in European Union countries, and
4. a review of environmental and health impact of major fireworks accidents.

All four reviews have delivered reports (deliverables D4-1 to D4-4) which are posted on the CHAF website.

Workpackage 5 – Instrumentation development

The quantitative information required from the practical workpackages was assessed and suitable instrumentation techniques were recommended or developed. A series of validation tests was also performed to assess the suitability of the instrumentation. This has generated three

deliverable reports:

1. a review of the data to be generated,
2. selection of the instrumentation, and
3. validated instrumentation

All three are reproduced on the CHAF website and will form the basis of a future article.

Workpackage 6 – Instrumented benchmarking.

One of the main objectives of this workpackage was to select a series of fireworks for testing using UN series 6 tests with additional instrumentation (mainly pressure transducers and thermocouples). Fireworks were selected to be in a clearly defined UN transport category (1.1 – mass explosion, 1.3 – major fireball and 1.4 – minor fireball) or likely to be on the borderline of UN 1.1/1.3 and UN 1.3/1.4 as benchmark examples. The UN series 6(b) and 6(c) tests were performed to give well defined UN transport classification of the fireworks, with the additional pressure and temperature data used for comparison to other workpackage results.

This workpackage has delivered its results in the form of reports which can be found on the CHAF website.

Deliverable D6-1 presents the rationale for the selection of fireworks types for the test series. These fireworks fall into three sets:

1. those chosen as reference materials; a 1.4G fountain, 1.3G waterfall, 1.3G Roman candle and a 1.1G report shell,
2. those chosen for shock initiation and at the 1.3/1.1G boundary; a Roman candle with report, a star shell, a report rocket and a star burst rocket,
3. those chosen for heat initiation; bag mines and waterfall.

Deliverable D6-2 presents the test plan and methodology and the final combined D6-3 and D6-4 reports give detailed results from the test series.

Workpackage 7 – Small-scale characterisation

This workpackage designed and tested small scale test apparatus to investigate the propagation of flame (or detonation) both within a firework and between fireworks in 1 and 2 dimensions. These were substantial tubes (1-D) and boxes (2-D) in which the propagation of the burning (or detonation) of fireworks could be investigated. This completed workpackage has produced two deliverables:

1. a methodology report setting out the mechanisms investigated and the test methods, and
2. a report on the application of the test methods and their findings.

Again, the results from this workpackage will be correlated with those from other practical workpackages.

Workpackage 8 – Medium scale characterisation of packaged fireworks

The medium-scale testing developed the small-scale work into a 3-dimensional test for examining time/pressure output from fireworks tested in their transport packages. The vessel used is an approximate 1 m^3 cylinder with instrumentation to measure internal pressure and temperature. This is currently in the early stages of testing. Findings will be reported via the website and in future articles for publication.

Workpackage 9 – Instrumented full-scale validation tests

This is a series of full-scale trials employing steel ISO containers (and, possible, concrete structures) to investigate hazards from specific firework types in mass storage. This workpackage was informed by previous workpackage results to select pertinent fireworks for test. These have been manufactured and testing will take place during 2005.

Workpackage 10 – Development of testing methodology

The final workpackage takes the results from the practical workpackages and will provide a series of recommendations on suitable tests to be carried out to predict the performance of bulk stored fireworks in the event of accidental initiation.

References

1 R. K. Wharton, "Recent European developments relating to pyrotechnics", *Proc.31st Annual Conference on Explosives and Blasting Technique*, ISEE, Orlando, Florida (Feb 6-9, 2005) pp 247-256.

2 European Commission project number EVG1-CT-2002-00074

3 J. Lambourne, "A matter of substance", *Fire Prevention*, Issue 356 (2002) pp 19-21.

4 "Factory explosion costs company UK£125,000", *Safety and Health Practioner*, Vol. 18, issue 2, (2000) p 5.

5 R. Merrifield, "Hazards Associated with the Storage of Fireworks", *J Pyro*, No 14 (2001) pp 1-14.

6 "Fireworks Blast Causes Fires, Shaking Houses but no Injury" New Zealand Press Association (WNZA), 6 March 2002.

7 "Kolding plant possibly overstocked", *The Copenhagen Post online*, http://www.cphpost.dk/get/83351.html, 04,11,2004.

8 S. G. Myatt, "The Effect of External Fire on Fireworks Stored in Steel ISO Transport Containers", *J Pyro*, No 16 (2002) pp 59-70.

9 S. G. Myatt and I. M. McKay, "Hazards associated with Handling and Bulk Storage of Fireworks", *Industrial Safety Management*, (Dec 2002) pp 6-9.

10 "*Recommendations on the Transport of Dangerous Goods*", fourth revised edition, United Nations, New York, (2003) pp 143-154

11 C. P. Weeth, "Enschede: Lessons to Relearn", *Proc. 6th International Symposium on Fireworks*, Lake Buena Vista, Florida (Dec 2001) pp 345-366.

Review of:

Firework Art

Mark Flemming

ISBN 0-9550621-0-1

Published by Rumble 2005

Reviewed by Tom Smith

Davas Ltd, UK

This is a very nostalgic book, giving examples of firework labels, posters and point of sale material over the period of my childhood as well as before.

The labels are exceptionally well reproduced, my only critisism would be that additional information, including the approximate date of the relevant firework, could usefully be appended to each label.

The introductory text is interesting, but not seemingly directly related to the illustrations that follow. It details the changes in the UK's fireworks industry, reflecting sadly on the general decline and rise in imports. It also , in the most general terms, equates the style of firework art to the social history of the day.

One of the most fascinating features of the labels themselves is the safety text - why is it that our parents' and grandparents' generations were able, seemingly, to enjoy their fireworks (and the firework art) without having to read, and probably ignore, reams of instructions, warnings and complience text?

This is a worthwhile addition to any firework enthusiasts library

See also http://www.firework-art.com

Events Calendar

Pyrotechnics and Fireworks

33rd International Pyrotechnics Seminar
July 16 - 21 2006, Fort Collins. CO, USA
Contact: Linda Reese, Appl. Res. Assoc. Inc.
10720 Bradford Road., Ste 110
Littleton, CO 80127, USA
Phone: +1-303-795-8106
Fax: +1-303-795-8159
email: lreese@ara.com
web: http://www.ips.org
http://www.ipsusa.org

Pyrotechnics Guild Int'l Convention
August , 2006, Appleton, WI, USA
Contact: Frank Kuberry, Sec. Treas.
304 W Main St
Titusville, PA 16354, USA
Phone: +1-814-827-6804
email: kuberry@earthlink.net
web: http://www.pgi.org

Listing of Fireworks Events - Worldwide
web: http://fireworksguide.com

Pyrotechnic Chemistry Lecture Course
At least 2 dates to be arranged in 2006
For more information please see
web: http://www.pyrochemistry.net

Energetic Materials

32nd Annual Conference on Explosives and Blasting Technique
Jan 29-Feb 1, 2006, Dallas, TX, USA
Contact: Lynn Mangol
Phone: 440-349-4400
email: mangol@isee.org

Fourth International Disposal Conference
13 - 14 November 2006 Katrineholm, Sweden
Contact: Klas Nyberg, KCEM,
Gammelbackavagen 6 SE-691 51 Karlskoga,
Sweden
Phone: +46 586 847 45
Fax: +46 586 847 49
E-mail: klas.nyberg@kcem.se

Propulsion

42nd AIAA/ASME/SAE/ASEE Joint Propulsion Conference
9 - 12 Jul 2006
Sacramento, California
Contact:
Phone: +1-703-264-7500
web: http://www.aiaa.org

High Power Rocketry

LDRS 2006
Contact: see web site
web: http://www.tripoli.org/calendar.htm

Model Rocketry

NARAM 2006
Contact:
web: http://www.naram.org
For other launch information visit the NAR Web site: http://www.nar.org

Future Events Information

If you have information concerning future explosive, pyrotechnics or rocketry meetings, training courses or other events that you would like to have published in the Journal of Pyrotechnics and on the website http://www.jpyro.com - please provide the following information:

Name of event, Date and place (City, State, Country), Contact information - including, if possible, name of contact person, postal address, telephone and fax numbers, email address and website

Journal of Pyrotechnics - Sponsors

Journal of Pyrotechnics wishes to thank the following sponsors for their continuing support

Individual Sponsors

Ed Brown
PO Box 177
Rockvale, CO, 81244, USA
phone: 719-784-4226
email: edwinde@cs.com

Gerald Laib
17611 Longview Lane
Olney, MD 20832, USA
phone: 301-744-4358
fax: 301-744-4784

Corporate Sponsors

Aerotech & Industrial Solid Propulsion Inc.
Gary Rosenfield
2113 W 850 N St
Cedr City, UT 84720, USA
phone: 435-867-9998
fax: 435-865-7120
email: garyr@powernet.net
web: http://www.aerotech-rocketry.com

Allied Speciality Insurance
Rick D'Aprile
10451 Gulf Blvd.
Treasure Island, FL 33706, USA
phone: 800-237-3355
fax: 727-367-1407
email: info@alliedspeiality.com
web: http://www.alliedspeciality.com

American Fireworks News
Jack Drewes
HC 67 Box 30
Dingmans Ferry, PA 18328, USA
phone: 570-828-8417
fax: 570-828-8695
email: afn@fireworksnews.com
web: http://www.fireworksnews.com

American Pyrotechnics Association
Julie Heckman
4808 Moorland Lane - Ste 109
Bethusda, MD 20814, USA
phone: 301-907-8181
fax: 301-907-9148
email: jheckman@americanpyro.com
web: http://www.americanpyro.com

Astro Pyrotechnics
Leo Autote
2298 W Stonehurst
Rialto, CA 92377, USA
phone: 909-822-6389
fax: 909-854-4747
web: http://www.astropyro.com

Black Cat Fireworks
Martin Guest
Crossland Hill, Huddersfield, W Yorkshire
HD7 7AD, UK
phone: +44-1484-640640
fax: +44-1484-485943
email: marting@blackcatfireworks.ltd.uk
web: http://www.blackcatfireworks.ltd.uk

Brooke * Mawhorr, PC
Douglass K Mawhorr
112 East Gilbert St., PO Box 1071
Muncie, IN 47305, USA
phone: 765-741-1375
fax: 765-288-7763
email: dimmawhorr@aol.com

Canadian Explosives Research Laboratory
Dr Phil Lightfoot, Manager
CANMET - 555 Booth St.
Ottawa, ON K1A 0G1, Canada
phone: 613-947-7533
fax: 613-995-1230
email: plightfo@nrcan.gc.ca
web: http://www.nrcan.gc.ca/mms/cerl

Combined Specialities International Inc.
John & Alice Allen
8362 Tamarack Village, Ste. 119
Woodbury, MN 55125, USA
phone: 651-855-0091
fax: 651-855-0088
email: jallen@combinedspecialities.com

Delcor Industries Inc
Sam Bases
19 Standish Ave.
Yonkers, NY 10710, USA
phone: 914-779-6425
fax: 914-779-6463
email: delcor@hotmail.com
web: http://www.delcor.com

European Pyrotechnic Arts Newsletter
Rob Driessen
Grenadierweg 55
Riemst, B 3770, Belgium
phone: +32-12-210-630
fax: +32-12-210-630
email: epan@pandora.be
web: htp://users.pandora.be/epan

Fawkes Fireworks
Tony Cardell & David Watts
89 Lingfield Road
Edenbridge, Kent TN8 5DY, UK
phone: +44-1732-862-862
fax: +44-1342-317-818
email: tony@fawkes.co.uk
web: http://www.fawkes.co.uk

Fire One
Dan Barker
863 benner Pike
State College, PA 16801, USA
phone: 814-238-5334
fax: 814-231-0799
email: info@fireone.com
web: http://www.fireone.com

Firefox Enterprises Inc.
Gary Purrington
11612 N Nelson
Pocatello, ID 83202, USA
phone: 208-237-1976
fax: 208-237-1976
email: custserv@firefox-fx.com
web: http://www.firefox-fx.com

Firework Professionals
Anthony Leyland
PO Box 19-912
Christchurch, 8030, New Zealand
phone: +64-3-982-3473
fax: +64-3-982-3474
email: firework@firework.co.nz
web: http://firework.co.nz

Fireworks
PO Box 40
Bexhill, Sussex TN40 1GX, UK
phone: +44-1424-733-050
fax: +44-1424-733-050
email: editor@fireworks-mag.org
web: http://www.fireworks-mag.org

Fireworks and Stage FX America
Kevin Brueckner
PO Box 488
Lakeside, CA 92040, USA
phone: 619-938-8277
fax: 619-938-8273
email: info@fireworksamerica.com
web: http://www.fireworksamerica.com

Fireworks Business
Jack Drewes
HC 67 Box 30
Dingmans Ferry, PA 18328, USA
phone: 717-828-8417
fax: 717-828-8695
email: afn@fireworksnews.com
web: http://www.fireworksnews.com

Fireworks by Grucci
Phil Grucci
1 Grucci Lane
Brookhaven, NY 11719, USA
phone: 631-286-0088
fax: 631-286-9036
email: philgrucci@aol.com
web: http://grucci.com

Fullam's Fireworks Inc
Rick Fullam
PO Box 1808 CVSR
Moab, UT 84532, USA
phone: 435-259-2666
email: rfullam_3@yahoo.com

Goex Inc.
Mick Fahringer
PO Box 659
Doyline, LA 71023, USA
phone: 318-382-9300
fax: 318-382-9303
email: email@goexpowder.com
web: http://www.goexpowder.com

High Power Rocketry
Bruce Kelly
PO Box 970009
Orem, UT 84097, USA
phone: 801-225-3250
fax: 801-225-9307
email: tra00015@aol.com
web: http://tripoli.org

IPON srl
Pagano Benito
Via Trofa
Ottavino, Napoli 80044, Italy
phone: +39-81-827-0934
fax: +39-81-827-0026
email: info@ipon.it
web: http://www.ipon.it

Island Fireworks Co. Inc.
Charles Gardas
N735 825th St
Hager City, WI 54014, USA
phone: 715-792-2283
fax: 715-7922640
email: islndfwk@pressenter.com
web: http://www.island-fireworks.com

Lantis Fireworks & Lasers
Ken Lantis
PO Box 491
Draper, UT 84020, USA
phone: 801-768-2255
fax: 801-768-2433
email: info@fireworks-lasers.com
web: http://www.fiireworks-lasers.com

MagicFire Inc
Paul McKinley
PO Box 896
Natick, MA 01760, USA
phone: 508-647-9645
fax: 508-647-9646
email: pyrotech@magicfire.com
web: http://www.magicfire.com

Martin-Baker Aircraft Ltd
David Chapman
Lower Rd, Higher Denham
Uxbridge, Middlesex UB9 5AJ
Great Britain
Phone: 44-1895-836-644
FAX: 44-1985-836-686
email: dchapman@martin-baker.co.uk
web: www.martin-baker.com

Martinez Specialities
Phil Martinez
208 Bossard Rd
Groton, NY 13073, USA
phone: 607-898-3053
fax: 607-898-3952
email: mr.squib@clarityconnect.com

Maratamaya Ogatsu Fireworks Co. Ltd.
1-35-35 Oshitate Fuchu
Tokyo, 183-0012, Japan
phone: +81 42-363-6251
fax: +81-42-363-6252
email: hanabi@mof.co.jp
web: http://www.mof.co.jp

Mighty Mite Marketing
Charlie Weeth
122 S 17th St
LaCrosse, WI 54601, USA
phone: 608-784-3212
fax: 608-782-2822
email: czweeth@pyro-pages.com
web: http://www.pyro-pages.com

MP Associates Inc.
PO Box 546
Ione, CA 94640, USA
phone: 209-274-4715
fax: 209-274-4843

Nilsson & Lee Pyrotechnics
Hans Nillson
Box 130
SE-372 22 Ronneby, Sweden
phone: +46-457-15600
email: info@pyrokits.com
web: http://www.pyrokits.com

Precocious Pyrotechnics Inc.
Garry Hanson
4420 278th Ave NW
Belgrade, MN 56312, USA
phone: 320-346-2201
fax: 320-346-2403
email: ppinc@tds.net
web: http://www.pyro-pro.com

Pyro Shows Inc.
Lansden Hill
PO Box 1406
LaFollette, TN 37766, USA
phone: 800-662-1331
fax: 423-562-9171
email: info@pyroshowusa.com
web: http://pyroshowusa.com

Pyrodigital Consultants
Ken Nixon
1074 Wranglers Trail
Pebble Beach, CA 93953, USA
phone: 831-375-9489
fax: 831-375-5255
email: purodig@aol.com
web: http://www.infinityvisions.com/pyrodigital

PyroLabs Inc.
Ken Kosanke
1775 Blair Road
Whitewater, CO 81527, USA
phone: 970-245-0692
fax: 970-245-0692
email: ken@jpyro.com

RCS Rocket Motor Components Inc.
Gary Rosenfield
2113 W 850 N St
Cedar City, UT 84720, USA
phone: 435-865-7100
fax: 435-865-7120
email: garyr@powernet.net
web: http://www.rocketmotorparts.com

RES Speciality Pyrotechnics
Steve Coman
21595 286th St
Belle Plaine, MN 56011, USA
phone: 952-873-3113
fax: 952-873-2859
email: respyro@earthlink.net
web: http://www.respyro.com

Rozzi Famous Fireworks
Arthur Rozzi
PO Box 5
Loveland, OH 45140, USA
phone: 513-683-0620
fax: 513-683-2043
email: art@rozzifireworks.com
web: http://www.rozzifireworks.com

Service Chemical Inc.
Ben Cutler
2651 Penn Avenue
Hatfield, PA 19440, USA
phone: 215-362-0411
fax: 215-362-2578
email: ben@servicechemical.com
web: http://www.servicechemical.com

Spirit of 76 Fireworks
John Bechtold
6401 West Highway 40
Columbia, MO 65202, USA
phone: 573-477-1776
fax: 573-477-1786
email: marketing@76wholesale.com
web: http://www.76wholesale.com

Starburst Pyrotechnics & Fireworks Displays Ltd
Bonnie Pon
2nd Fl-Sui Hing Hong Bldg-17, Commissioner St
Johannesburg, Gauteng 2000, South Africa
phone: +27-11-838-7705
fax: +27-11-836-6836
email: info@starburstpyro.co.za
web: http://www.starburstpyro.co.za

Western Pyrotechnics Inc.
Rudy Schaffner
PO Box 176, Holtville, CA 92250, USA
phone: 760-356-5679
fax: 760-356-2155
email: rudys@holtville.net

Sponsorships

No advertising as such is printed in the Journal of Pyrotechnics. However a limited number of sponsors have been sought so that the selling price of the Journal can be reduced from the listed cover price. The costs of being a sponsor foran issue of the Journal of Pyrotechnics is $70 per issue for businesses and organisations and $35 for individuals. In addition to a listing in the sponsors section of the Journal, full sponsors receive two free copies of the sponsored journal [one copy for individual sponsors]. Additionally, if you so desire, we will provide a link from the Journal of Pyrotechnics website (www.jpyro.com) to the sponsor's website or email address - or simply a company name and contact details.

Additionally it is possible to insert a "flyer" for distribution with the Journal on payment of a modest fee. Please contact the publisher or managing editor for more details

Information for Readers

Editorial Policy

Articles accepted for publication in the Journal of Pyrotechnics can be on any technical subject in pyrotechnics. However, a strong preference will be given to articles reporting on research (conducted by professional or serious individual experimeters) and to review articles (either at an advanced or tutorial level). Both long and short articles will be gladly accepted. Also, responsible letters commenting on past Journal articles will be published along with responses by the authors.

Publication Frequency

The *Journal of Pyrotechnics* appears approximately twice annually, typically in mid-summer and mid-winter.

Subscriptions

Anyone purchasing a copy of the Journal will be given the opportunity to receive future issues on an approval basis. Any issue not desired may be returned in good condition and nothing will be owed. So long as issues are paid for, future issues will automatically be sent. In the event that no future issues are desired this arrangement can be terminated at any time by informing the publisher. Additional discounts are available for payment in advance for issues of the *Journal of Pyrotechnics*. Please contact the publisher for more information

Back issues

Back issues of the Journal will be kept in print permanetly as reference material. Shortly, these will also be available online by subscription at http://www.jpyro.com

Caution

The experimentation with, and the use of, pyrotechnic materials can be dangerous and may require licences or permits in certain countries; it is felt to be important for the reader to be duly cautioned. Without the proper training and experience no one should ever experiment with or use pyrotechnic materials. Also, the amount of information presented in this Journal is not a substitute for necessary training and experience, nor does it remove the relevant application of National or local laws and regulations.

A major effort has been undertaken to review all articles for correctness. However it is possible that errors remain. It is the responsibility of the reader to verify any information herein before applying that information in situations where death, injury or property damage could result.